REMOTE SENSING OF AGRICULTURAL SALINITY

by

PETER HICK

Presented as part of the requirements for the award of

the Degree of Master of Applied Science, of the

Curtin University of Technology.

Perth, Western Australia

December 1987

REMOTE SENSING OF SALINE SOILS

ABSTRACT

Salinity represents the major environmental threat to arable land in Western Australia and many other parts of the world. This study was designed to establish criteria for a practical remote sensing system using the visible, reflected and shortwave infrared for the early detection and mapping of salinity. The results are principally from a group of study sites on the CSIRO's Yalanbee Experiment Station, and from other significant sites during the agricultural cycles of 1985-7.

Analysis of imagery from the Geoscan Multispectral Airborne Scanner showed that best discrimination between study sites affected by salinity, and those not affected, was provided by bands 3 (650-700 nm), 4 (830-870 nm) and band 6 (1980-2080 nm). The maximum discrimination occurred in a September 1986 flight (spring-flush). Although excellent discrimination was also evident in August and November in 1985, this could not be reproduced in November 1986. The visible and reflected infrared bands 3 and 4 featured prominently, but the significance of the short wave infrared bands was evident especially when vegetative ground cover became a less dominant factor.

Field spectra collected over the same period with the Geoscan Portable Field Spectroradiometer (PFS) supported the aircraft data to a certain extent. Detailed analysis of the fine non-correlated structure of narrow constructed bands, from PFS data, indicated that improved discrimination between sites could be provided over a wider time window extending into the summer and autumn. This is when weather-related conditions, i.e. cloud, soil moisture and sun angle, are more conducive to extensive surveys.

The importance of at least one narrow band centred near 1985 nm was determined. Laboratory spectra of bare soil from the sites measured on an Hitachi Spectrophotometer also proved the importance of the shortwave region adjacent to the 1900 nm water absorption.

The study evaluated the spatial and spectral characteristics of existing satellite systems such as Thematic Mapper and the Multispectral Scanner on the Landsat series and determined that a spatial resolution of about 20-30 metres was most appropriate for detection of salinity at a scale whereby management could be implemented.

Ground electromagnetic techniques were evaluated during the study and the EM-38 Ground Conductivity Unit proved valuable for characterizing salinity status of the sites. The Lowtran Computer Code was used to model atmospheric attenuation and results indicated that the positioning of a narrow shortwave infrared waveband, centred at 1985 nm, is possible.

ACKNOWLEDGEMENTS

I am deeply indebted to the CSIRO, and the National Soil Conservation Program, without whose support this work could not have been done. Dr Frank Honey and his staff at Geoscan Pty Ltd, provided the airborne and field hardware. Dr Claude Collett and his successor, Mr Bill Larson, as the principal supervisor, provided help and friendly guidance during the preparation of this document. Colleagues and friends, Dr Norm Campbell, Mr Jim Davies, Dr Harri Kiiveri, Professor Ron Lyon, Professor Paul Tueller, Mr Bill van Aken, Professor Peter Crown, Mr Tony Rea, Mr John Charlich, Miss Jan Ward, Dr Jim Davies, and Mr Ian Tapley, have all played important parts in this study. Special thanks are offered to Mr Eric Bettenay for overall supervision, and Miss Stacey Melvold who helped prepare this document.

TABLE OF CONTENTS

CHAPTER ONE

CHAPTER TWO

CHAPTER THREE

FIGURES

TABLES

CHAPTER ONE

1.1 INTRODUCTION

1.1.1 Aims

The aim of the study is to provide a scientific basis for the design of a remote sensing system which will be of maximum benefit for the early identification of land affected by salinisation. From this work, it will be possible to assess the relative usefulness of current and future spaceborne and airborne land sensor packages covering the visible, reflected and shortwave infrared regions, using Western Australian examples but with conclusions which are more widely applicable.

Concisely, the aims are:-

1) to optimise maximum spectral discrimination at useable wavelengths, or multiple wavebands, which describe the characteristics of saline and non-saline lands;

2) to determine those times in a normal year's agricultural cycle at which maximum discrimination can be made; and

3) to determine the most appropriate ground spatial resolution to discriminate saline affected targets from the surrounding land.

1.1.2 The Problem - The Philosophy

Contributions to the solution of the salinity problem could come from hydrology studies, as the salt is brought to the root zone by rising water tables; from plant physiology studies, as the loss of plant growth is the economic result; or from soil physics, as the problem could be encouraged to wash away down the creek. This thesis contributes to none of these courses, but implicitly all must be considered, as this is a "Remote Sensing" study and only aims to determine maximum discriminability of salt-affected land from its background which may enable implementation of remedial management. Care must be taken not to think that there is an absolute waveband, pixel size or time of year that will always discriminate high salt risk areas from those areas less at risk.

The identification of salinity using spectral methods has attracted considerable research in Australia and throughout the world (Honigs et al. 1983). Hirschfeld (1985) suggests that there are two reasons for this interest. One is the simplicity of laboratory spectral measurement and the other is the compatibility with remote measurements from aircraft or orbiting spacecraft. He comments that "at first glance, the determination of salinity by infrared spectroscopy is so implausible as to seem ridiculous....Not only does moisture give an exceptionally strong infrared background, but also sodium chloride is the archetype of an infrared transparent material, having no absorption bands whatever in the near (or middle) infrared". Hirschfeld (1981) suggests that "sodium chloride is capable of modifying the absorption bands of moisture in a characteristic and measurable way".

Chaturvedi et al. (1983), in their review of remote sensing of salinity, presented numerous cases where sensors in the visible and reflected infrared regions could identify intermediate to mature saline seeps. They also note that these findings were supported by Dalstead in his M.Sc. thesis, who indicated that the thermal infrared regions could delineate incipient seeps at certain times of the year. Thermal data were collected in this study, and at some stage may provide a basis for studies, but these data are uncalibrated and as no high resolution (< 120 m) spaceborne systems are proposed, they have not been included. Horton et al. (1977) identified in his experiments well-developed saline seeps but could not reliably identify incipient or potential seeps.

A large, NASA-funded, project during 1978-9 conducted experiments for detection of saline seeps in South Dakota, USA, using airborne remote sensing in the visible, infrared, thermal and microwave regions (Carver and Bush, 1979). Their conclusions failed to support the use of near infrared, or thermal infrared but did allude to a potential use for passive microwave. Microwave responses to soil-water electrical conductivity at limited spatial resolution was reported in passive systems and in an active system at the same wavelengths (C and L bands), an even stronger response was registered. However, Chaturvedi et al. (1983, p.250), in contrast to the findings reported by Carver & Bush (1979), were less optimistic about the use of either passive or active microwave systems.

Most studies to date, for example, May and Peterson (1976), have been restricted to the available spectral bands on existing spacecraft, which, although useful for vegetation studies, were not selected specifically to detect spectral characteristics associated with incipient salinity. For this study, a unique combination of local knowledge, instrumentation and hardware laboratory and field support enabled an extensive detailed evaluation of visible, reflected and shortwave spectral regions.

1.1.3 Economic Considerations

Salinity has an impact in many ways and its cost to society may be categorised in the following ways (Peck et al. 1983, p.39):

i. Costs associated with use of saline water;

ii. Costs incurred by users of salinised land;

iii. Costs incurred to overcome salinity of water supplies; and

iv. Costs of alleviating the impact of salinity on land resources.

The first two can be considered as "damage costs", the other two as "abatement costs". The total cost of salinity was calculated, from Peck, to be $93 million in 1982. This figure is an estimate of all costs due to forms of salinity in all states of Australia. The estimate for annual productivity loss due to dryland salinity was between $16-22 million, with Western Australia having the largest affected area within Australia.

There is a fundamental desire for information on the extent of current loss of production from agricultural salinity, and the magnitude of any future extension of the problem. It is also then necessary to assess implications for other land uses and to study the long-term impact of current land use. Dryland agriculture, urban water supply, forestry and recreation needs all compete, and the allocation of land was historically based on short-term perception of production of food and fibre and the available technology to maximise returns. This was the basis for land clearing for agriculture in Western Australia.

It has long been recognized that the hydrological balance was changed by clearing for agriculture and that salinisation of land may result. Documented evidence of salinity encroachment has been provided by (Teakle 1938, p.434-52; Lightfoot, et al. 1964, p.396;

Malcolm and Stoneman 1976, p.42, Peck and Hurle 1973, p.648.). Occasional estimates of the extent of salinity were obtained by questionnaire. In 1955 and again in 1962, in conjunction with the annual statistical returns, farmers in Western Australia were asked to supply estimates of salt-affected land on their properties. In the 1955 survey the data were collated over statistical divisions, but in 1962 details were collected on a shire basis. The questions asked obtained the same basic information in each case, with different additional questions in each survey.

In 1974, a further survey was conducted in co-operation with the Australian Bureau of Statistics (ABS) using questions covering only the basic information. The ABS prepares the forms annually for statistical returns, relating to area and types of crops, etc. from farmers. In the 1974 return the following further information was sought, "Area of salt-affected land at 31 March 1974 which was previously used for crop or pasture."

Nulsen (1981, p.88), in his survey of the Wongan Hills Shire, used stereo monochromatic air photographs at a scale of 1:20 000 to delineate areas that in the winter-spring of 1977 "would grow plants no less salt tolerant than sea barley grass, Hordeum marinum. ." This was supported by road traverses and farmer interviews.

The cost of these surveys are not documented, but these examples of recent surveys are cited to support the case for survey systems based partly on remotely sensed data,probably incorporated with ancillary data sets,to provide information for:

i precise spatial extent of existing salinisation;

ii monitoring expansion or contraction of affected land; and

iii baseline information prior to cultural changes.

1.2 BACKGROUND

1.2.1 Salinisation

The process of salinisation of agricultural soil has probably existed for as long as man has been practising the cultivation of plants for his benefit. The dimension of the problem has paralleled man's ability to alter the native vegetation (at an unprecedented rate) with the use of mechanical and chemical farming techniques.

Soil salinisation is the process of salt accumulation in the soil to the extent that plant growth and the soil's physical properties are affected. Soil is considered as saline when it contains more than 0.1% (loams + sand) or 0.2% (clay loams and clays) of NaCl (by weight) in the surface to 20 cm. "Salinity" describes the concentration of soluble salts in a soil, the most common ions being sodium (Na^+), potassium (K^+), magnesium (Mg^{2+}), calcium (Ca^{2+}), chloride (Cl^-), bicarbonate (HCO_3^-) and sulphate (SO_4^{2-}). Chlorides of sodium and magnesium dominate the ionic species in the majority of Australian soils (Northcote & Skene 1972) (Bettenay 1986).

The soil salts have similar composition to sea water, except for accumulated nitrates. Atmospheric accession of salt in rainfall has been measured in Western Australia and Victoria. There is a decrease in saltfall with distance from the coast (Hingston and Gailitis, 1976). Salt inputs vary from about 300 kg ha^{-1} near the coast to less than 50 kg ha^{-1}, 150 km inland. The authors found the relationship -

$$F = 1108\ d^{-0.735}$$

where F is chloride fall in kg ha^{-1} yr^{-1} and d is distance from the ocean in km.

For the typical deep-weathered soil profile at Yalanbee, with annual salt input in 600 mm rainfall of 56 kg ha^{-1}, accumulation of 10^6 kg ha^{-1} of salt could be accomplished in the order of 20,000 years, allowing a small loss of salt each year (Dimmock et al. 1974, p.66). This rate of atmospheric accession has undoubtedly varied through geological time and changing climatic conditions.

The areas of agricultural degradation due to salinisation in Australia total more than 420,000 ha, and, with approaching double that figure in the North American continent, the current research effort is justified even without the consideration of the effect of salinity on potable water supplies.

The emphasis in this study is on the detection of early stages of salinisation in areas of dryland agriculture in semi-arid environments, (i.e. in areas where the potential evaporation may exceed rainfall), and in Mediterranean environments where there is a period of excess rainfall over evaporation for the winter months. These areas have the potential for salt concentration at the surface due to emerging groundwater, with evaporation equal to or less than the groundwater seepage. "Seepage" or "Saline Seeps" are the accepted terms for areas where salts accumulate at the soil surface as a consequence of the groundwater discharge from an unconfined or confined aquifer. "Seeps" describes the most common form of salinisation around which have developed numerous variations dependent on salinity, pH, landform, drainage etc.

1.2.2 Salinity in Western Australia

The western third of the Australian continent contains in part an ancient Precambrian shield of crystalline Archean rocks overlain by deeply weathered lateritic soils which contain large quantities of oceanic/atmospheric-derived salts. The south-western corner of the shield supports extensive dryland agriculture in a broad belt approximately from latitude 27 degrees south to the south coast at a latitude of 35 degrees south, and east to Longitude 125 degrees East (Figure One).

Winter (June-September) rainfall ranges from >1500 mm near the coast to <300 mm at the eastern limit of cultivated agriculture some 300 km inland. Mild, wet, Mediterranean-type winters provide

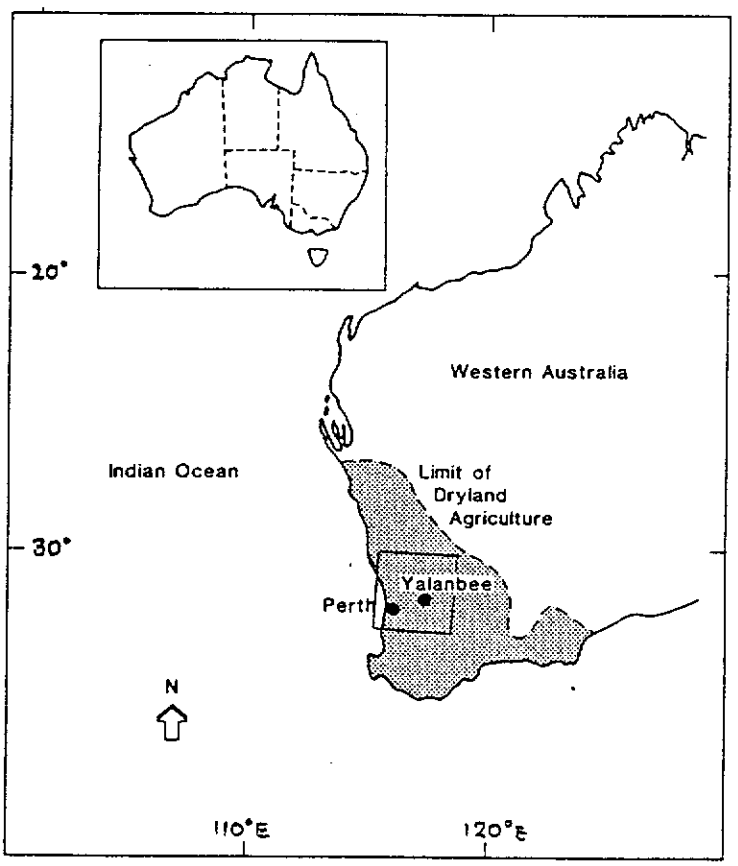

Figure One (a) - Location map depicting the dryland agricultural belt in the south west of Western Australia. The position of the Thematic Mapper Image, Figure One (b) is shown here and this area also includes the large scale map segment around Yalanbee, Figure One (c).

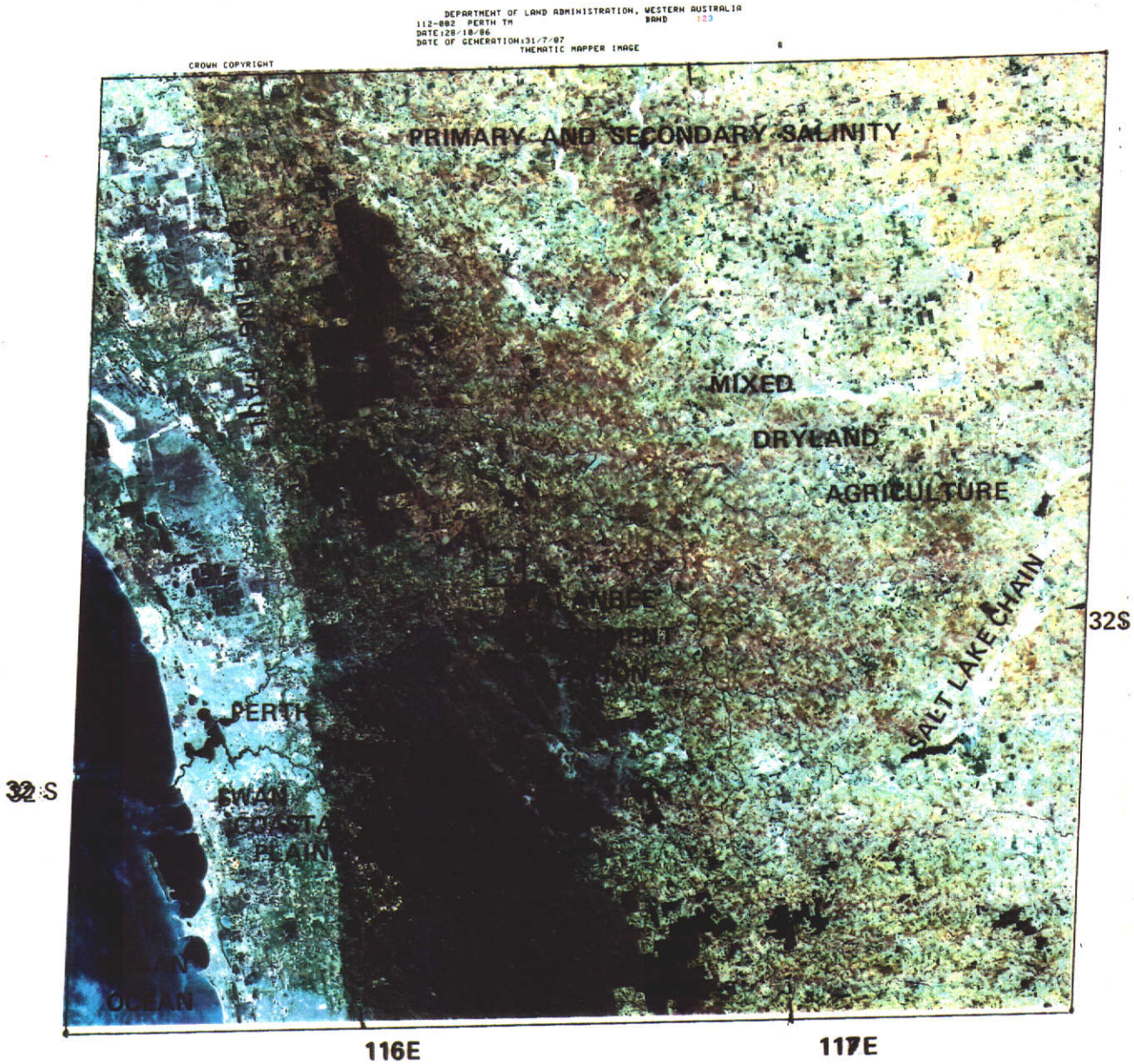

Figure One (a). Thematic Mapper image of Perth, see inset Figure one. Landsat 5 TM Bands 1,2 + 3 giving "true" colour composite on 16 October 1986 (Path/Row 112-082)

Figure One (c). Part of the Woorooloo 1:1000,000 Topo Sheet No. 2134 showing Yalanbee Experiment Station

moisture for the extensive pasture and wheatlands. Hot, dry summers, from December to March, provide little or no rainfall for annual plant growth. Perennial growth relies on access to deep, normally inaccessible, groundwater. Approximately six million tonnes of hard wheat, principally for export to European and Asian markets, are shipped from coastal ports. The production of wool, sheep and cattle is of equal importance.

Surface soil salinity is classified as primary or secondary in origin. Primary salinity is that which was present in the landscape in the form of extensive salt lake chains and lacustrine soils prior to the clearing of native vegetation for agriculture (Burvill 1947, pp.9-19, Bettenay et al., 1962). Secondary salinity is that which is subsequent to, and caused by, agricultural use of the land. The area of land affected by primary salinity remains relatively constant, while clearing of native perennial vegetation, mostly during the last 100 years, has caused an increase in the area affected by secondary salinity. Figure one (b) shows examples of primary salinity and also illustrates the extensive clearing of native vegetation. Only the state forest and the uncleared remnants, usually nature reserves, remain; these show as dark green.

Associated increases in stream salinity have also occurred and have resulted in frequent loss of urban and on-farm water supply. The current estimate that 264,000 ha of land in Western Australia is affected by secondary salinity is based on Malcolm and Stoneman (1976, pp.42-49) and Henschke (1980, p.116). Despite the apparent seriousness of the salinity problem, only limited documented estimates of the specific areas affected are available.

1.2.3 Historic Remote Sensing of Salinity in Western Australia

Remote sensing techniques have been investigated as a method of assessing the location and extent of secondary salinity and to monitor any changes resulting from management practices (Estes & Simmonette 1978).

As noted in section 1.1.3, the Western Australian Government produces a regular statement on the extent of secondary agricultural salinity derived from photographic surveys and farmer questionnaires. With the advent of satellite-derived digital imagery, a study (Honey et al. 1984) was commenced to evaluate the use of such data to complement the salinity mapping and monitoring.

Early attempts to use Landsat MSS data were little more than enhancement of autumn imagery for "photo-interpretation". Late summer/autumn imagery was available and thought to be adequate. This was based on experience gained from air photo surveys and from the knowledge that secondary salinity seemed to be most readily visible at these times. This approach proved unsuitable, due to the confusion with other land surfaces which displayed the spectral characteristics of bare soil.

An alternative hypothesis was based on the experience that the best discrimination of salt areas was in the "spring-flush" (Hick et al. 1984). At this time, those areas remaining without vigorous vegetation were readily identified by their spectral characteristics. While this introduced a range of cover classes other than saline, these other classes had characteristics which could be isolated digitally, topographically, or were of a static nature and hence could otherwise be accounted for (examples include roads, gravel pits, roaded catchments, etc).

In Western Australia, an evaluation of Landsat MSS CCTs indicated that detection of known bare salt areas could be made during the period of maximum growth of crops and pastures, (June-Oct). Data set from three dates were merged into a 12 -band MSS file and a parallelepiped classifier was used based on a mean of the pixel values within the training site plus and/or minus one standard deviation. Use of a higher standard deviation was rejected on the basis that the misclassifications highlighted the extreme variability even within training sites. Improved accuracy of classification was achieved by having a large number of narrow classes. Highly saline areas were differentiated in part by the rate of cover change during the year. Road and railway reserves have similar trends of vegetation change and this fact appears to preclude the separation of salt areas from these reserves in some cases. This was evident by misclassifications (errors of commission) along these often linear features. Similarly, a number of misclassifications appeared on bare soil areas high in the landscape. It is reasonable to assume that saline areas are areas of groundwater discharge rather than recharge, and as such, are almost exclusively in low to midslope positions, rather than high in the landscape. For the study area, inspection of the 1:100,000 map with 20 m contours indicated that significant misclassifications

could be removed by incorporation of specific altimetric data. These data in digital form, used as another band in the classification file, enabled the removal of misclassifications in high landscape positions.

1.2.4 Spectral Reflectance Background

The fundamental measurable remote sensing quantity for a picture element (pixel) is its spectral radiance. Spectral characteristics can be most easily explained in the visible region of the electromagnetic spectrum using "reflected-light" as the example. The sun is a source of electromagnetic radiation of which a small portion, from 380-760 nanometers, can be perceived by the retina of a human eye. In this study all wavelengths (λ) are in nanometres (nm). Wave number is $\frac{1}{\lambda}$ or the frequency/cm.

A visible object exhibits a particular colour because it reflects light. Pigments may absorb a portion of "white" light and reflect other portions, and the wavelengths absorbed or reflected give the perception of colour. A diffuse near-perfect reflector (or Lambertian surface) would ideally reflect all wavelengths and appear white as is nearly the case with $BaSO_4$ or Halon standards. Certain pigments may absorb all light and would appear black as they reflect no light.

Historic arguments about the nature of light canvassed the view that light consisted of minute particles. The Dutch scientist Huygens (1629-1695) disputed Newton's particle theory and promoted light-waves theories. The demonstration that waves may be bent around a barrier, or diffracted, supported the wave theory and during the 18th century Thomas Young was able to create diffraction patterns by passing light through slits. The history of light theories is well covered in Murphy & Smoot (1982, p.267-270).

Electromagnetic radiation at some frequencies interacts with molecular processes (Schaper 1976, p.86). Gamma and x-rays interact

with both atoms and molecules by adding or subtracting energy from the surrounding electrons. The molecular state may be affected in various ways, either by vibration or rotation of the molecules. Transitions of the electronic state are a result of interaction with ultra-violet and visible light, whereas vibration and rotation are associated with short-wave infrared (SWIR) or thermal infrared (TIR) radiations. The SWIR, approximately 1,100-3,000 nm is reflected energy from the sun. This varies as a function of albedo and angle of incidence. TIR is emitted energy.

If radiation having a broad spectrum of energies (e.g. sun-light), traverses a cloud of molecules of a given type, certain wavelengths are absorbed by the molecules, giving rise to an "absorption spectrum". Some of the energy will be retained to emit radiation, giving rise to an "emission spectrum".

An absorption line can be measured spectrally when a molecule interacts with (i.e. absorbs) a photon. As the number of molecules between the source of energy and the receiving/detecting apparatus increases, the number of photons of that energy that is absorbed will increase; that is, the absorption line gets "deeper". The proportionality constant is basically a probability that a "collision" between a molecule and a photon will result in that photon being absorbed.

This assumes that the energies of the photons absorbed by the molecule are defined with infinite precision. In fact, it is found that the molecule will absorb not only the specific energy but also a small range around that value. The range is frequently smaller

than the distance (in energy) from the next absorption so that the technique can retain its basic validity, i.e. the absorptions are separable.

Examination of the spectrum of a molecule shows that there is a distinct regularity in the absorption features. Whether this regularity remains is dependent on the type of molecule involved. Simple molecules retain considerable regularity, whereas others (water vapour [H_2O] for example), display a totally random array of individual lines. In all cases, however, the arrays of lines group together into what are called absorption bands. Analysis of such bands shows that they result from transitions between vibrational states of the molecule, and the "fine structure" of the individual absorption lines within the band are a consequence of transitions between rotational states within the vibrational states.

The atmosphere contains molecules which absorb infrared radiation at particular wavelengths. Between these regions, "atmospheric windows" occur. These are regions where attenuation due to atmospheric gases is minimal, and hence they permit observations of the earth's surface from an airborne or spaceborne sensor.

Figure Two graphically represents the atmospheric windows between 400 and 2600 nm. Against this are shown the positions of the bands installed on the Geoscan scanner and the two scanners aboard the Landsat series of satellites. A more complete list of spaceborne and airborne sensors is included in Appendices One a & b.

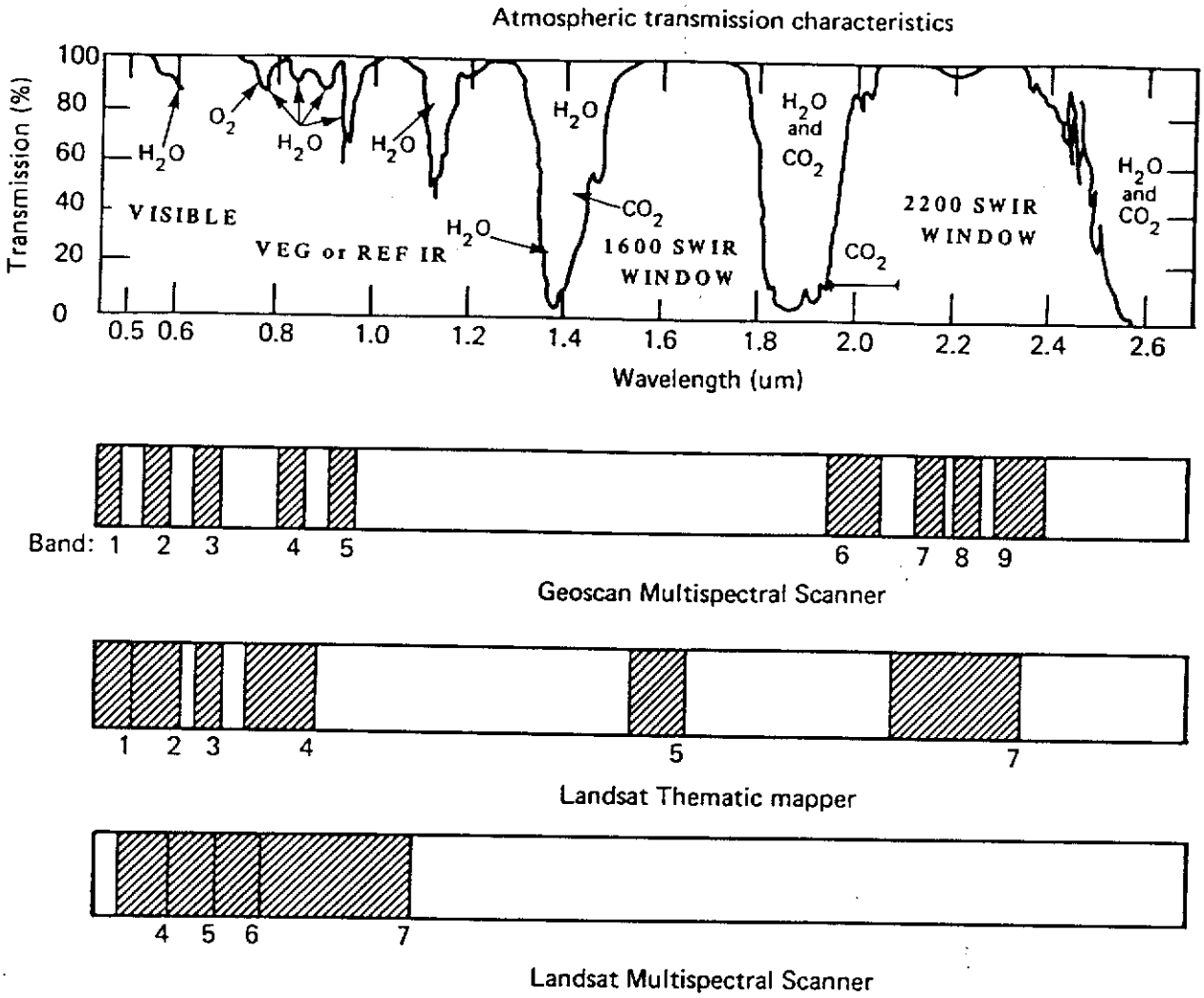

Figure Two. Wavebands covering the visible and near infrared incorporated in the Geoscan Airborne Multispectral Scanner, and the Landsat Thematic Mapper and Multispectral Scanner. (Also see Appendices One a & b.)

1.2.5 Measurement of Reflectance

Spectral measurements of field sites were routinely recorded using both an Hitachi laboratory spectrophotometer and the Geoscan portable field spectroradiometer (PFS). Basically, reflectance of a target may be measured in two ways: in the laboratory, artificially illuminated; or in the field with solar illumination. These approaches provide different results for several reasons. Illumination conditions are more easily controlled in the laboratory, but the field-of-view is different for laboratory, field and aircraft measurements. In laboratory studies, for example, a single leaf, or soil sample, may be analyzed, whereas in the field the sample usually becomes larger as a function of distance from the target. Thus, depending on its altitude, a narrow-field-of-view instrument may "see" anything from several leaves to a whole paddock, and as the field-of-view becomes larger, the target becomes a composite of leaves, stalks, soil, shadow, etc. With increasing altitude, atmospheric effects become more important, and scattering and absorption effects on radiance are enhanced. Target radiance is also influenced by scattered radiance from outside the instrument's field-of-view.

Reflectance is the ratio of the radiant flux actually reflected by a target surface to that which would be reflected into the same reflected geometry by an ideal perfectly diffuse (Lambertian) standard surface. For small fields of view, such as those encountered with field spectroradiometers, the term bidirectional reflectance factor is used (Stoner and Baumgardner 1981, p.1426). This describes the measurement from one direction being the viewing

angle of the instrument and the other direction being the solar zenith and azimuth. The bidirectional nature of the reflectance factor, $R(\theta_i,\phi_i;\theta_r,\phi_r)$ is illustrated in Figure Three for incident and reflected beams where (θ_i,ϕ_i) and (θ_r,ϕ_r) are the zenith and azimuth angles of the incident and reflected beams respectively. In the field, R can be approximated by taking the ratio of the instrument response when viewing the target V_t to the instrument response when viewing a level reference surface V_r such that

$$R_t(\theta_i,\phi_i;\theta_r,\phi_r) = \frac{V_t}{V_r} R_r(\theta_i,\phi_i;\theta_r,\phi_r)$$

where $R_r(\theta_i,\phi_i;\theta_r,\phi_r)$ is the bidirectional reflectance factor of the reference surface; this term corrects for the nonideal reflectance properties of the reference surface. This relation assumes that (1) the instrument response is linear to entrant flux, (2) the diffuse component of irradiance is negligible, (3) the reference surface is irradiated and viewed in the same manner as the target, and (4) the aperture is sufficiently distant from the target (Bowker et al., 1985, p.3).

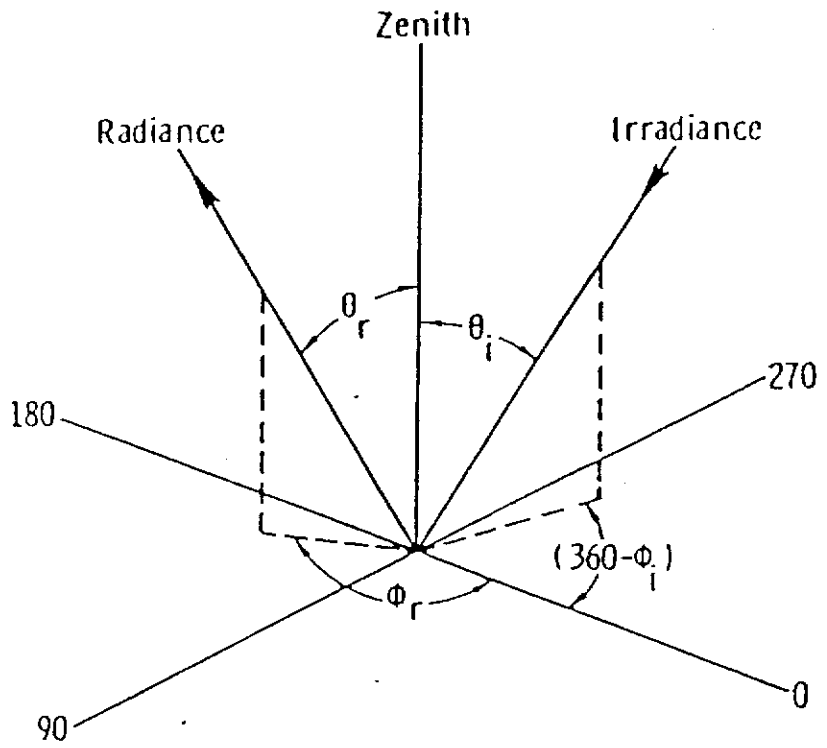

Figure Three. Bidirectional Reflectance
(adapted from Bowker et al.)

Field and laboratory calibration procedures consist of the comparison of the instrument response between the target and a level, spectrally-flat reference surface. This approach assumes that the sample target is nearly independent of the incident irradiation and atmospheric conditions at the time of measurement. The basis for bidirectional factor measurements allows for direct comparison of field-collected and laboratory-collected data. Stoner et al. (1980, p.572) showed experimental results verifying the validity of comparing laboratory and field-measured spectral response in moisture-controlled conditions. Spectral analysis

in controlled laboratory conditions allows for great flexibility to study a diverse range of soils from scattered field sites independent of varying sun illumination.

Soil radiance from airborne MSS data was compared with laboratory reflectance spectra of soil (May and Peterson 1975, p.211). They showed that laboratory-derived reflectance gave good agreement with the airborne data for bare soil situations.

In laboratory measurements of reflectance, a small sample of the target is usually analyzed using a spectrophotometer with an integrating sphere attachment. Two methods of measuring reflectance with an integrating sphere are possible. In the 'substitution method', the sample and reference are placed in turn at the sample aperture and the ratio of respective photocell readings is determined. In the 'comparison method', both sample and reference are placed in separate apertures, the illuminating beam is switched from one to the other, and the ratio of the respective photocell readings is determined. The 'substitution method' is generally implemented in spectroradiometers and the 'comparison' method is employed in spectrophotometers. The instruments used in this study are described in detail in Chapter Two and their specifications are appended.

1.2.6 Spatial Resolution, Element Size

Spatial resolution can be considered as the minimum cell or element distinguishable on an image. At this level, confusion often abounds as to the distinction between "resolution", "detectability" and "precision". An apparent object may be smaller than the nominal minimum "element-size", or because of its geometric configuration, it may appear on imagery, giving an erroneous perception of what is actually the smallest resolvable feature. Features with high contrast to their background may be "detectable" when in fact their spatial dimension is smaller than the minimum spatial resolving power of the instrument. Similarly, linear features can often be discerned when their width is much less than the instrument's instantaneous field of view (IFOV). This aspect has important implications for the detection of salinity. Often salinity is associated with streams and drainage lines, or occurs as "fringing" features, which are often both high-contrast and linear.

The term "nominal spatial resolution" is used to subdue the notion that a specific measurement of resolution, i.e. 10 metres, is in fact that given figure. The resolution depends upon the characteristics of the detector and is only the mean measurement for a spot on the ground which is then divided into equal parts by the number of samples in each line. An image grid, or raster, is created to reproduce the ground characteristics.

With the advent of the Landsat series of satellite, with a nominal 57 x 79 metre picture element (pixel), some reassessment by investigators was required as to what actually needed to be resolved to provide boundary information. The early complaints, by land

managers, about Landsat MSS data were nearly always that the spatial resolution was too coarse. It was felt that if individual trees, roads, fences and other boundary features could not be clearly seen, then it would not be possible to quantify the constituent matrix. As a consequence, during the late 1970's, satellite design was influenced by pressure from groups seeking higher spatial resolution; for example Landsats 4 and 5 decreased nominal pixel sizes to 30 metres, while the French SPOT satellite has a 20 metre multispectral scanner and a 10 metre monochromatic instrument.

The nominal pixel size is the spatial resolution of a sensing system, and depends upon the geometry of the instrument. The optical components of focussing, focal length, and detector size determine the angle of the IFOV. The height above the measured surface determines the ground coverage. Assuming the land surface is flat and the height constant, the sample at nadir would represent one pixel of determined size. Earth curvature, terrain irregularities, pitch, roll and yaw and scan angle affect pixel geometry and hence nominal spatial resolution.

1.2.7 Atmospheric Modelling - The Lowtran Code

To predict the effects of the atmosphere on total radiation from the sun, a group of models has been compiled to calculate, for given parameters, the atmospheric transmittance for a given wavelength. These models, generally known as Lowtran 6 computer code (Kneizys *et al*. 1983), calculate transmittance and radiance over the range from 250 nm to 28,500 nm, or in wave numbers (cm^{-1}) from 350 to 40,000 cm^{-1}. The average steps are 20 cm^{-1}. The code uses a single-parameter band model for molecular absorption and includes the effects of continuum absorption, molecular scattering and aerosol extinction. Refraction and earth curvature are included in the calculation for an atmospheric slant path, allowing calculation for edge pixels etc. The code contains representative atmospheric and aerosol models, as adopted for this study; there is also an option for user-derived data to be incorporated.

For this study, the aim was to determine the total solar illumination reaching the ground and then to calculate the effects on the reflected energy reaching the detectors in both the Geoscan portable field spectroradiometer (PFS) and the airborne multispectral scanner (MSS). Calculations of transmissions have been plotted for a range of atmospheres from very moist (tropical) to very dry (sub arctic), using rural atmosphere models and covering the range of heights flown by the scanner. Nadir and edge pixel calculations are also reported in Chapter Three (3.2.6).

1.3. THE STUDY AREA

1.3.1 Yalanbee Experiment Station

In December 1962 CSIRO purchased a largely uncleared, 1150 ha, property near the small township of Bakers Hill. This property, "Yalanbee", is 72 km east of Perth, about 1 km south of Bakers Hill on the Great Eastern Highway, Figure One and One (c) (location map). The property was cleared, over the next 12 years, to enable a diverse range of experiments, including those on fertilizer applications, crop and pasture production, agroforestry and silviculture, domestic and native animal behaviour, production and nutrition, farming systems, and, of importance to this study, hydrologic studies relating to salinity and water supply. The rainfall of 580 mm per annum, most of which falls in winter, affords a growing season of 5.5–6 months.

When the property was purchased, the only evidence of salinity was "a trickle of brackish water in the creeklines during summer months" (E. Bettenay, pers. comm.). By 1967, the author, with others, reported and pegged small patches of failed pasture and other evidence of saline encroachment adjoining the major creekline entering the western boundary of the property. This creek, known locally as Crocodile Creek, has a catchment area of 710 ha above the main saline scald evident today, and about 40% of this catchment is on the CSIRO property.

After clearing in 1963, the valley through which Crocodile Creek runs was one of the most productive parts of Yalanbee. Currently more than 86 ha of this valley has been lost from production due to salinity and a significant amount is directly under threat. The data on the extent of salinity at Yalanbee have not yet been published. From observations, salinity does not increase at a

steady rate, but rather has a stepwise progression, with the greatest increase following winters of heavy rain (E. Bettenay, pers. comm.).

The following are estimates, made by Bettenay, based on interpretation of air photos for areas badly affected by salt (see Table One, Available Photography).

Yalanbee	Area saline (ha)	% of catchment
1966	0	0
1967	trace	trace
1968	5.5	0.8
1977	70	9.9
1983	80	11.3
1985	86	12.1

The reason for the development of these extensive saline areas lies in the soils and landform, and in the extent of dissection into the deeply lateritic weathered profile. The higher parts of the catchment are remnants of the old lateritic surface and comprise deep sands, gravels and blocky lateritic duricrust which probably provide intake zones for a partially confined water table.

The valley sides have mainly duplex soils in which a perched aquifer develops at shallow depths in winter months. The valley floor upstream from a granite barrier has complex duplex soils overlying a siliceous hardpan which appears to act as an aquitard or a partially-confining layer above the very saline groundwater. Soil profiles store considerable quantities of soluble salts; in the Yalanbee region it has been calculated that a salt storage in the order of 1 million kilograms per hectare occurs (Dimmock et al. 1974, p.63).

YALANBEE EXPERIMENT STATION - AERIAL PHOTOGRAPHY

24.11.60	B/W	1:15,000
10. 3.67	B/W	1:15,000
21. 7.69		1: 4,000
16. 6.70	Colour + Colour IR	1:10,000
20.10.70	Colour + Colour IR	1: 4,000 + 1:15,000
6.11.72	B/W	1:10,000
4.10.73	Colour	1:10,000
27. 9.74	B/W	1:10,000
16.11.76	Colour + Colour IR	1:40,000
27. 1.78	Colour + Colour IR	1:10,000
15.10.78	Colour	1: 5,000 (approx.) 70 mm
19. 5.80	Colour + Colour IR	1:10,000
4.12.80	Colour	1:30,000
10.10.81	Colour	1:30,000
15.12.82	Colour	1:10,000
29. 1.85	Colour	1: 5,000 + 1:2,000 (approx) 70mm
31.10.85	Colour	1:16,000 70mm

Multispectral Scanner Flights *(GEOSCAN MKI)

30. 1.84	5,000 ft ASL *
6.12.84	7,000 ft ASL *
29. 3.85	6,000 ft ASL *
28. 8.85	7,000 ft 4,000 ft ASL *
11.10.85	AIS,TIMS,TMS, C-130 (NASA-JPL-CSIRO)
25.11.85	7,000 ft ASL *
18. 2.86	10,000 ft 7,000 ft and 4,000 ft ASL *
26. 3.86	7,000 ft ASL *
4. 4.86	7,000 ft ASL *
6. 9.86	7,000 ft ASL *
18.11.86	7,000 ft 4,000 ft ASL *
30. 1.87	7,000 ft ASL *
26. 3.87	7,000 ft ASL *

Table One. Photographic and digital image archive, covering Yalanbee, used to trace the effect of salinity.

Hydrologic studies indicate that groundwater pressures have increased due to clearing of the deep-rooted perennial native vegetation for the introduction of shallow-rooted annual crops and pastures. This also affects infiltration rates in the recharge areas which has affected both partially-confined groundwater and perched aquifers. These together have led to increased salinity, and waterlogging, and the subsequent accumulation of evaporites.

The studies by CSIRO at Yalanbee indicated its suitability as a study site representative of the higher rainfall regions of the Western Australian agricultural districts. It is typical of a large tract of land which runs down the eastern margin of the Northern Jarrah Forest Figure One (a). This land is important for several major reasons. Significantly, it is highly regarded agriculturally for grazing and cropping, and commands premium land values. The relief, good timber, reliable rainfall, reasonably fertile soils and proximity to services make this land sought after.

In many cases this region, of which Yalanbee is representative, forms the headwaters for westward-flowing rivers which are either currently used for urban and rural water supplies or are 'ear-marked' for this use in the future. A very high proportion of the subcatchments, of similar order to Crocodile Creek, are contributing high levels of salts to these systems. Concern as to the impact of this has lead to clearing controls in some catchment areas, e.g. Wellington Dam catchment including the Collie, Bingham and Harris River systems. Deteriorating water quality is held, by many, to be of greater importance than the loss of agricultural production.

The intensive study, reported here, on the Yalanbee Experiment Station is part of a wider study involving a diverse range of soils, rainfall and management practice with national implications. Yalanbee was chosen as the prime test area for development of techniques because of the control which can be exercised over stocking, cropping, etc.

1.3.2 The Study Sites

The major salt affected area at the Yalanbee Experiment Station is the Crocodile Creek area which, as previously mentioned, was formerly productive land. Adjacent to this seep are areas which carry a range of vegetation having varying tolerance to salinity. It is evident that expansion of the Crocodile Creek salt seep is still continuing. This study attempts to determine spectral characteristics which may indicate where the expansion will occur.

Eight sites were selected, representing a range of situations occurring in the vicinity of the Yalanbee salt seep (see Appendix Two). They were selected in the field initially on the basis of the visual uniformity of their vegetation at peak growth in the spring. Some refinement of their positions followed using electromagnetic induction techniques and detailed vegetation and soil profile descriptions. Their uniformity beyond the sites was also checked on recent photography and imagery to minimise the border effects when extracting the pixel values.

Salt tolerance in introduced annual pasture species varies. On the basis of the anticipated spectral response of certain types of vegetation, pure or uniform mixtures of species were selected to represent cover classes which would indicate the salinity status. The sites were pegged within reasonably uniform areas, and were approximately 21 metres square. This size was chosen following the decision to initially fly sites with the Geoscan Multispectral Scanner at 7000 ft(2130 m) above ground level (AGL), which produces approximately 7 metre sub-nadir spatial resolution; thus the sites represent 9 pixels in a 3x3 configuration (Figure Four).

Proximity to nearby features identifiable on MSS images was recorded to enable precise location of pixels for extraction of the digital values.

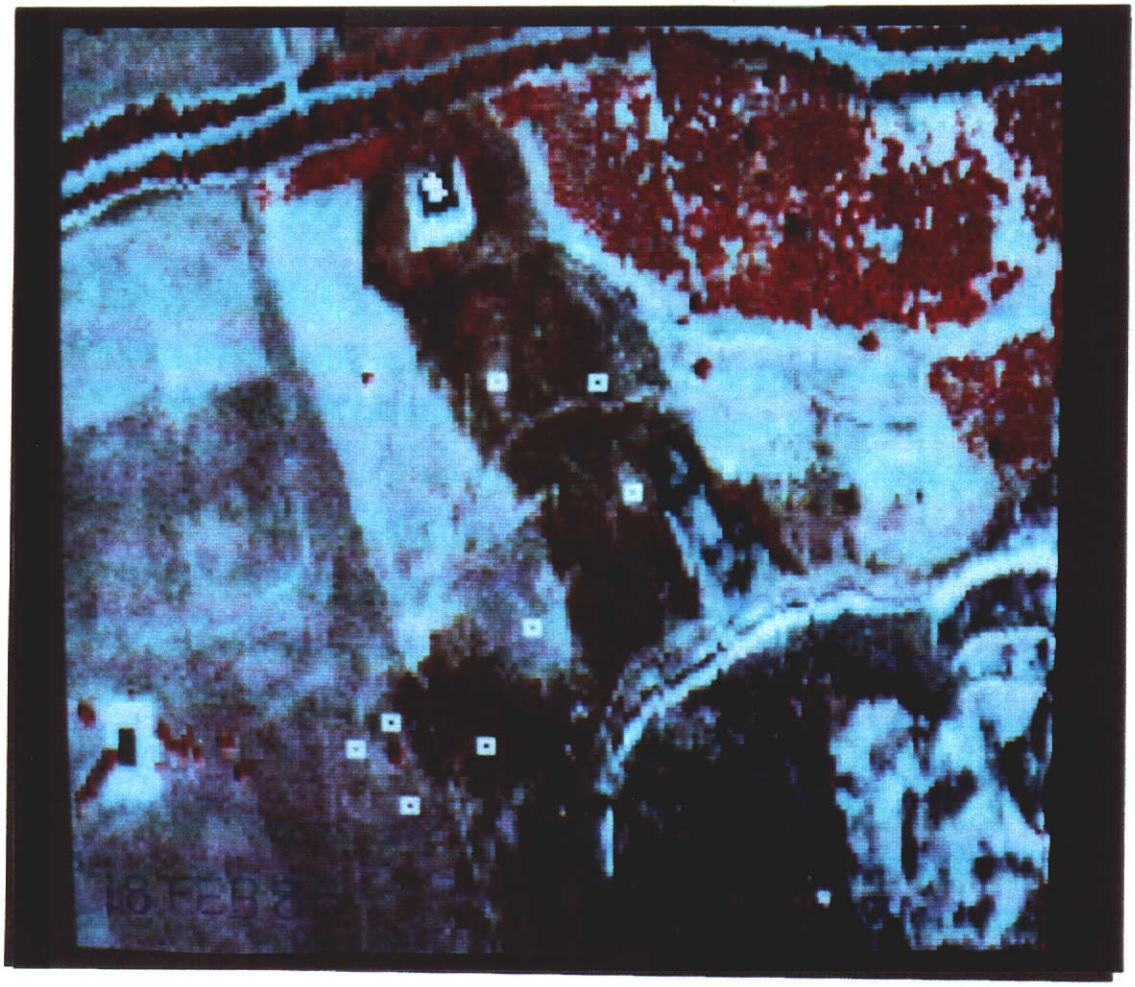

Figure Four. Study sites on Yalanbee with Data Extraction Points Embedded. This is a subsection of a Geoscan Multispectral Scanner Image from 18 FEB 1986 and is a colour composite from bands 4(R) 3(G) 2(B) (see Figure Two). Berry Brow Road (running N-S) appears across the top of the image and the sites are numbered from the bottom as 1,2,4,3,5,6,8+7 (Figure Eight).

CHAPTER TWO

METHODOLOGY AND INSTRUMENTATION

2.1 METHODOLOGY

2.1.1 Study methods

The purpose of this work was to test the hypothesis that there are wavebands in the visible to shortwave infrared (400-2500 nanometers) which, at a specified time of the year, will provide better discrimination of land at risk from salinity encroachment than those currently available on existing satellite or airborne systems (refer to Section 1.2.3.). It was proposed to select and test wavelengths, as discrete wavebands of specified width, for selected test areas where the nature and degree of salt encroachment is well documented (refer to Section 1.3). Additionally, the sample size, or minimum mean ground resolution, which can be practically considered as representing an identifiable, manageable part of that land will be determined (refer to Section 1.2.6).

The major consideration in identifying salinity problems lay in the cultural practices employed in farm operations. Plant succession in relation to increasing salinity is reasonably well ordered and in many cases both the distinctive spectral and phenological characteristics of the volunteer plant communities are sufficient to diagnose degradation due to salinity. However, for more than 50% of a normal year, the ground surface of approximately 40% of the agricultural areas can be considered spectrally as bare soil, thus removing the diagnostic value of plant succession. This occurs as a result of the following:

i Cropping practices ie, ploughing and sowing in April/May;

ii Thin patchy or slow winter growth;

iii Fallowing;

iv Hard grazing of post-harvested stubbles in successive cropping programs;

v Hard grazing of annual pastures; and

vi Mechanical harvesting of clover seed.

The study methodology was designed to address the problem of cultural practices in salinity identification and to collect appropriate data to allow the analysis and determination of factors which affect the identification of salinity. Sites were chosen at Yalanbee Experiment Station to represent a range of saline situations. These sites were accurately described in terms of their static characteristics, i.e. soils, slope, etc., and then regularly revisited to describe their dynamic characteristics such as vegetation, soil moisture, salinity, electromagnetic conductance (EM38) (refer to Sections 2.2.4 and 3.3.1). Concurrent with these visits, soils were sampled for laboratory spectral analysis (Hitachi spectrophotometer) (refer to Sections 2.2.1 and 3.2.3) field spectra were recorded with a portable spectroradiometer (PFS) (refer to Sections 2.2.2, 3.2.4) and the Geoscan Airborne Multispectral Scanner was flown over the sites. Samplings were timed to coincide with major seasonal phenology of the vegetation.

Data were analysed to test the suitability of spectral wavebands installed on existing aircraft and satellite sensing systems, and the probability that other wavelengths, at other times of the year, and at different ground resolution, will provide improved discrimination of land at risk from salinity encroachment. Lowtran calculations were analysed (refer to Sections 1.2.7 and 3.2.6) to determine the spectral regions where atmospheric windows would permit band location.

2.1.2 Field methods.

Site descriptions in Appendix Two include the condition of the eight sites at selection, and seasonal data for each sampling.

The methods used to describe the characteristics of each site conformed with the following standards of description and measurement. Soils were hand augered down to the B horizon, usually between 50-100 cm. The surface A1 and A2 horizons were described with sampling intervals each 10 cm at depth. The augered spoil samples were field textured, and had pH and wet Munsell colours recorded. Percent gravel and mottles were estimated, enabling subdivision into principal profile forms, and each profile was allocated a Northcote classification (Northcote 1960). Profile moisture samples were sealed in plastic bags and weighed immediately on return to the laboratory. These samples were then dried at $40^{o}C$, reweighed and sieved through a 2 mm sieve to remove loose organic matter and gravels. Laboratory spectra were measured on these samples.

For salinity determinations, 20 grams was subsampled, mixed 1:5 with distilled water, shaken for a minimum of 1 hour and then, after a minimum of 12 hours to allow settling, the electrical conductivities (EC) were measured. Johnston et al. (1982) determined the relationship between electrical conductivity and total concentration of soluble salts in Western Australian soils as:

$$TSS = 4.796k - 4.83 \text{ for } 2.9 < k < 152$$

$$Cl^{-} = 1.938k - 0.59 \text{ for } 0.4 < k < 5.73$$

$$Cl^{-} = 2.946k - 6.37 \text{ for } 5.73 < k < 254$$

where k is the electrical conductivity (mS m^{-1}), TSS is the total soluble salts (mg/l^{-1}), and Cl^{-} is chloride concentration

(mg/l^{-1}) of the extract. Electrical conductivities were measured at a constant temperature of 25°C using a Radiometer-type CDM2 conductivity meter with a flow conductivity cell with a cell constant of 0.50.

Organic matter was determined using Loss On Ignition (LOI) technique as described by Piper (1944 , p.59). This technique involves firing the sample at 600°C and measuring the weight loss.

EM-38 Electromagnetic induction ground conductivity readings were recorded after initial calibration and nulling to the manufacturers specification. These readings were made, both vertically and horizontally, in a standard pattern from the N.W. corner peg at each sampling date. The reason for the inclusion of EM 38 data is covered in Section 2.1.4.

Vegetation sampling was done at two levels. Firstly, the plant distribution over the entire site was estimated and described. Secondly, a more detailed description on the basis of bulk biomass was made of a pegged 1 metre quadrat in the centre of the site.

At each sampling, or as cloud-free weather permitted, field spectra were measured with the Geoscan Portable Field Spectroradiometer (PFS). The method of sampling was carried out under the following conditions:-

1) Maximum sun elevation plus or minus two hours.
2) The PFS was oriented towards the sun's azimuth.
3) No visible cloud whatsoever was tolerated.
4) Standard reflectance targets calibrated and stored before each site. ($BaSO_4$ painted plate)
5) One metre above the ground, giving sample spot size of 200 sq cm (approximately) at nadir.

6) Between fifteen and thirty samples uniformly distributed on a regular grid across the site, the total number of spectra recorded being dependent on available sunlight hours.

The spectra were down-loaded from the PFS onto a microcomputer and stored on floppy disk in the field. These data were then transferred to a minicomputer for plotting and statistical analysis.

Sampling schedules were governed to some degree by the availability of the MSS scanner and appropriate flying weather. The constraints placed on the airborne data acquisition related to cloud-free conditions, sun elevation, sun azimuth and absence of rain for, ideally, 7 days to enable dry soil conditions prior to flights. Most missions were planned as near to midday as possible (although this was less critical in mid-summer), always flown directly into or away from the sun to ensure uniform "across-track" illumination, and, with the aid of a drift site, the ground sites were positioned as close as possible to nadir from the aircraft track. These sites were then displayed on the image processing system (IPS) using an enhancement which gave good visual discrimination between sites. The site centres were located using the zooming capabilities of the IPS and the pixel values and their coordinates were extracted for statistical analysis.

The statistical technique used was robust canonical variate analysis (Campbell 1982). Briefly, this procedure produces linear combinations of spectral bands which are uncorrelated within groups and which maximize the ratio of between to within group variability. Atypical pixels are also identified and downweighted.

The aim of the procedure is to produce a lower dimensional representation of the data which can be plotted to display real group differences.

At each date the eight, 3x3 pixel, sites were augmented by additional training sites to improve the estimation of the within-groups variation. These areas were selected on the basis of their uniformity on the imagery and represented large areas of crop, pasture, woodland plantations, etc. The between-groups variability was computed from the means of the 8 training sites only, as well as for a contrast of the non-saline and the saline sites.

2.2 INSTRUMENTATION

This section describes briefly the principal instruments used in this study. Additional specifications are included as appendices. The airborne scanner and the portable field spectrometer are both prototype development instruments, the Hitachi was modified for this study and the EM 38 was used as directed by the manufacturer.

2.2.1 Hitachi Spectrophotometer

Laboratory measurement of reflectance spectra, using the 'comparison method', were made in this study using an Hitachi model 340 UV-VIS-NIR Recording Spectrophotometer (refer to Appendix 4 for specification). This instrument is fitted with an integrating sphere which integrates reflectance from the sample from all directions, thus minimizing the variation due to particle size and orientation. A data-handling device couples the instrument to a micro or minicomputer. For this study, modifications were implemented to enable horizontal presentation of undisturbed soil samples to the normally vertical aperture of the integrating sphere. Initially a polished periscope was tried which presented an image of the sample mounted horizontally to the aperture of the sphere (Hick and Macham 1986). Losses of reflected energy were of the order of 60-80% from samples which had mean reflectance of only 10-20% of the reference. This was considered unacceptable.

After consultation with the manufacturers the machine was "wall mounted", thus enabling the presentation of samples to the now horizontal aperture of the sphere. This was done and the machine has since given reliable results. This reduces the risk of contamination of the reflective halon coating of the sphere.

2.2.2 Portable Field Spectroradiometer

The GEOSCAN Pty Ltd Portable Field Spectroradiometer (PFS) (Honey and Daniels 1984) was designed for the measurement and recording of reflectance spectra over the range 400 to 2500 nm. The instrument is a compact, modular system powered by rechargeable lead acid batteries carried in a backpack. Recording a near continuous spectrum involves pointing the instrument at a target and pressing a trigger, or alternatively a predetermined number of spectra may be averaged. Spectra of targets are displayed on a liquid crystal display (LCD) incorporated into the instrument. Up to 240 spectra may be stored in the bubble memory of the system for subsequent dumping to mass storage. Data are stored internally as 8-bit data, with 256 data points per file. Previously recorded spectra may be displayed on the LCD for comparison.

Software to control the spectroradiometer, to display and print the spectra, and to download the data to peripheral devices, was provided with the instrument. The PFS is comprised of three modules:

(i) The telescope module, which collects the reflected visible and short-wave infrared (SWIR) energy, reflecting it through a small aperture into (ii) the scanning and detection module, in which the focused energy passes through the OCLI circular variable filter onto a composite silicon/lead sulphide detector. After amplification, the signals from the detector are then digitised in (iii) the microprocessor control and storage module. During the recording sequence, the spectra are displayed on the 160 x 128 LCD. These spectra may be overwritten, or may be stored into the 1-megabit

bubble memory. This form of memory allows the PFS to be turned off for transport, battery charging etc. without loss of data.

The PFS is capable of measuring either absolute radiance, or reflectance relative to a standard, such as barium sulphate. Reflectance mode was normally chosen to produce comparable results. Reflectance mode is selected after recording a spectrum using the $BaSO_4$ plate; setting of the gains of both the visible and infrared amplifiers is then automatic. All spectra measured are then of reflectance, calculated relative to the spectrum recorded immediately prior to selecting the reflectance mode.

To facilitate control over height and perpendicularity of PFS measurements a trolley, based on a "golf-buggy", was constructed. Its design allowed adjustments to height and direction and also carried the battery packs, thus enabling more efficient use of the instrument.

2.2.3 Geoscan Airborne Multispectral Scanner

The airborne multispectral scanner, also developed and supplied by Geoscan, is a modular, stabilized system capable of recording data in narrow spectral channels over the range 400 to 12,500 nanometers. Data from the system are recorded onto a Winchester disc, then backed up in computer-compatible form onto 1600 bpi magnetic tapes. A real-time interactive colour display unit enables rapid determination of image quality during recording, and allows important features to be identified. The basic modules which comprise the scanner are included in the appendices.

The scanner system was designed to fit in a small, twin engine light aircraft which has a standard 18" (450 mm) hole for a reconnaissance camera. At present, the scanner is installed in an unpressurised Beechcraft Queenair, owned by Kevron Aerial Surveys on long term charter to Geoscan Pty Ltd.

Initially, the scanner was operating with 11 channels, with the following bandpasses:

Channel	Bandpass (nm)
1	450 - 500
2	550 - 600
3	650 - 700
4	830 - 870
5	930 - 970
6	1980 - 2080
7	2160 - 2190
8	2205 - 2235
9	2300 - 2400
10	9800 -10200
11	11050 -11450

Channels in the thermal IR region, with wavelengths of 7,500 - 8,000 and 8,500 - 9,000 nm, were added later.

The data acquired with the scanner over the salinity test sites has generally been of excellent quality, both from a radiometric and geometric sense. Some early striping problems due to an unstable voltage reference on the A/D converters, and noise due to ground loops in the amplifiers, have been corrected.

Two effects were noted to cause some degradation of the raw scanner data. The most apparent of these effects is the variation in atmospheric backscatter into the field of view of the scanner, resulting in considerable variation in contrast and brightness across a scene. Geoscan Pty Ltd has developed software which compensates for variations due to "across-track" illumination. The salt sites were flown on sun azimuth dependent flight lines, i.e. into or away from the sun, to minimise the asymmetry of illumination changes.

The second degrading effect on the imagery was due to misregistration of the visible module and the thermal infrared module. This resulted in a two-scanline offset, combined with a non-linear variation in the relative pixel positions along a scan line. Geoscan has a correction and resampling algorithm which reduces the pixel-to-pixel registration errors to less than 0.125 pixels (Honey, pers. comm.).

2.2.4 Geophysical Ground Electromagnetics

Although this is not a spectral remote sensing technique its inclusion in the study does have relevance for site selection, and to assess the possible relevance of Airborne EM Systems currently available.

Soil electromagnetic resistivity depends upon many factors including soil moisture, texture and salinity. Generally a correlation exists between measured soil resistivity and soil salinity (De Jong et al. 1979 p. 810). Australian experience supports this; for example, Williams (1983 p.2) stated that approximately 70% of the (ECa) values can be explained in terms of soluble salts. The remaining 30% relates to mineral, textural and moisture content. The depth of soil measured depends upon the frequency of the transmitter, distance between the coils, their orientation to the soil surface and, to a lesser extent, on the actual conductivity of the soil.

The technique relies on an electrical current being applied to a coil, or transmitter, then measured at another coil or receiver, and the resistivity between them measured (McNeill J.D. 1980). When the transmitter coil is energised, circular electrical currents are induced in the soil which are directly proportional to the bulk electrical conductivity (EC) of that soil. Each of these current loops generates a magnetic field which is proportional to the current flowing in the loop. Part of that magnetic field is intercepted by the receiver and creates an output linearly related to apparent soil electrical conductivity (ECa) or resistivity.

The EM-38 instrument, manufactured by Geonics Ltd, used for this study, is a light-weight portable device approximately one metre long with internal coils at each end.

CHAPTER THREE

3 RESULTS

3.1 SPATIAL RESOLUTION

3.1.1 The Yalanbee Example

Since 1960, 25 photographic and electronic imagery missions have been acquired over Yalanbee (Table One); photogrametric scales have ranged from 1:2,000 to 1:40,000. Invariably the ground resolution decision was made in an arbitrary fashion based on limitations of finance, navigability and a minimal perception of which ground features needed to be resolved. The availability of powerful magnifying stereoscopes coupled with excellent film and reproduction techniques indicates that extensive waste has probably occurred in expensive low altitude air photo missions. Rarely have the air photos of Yalanbee been interpreted to the limit of the resolveable features contained therein.

The value of stereo air photographs to delineate salinity and landforms which may be at risk is in no way underestimated in this study. Aerial photographs are generally accepted to have maximum spatial information for remote sensing, but many consider that, technically, they cannot be taken any further. Aerial photographs normally lack geometric control, lack photosensitivity control, have variable processing control and have limited spectral coverage into the near infrared, and have no short-wave or thermal infrared response.

Low-cost, monochromatic, small-scale air photographs are widely available; their actual cost is absorbed in benefits already gained from the mapping exercises for which they were commissioned. Larger

scale colour or colour I.R. photography has larger associated costs but is still very cost effective when compared with mapping exercises based upon ground traverses and field sampling.

Figure Five is an aerial photograph centred on the Crocodile Creek study area. It was taken using a WILD RC10 Camera with a 152 mm lens at a height of 1,530 metres AGL (1,830 m above sea level - ASL) giving a nominal photogrametric scale of 1:10,000. The photo was taken near midday on 12 December 1982 and was part of a run designed to give 60% overlap providing a stereoscopic exaggeration.

Superimposed on this photograph is an example of the level of salinity mapping usually extracted from scales of this order (Nulsen 1981, and pers. comm.), with an overlay demonstrating nominal pixel resolution from a range of multispectral sensors (see Appendices One a & b). The largest square represents, at the photo scale, a 1.1 km square which is the nominal sub-orbital ground resolution for the Advanced Very High Resolution Radiometer (AVHRR) on board the NOAA series of polar-orbiting meteorological satellites. Within this square is a 12 x 10 pixel matrix simulating the nominal resolution of the Landsat Multispectral Scanner (MSS) (see Figure Six). The half pixel offset is a function of earth rotation and the design of the instrument which "sweeps" 6 lines each scan. Nominal examples are also given of the resolution of the Thematic Mapper on Landsats 4 and 5 (also see Figure Seven) and the multispectral scanner on the French SPOT satellite (launched in Feb 1986). Grids representing 6 and 10 metre pixels as recorded for this study by the Geoscan Airborne Multispectral Scanner are also included.

Figure Eight is an aerial photograph taken with a window-mounted, motor-driven, 70 mm Hasselblad camera fitted with an 80 mm

lens (Hick and Tapley, 1981, p.6). The photoscale of this enlargement is approximately 1:4000. An overlay includes the sample sites and nominal grid indicating airborne multispectral scanner pixels of about 7 metres. This overlay shows the distribution of 7 metre pixels over the sites and the problems of orientation of the 3x3 pixel samples.

An example of the loss of information as spatial resolution changes is given in Figures Seven a,b,c & d. These images were prepared synthetically by aggregating pixels within the image processor. They do however give an indication of the loss of definition of such features as tracks and trees but the major elements of the land affected by salinity remain.

The sample extracted from the Geoscan MSS data of 3x3 pixels provides a limited indication of variability both across sites and inherently within the data. Larger samples are extracted from uniform areas of pasture, crop, bush, dam water, rock etc. and these have been included in the statistical analysis both for variability on a particular date of acquisition and between dates of acquisition.

Degradation of pasture from the effects of rising saline groundwater progresses in steps following winters of heavier than normal rains (Bettenay, pers. comm.), the effect becoming evident as evaporation concentrates the salts during the following summer. These areas develop and expand on topographically controlled "fronts" over the next 2-20 years. Annual increases may range from 0-50 metres, but is most likely to be 10 metres per annum in early years, again dependent on the seasonal conditions. Resolution becomes a trade-off with cost of acquisition.

Results, from this work, indicate that the study sites which are approximately 20-30 metres square, reasonably uniform, and spectrally separable, are of the order of the area of the minimum spatial resolution. The saline encroachment at Yalanbee around which sites 1-5 are located, is currently 80 metres wide and the pasture is degrading on a front approximately 20 metres ahead of the scald (see Figure Four). The Thematic Mapper image, Figure Seven, (top and bottom) with its 30 metre spatial resolution, does show the general outline of this advancing saline front as a green line only 1 pixel wide near the sites. This tends to indicate that image pixels of the order of the area of the sites i.e. (20-30 m) provide adequate discrimination, to determine the location and direction of expansion of salinity to implement whatever hydrological or agricultural remedial management is considered relevant.

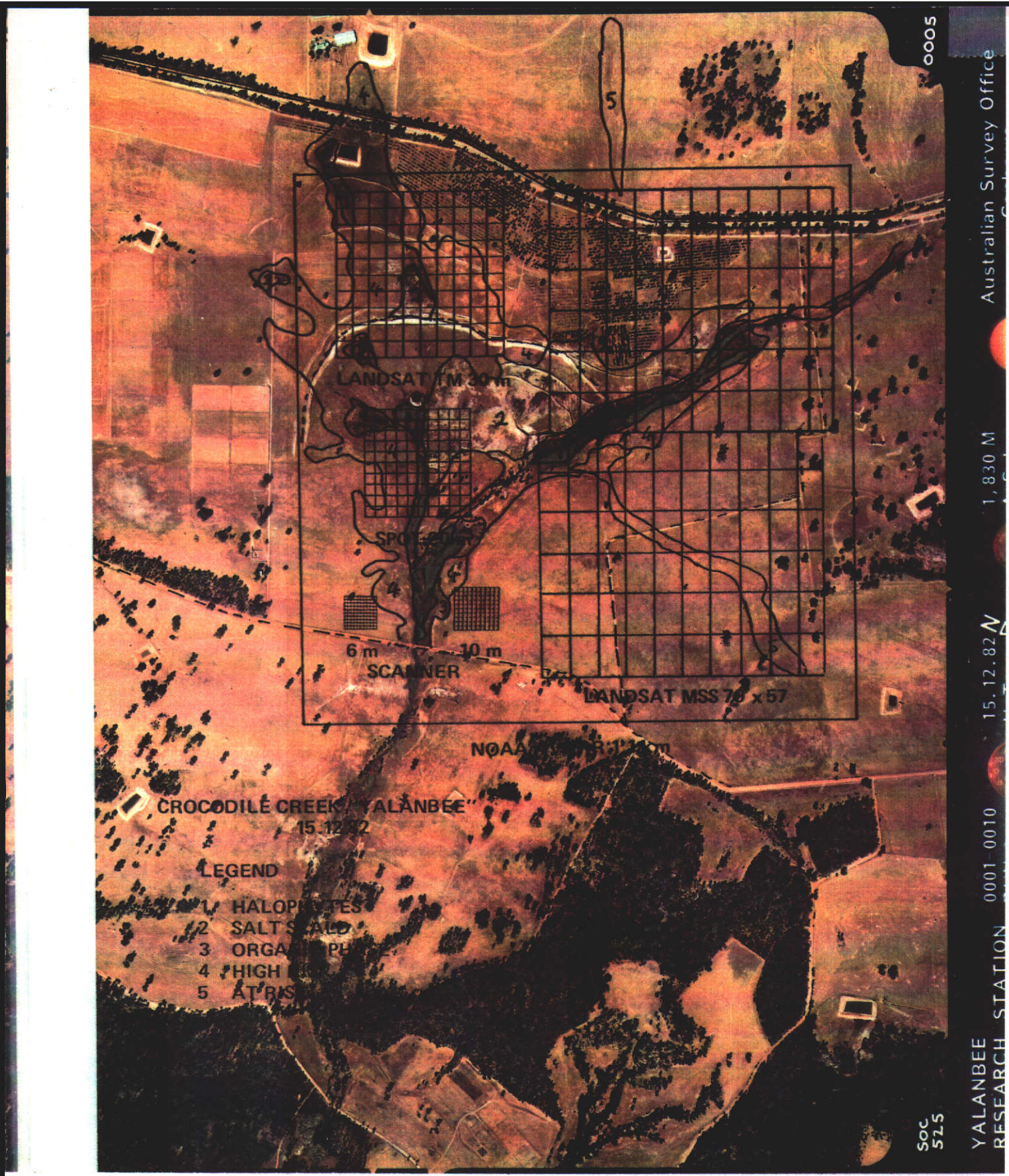

Figure Five. Aerial photograph of the salt scald on Crocodile Creek, Yalanbee, with overlays indicating a level of salinity mapping based on air photo interpretation and varying spatial resolutions. The outer square is the nominal 1.1 km resolution of the NOAA-AVHRR, within that the 79 x 57 m Landsat MSS sample, the 30 metre Landsat Thematic Mapper, SPOT-IMAGE 20 metre HRV and two examples of nominal airborne scanner pixels.

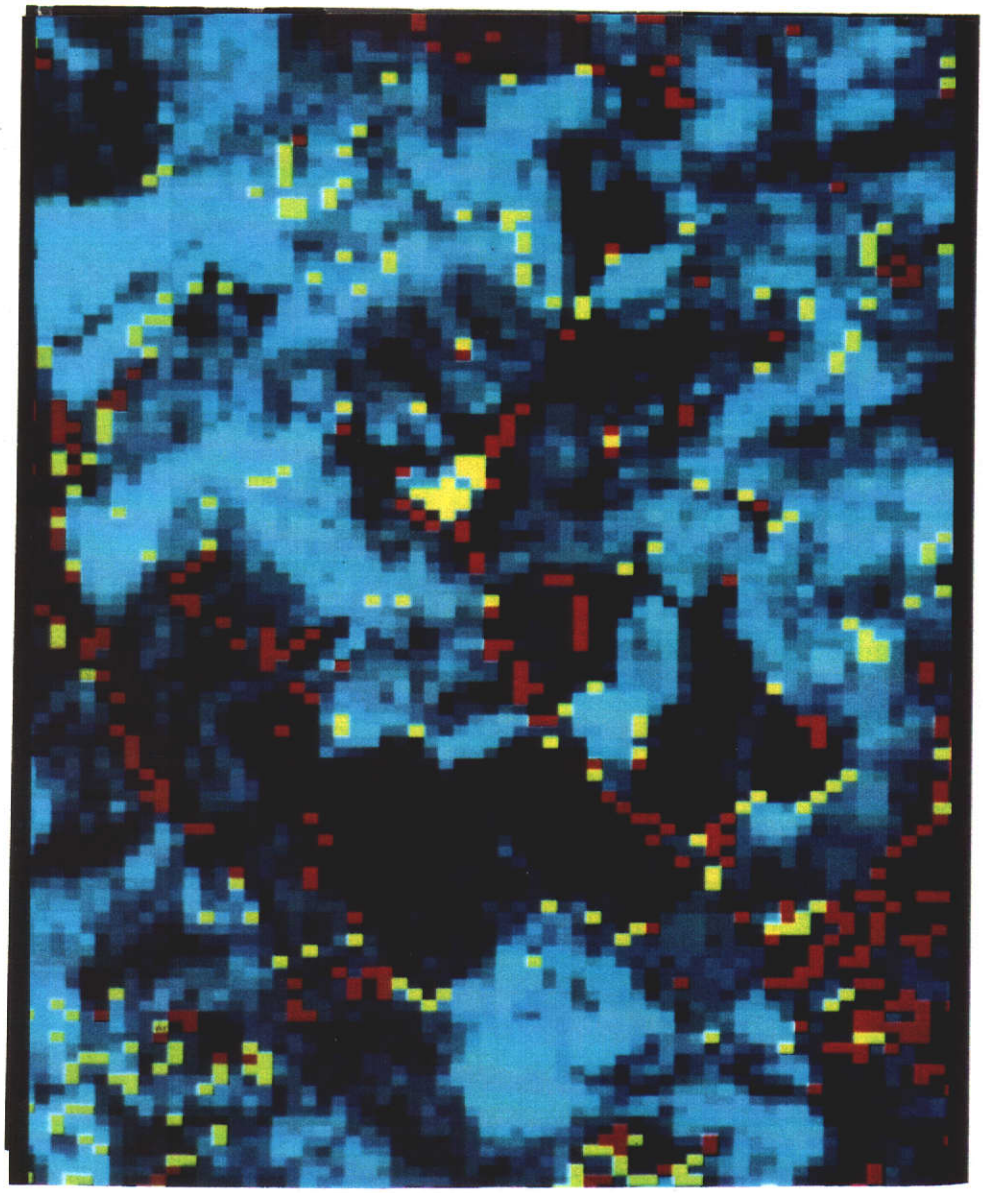

Figure Six. Classified Image of Crocodile Creek, Yalanbee from Landsat 2 Multispectral Scanner 24 Oct 1981 (120.082) - This image is at an approximate scale of 1:40,000 - individual pixels are evident and there are two classes mapped leaving an unclassified "grey-scale" of MSS band 2. Red is saltland vegetation, yellow is salt scale - the study area is the group of yellow pixels near the centre. North is to the right hand side.

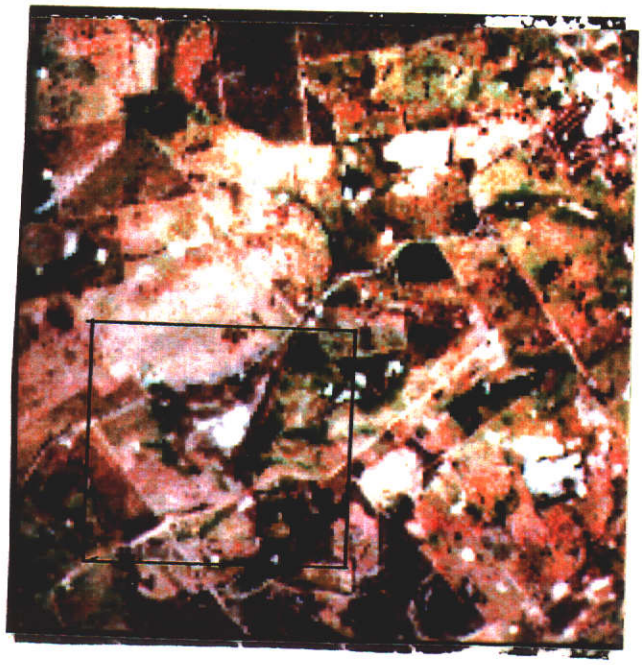

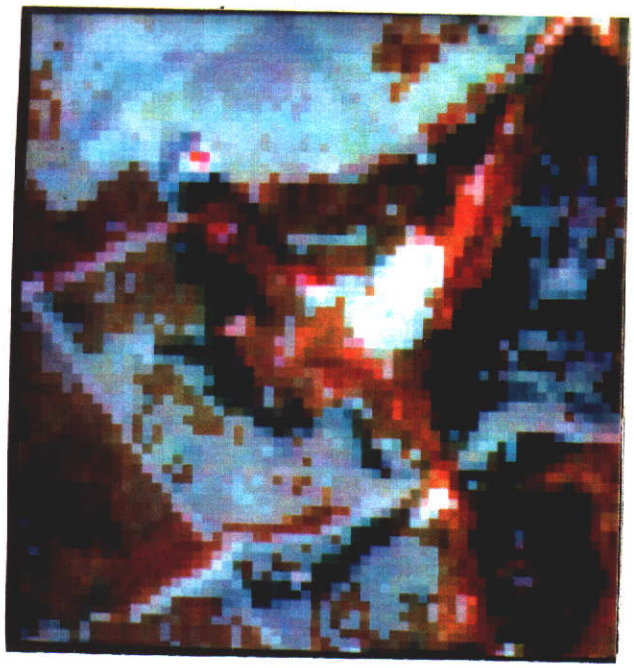

Figure Seven. Colour Composites from Landsat Thematic Mapper for Yalanbee (Perth 112-082 28.10.86). The top example is at a scale of approx. 1:60,000 which covers an area of 25 sq km and represents a "true-colour" ie uses the visible bands in composite. The lower example is a subset of the top image and uses "False-Colour" ie Infrared band is composited with a visible band to produce an image highlighting the vegetation and salt areas. This image is at an approximate scale of 1:20,000. North is to the right hand side.

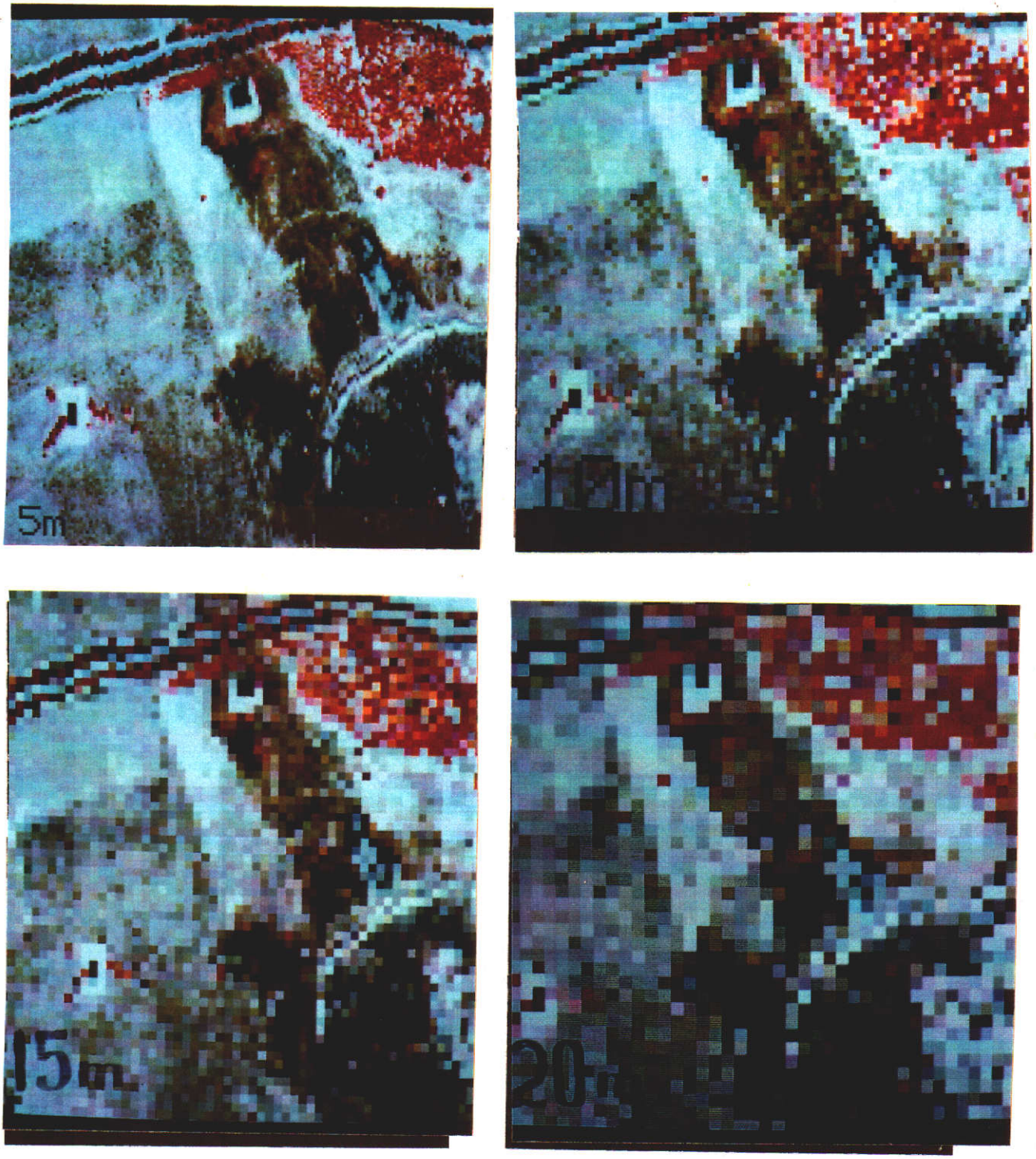

Figures 7A, B, C, D are enhanced images from the Geoscan Airborne Multispectral Scanner using bands 2 (Blue), 3 (Green) and 4 (Red) to show approximate pixel resolutions of 5,10,15 and 20 metre resolution.

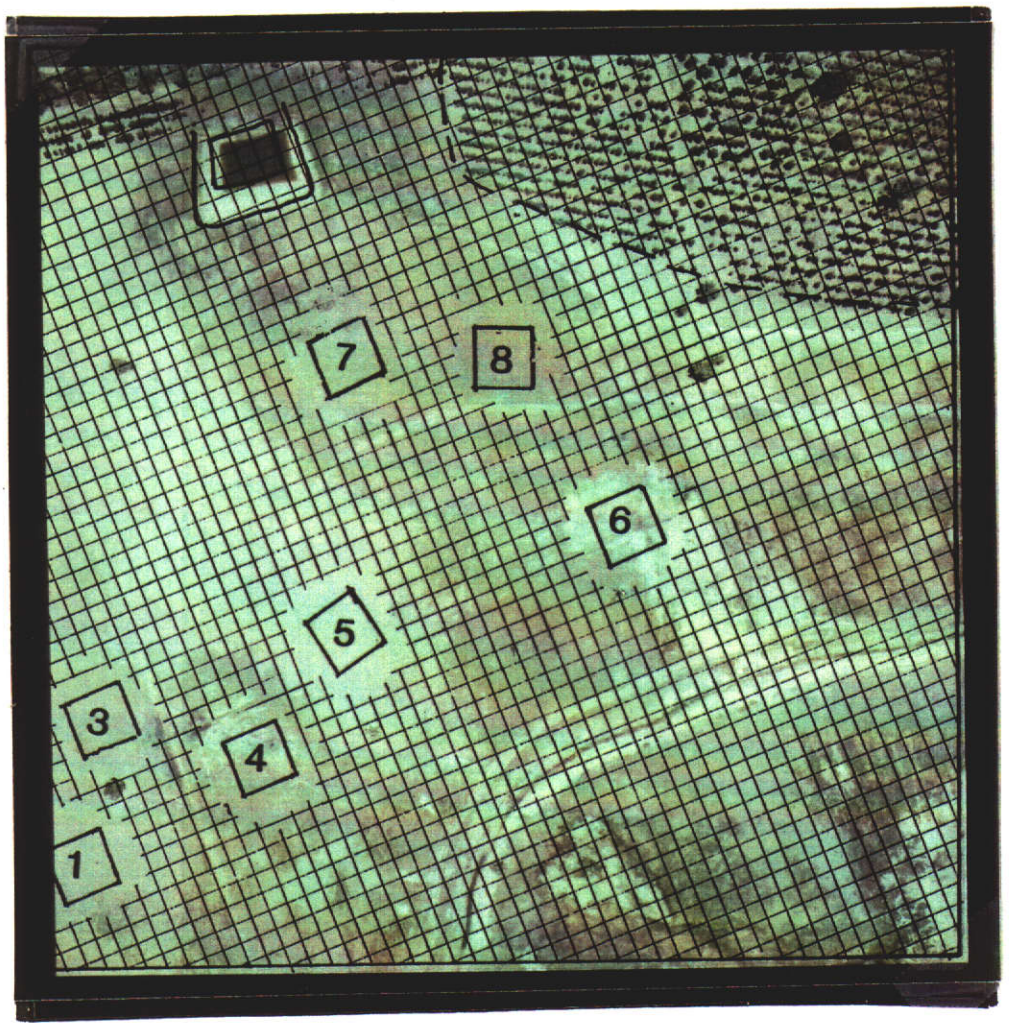

Figure Eight. Aerial Photograph of Crocodile Creek Catchment with sites and a nominal 7 metre pixel overlay. Site two lies off the image 25 metres south of site three.

3.2 SPECTRAL ANALYSIS

3.2.1 Spectral Analysis of Soils

Spectral analysis of soils has been the subject of extensive studies in the United States since the 'mid-sixties'. The findings of the groups at Stanford University led by Prof. R.J.P. Lyon, and at Purdue University by Stoner and Baumgardner (R.J.P. Lyon pers. comm.), similarly conclude that: "The capacity to measure both visible and infrared reflectance adds a new dimension to the possible use of soil spectra to explain soil characteristics and to predict soil response to different management conditions. Field and laboratory soil spectral characterization helps define the extent to which intrinsic spectral information is available from soils as a consequence of their composition and field characteristics."

X-ray diffraction (XRD) studies indicate that the mineralogy of the surface soils vary only slightly on the study sites at Yalanbee. They all show an abundance of quartz with minor amounts of kaolin and traces of anatase (CSIRO Unpub. data). The major variation is in the organic matter, both in quantity and type.

Organic matter, determined by Loss on Ignition (LOI), appears in Figure Nine. Overall soil reflectance (albedo) generally decreases as the organic matter content increases. The constituents, which include humic and fulvic acids and non-specific compounds such as decomposing plant residues, affect reflectance to differing degrees. Krishman et al. (1980 p.1282) reported that reflectance from the visible region is more closely related to organic matter content of soil than measurements from the infrared region.

As displayed in Figure Nine, most soils show considerable uniformity and a general increase in reflectance from 400 to

1,850 nm, with usually a decrease thereafter. This is in contrast with the reflectance spectra of green vegetation as presented in Section 3.2.2 (Figure Thirteen) where it has been possible to subdivide the three different reflectance curves into classes of shapes and magnitude. The properties which determine soil reflectance are: mineral composition, texture (particle size), structure, organic matter and moisture content. Mineral composition, organic matter and moisture are the main factors governing spectral absorption of radiation (Bunnik 1981 p.47). Texture and structure determine the degree of shading and facets of reflection. Soil moisture is retained in the pores between the particles by a capillary process and by the "hydro-attractive" properties of the organic matter and "hygroscopic" characteristics of salts. Increasing moisture content results in a decrease in reflectance at all wavelengths. Maximum decrease occurs in the water absorption regions near 1400 nm, 1900 nm, 2200 nm and beyond 2500 nm.

The importance of the effect of moisture on spectra, especially in the SWIR regions, cannot be underestimated (Bowers and Hanks (1965), p.132). These authors showed the effect of moisture on spectra and this is supported in Figures Nine and Twelve. This is the reason for the requirement, that ideally no rain should precede a scanner flight for 7 days, as stated in the methodology (Section 2.1.6).

Moisture associated with vegetation shows the same characteristic spectra as moist soil. The value of the SWIR region can then only be considered when bare soil conditions prevail, or dominate over dry or senescent vegetation which has been subjected to uniform atmospheric conditions.

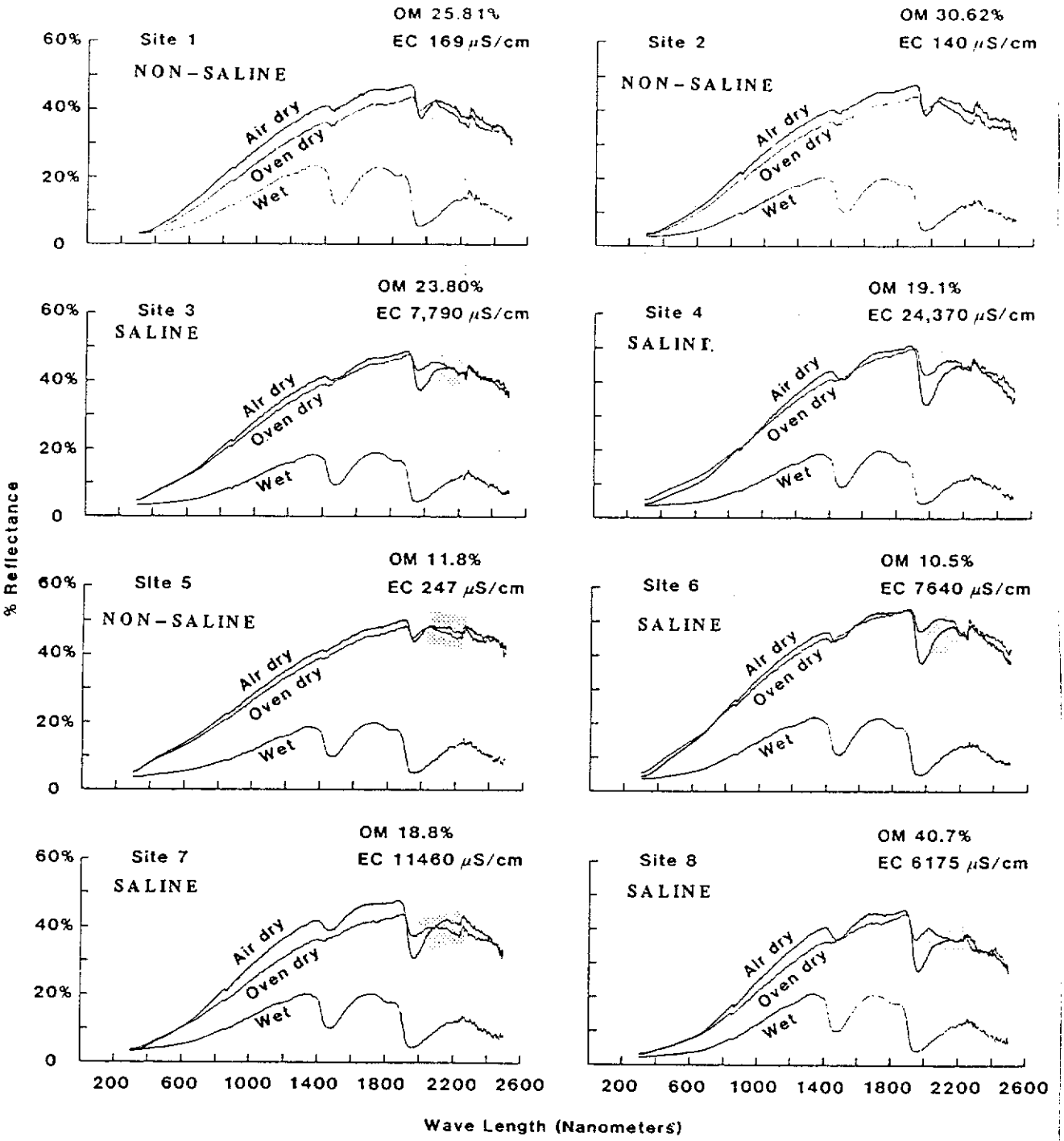

Figure Nine. Bare soil laboratory spectra for the eight Yalanbee sites. Sites 1,2 and 5 with ECs between 140-247 µS/cm represent the non saline samples and 3,4,6,7 and 8 with ECs between 6,175-24,370 µS/cm are soil samples from saline sites. Organic matter (OM) determined by Loss On Ignition (LOI) are included.

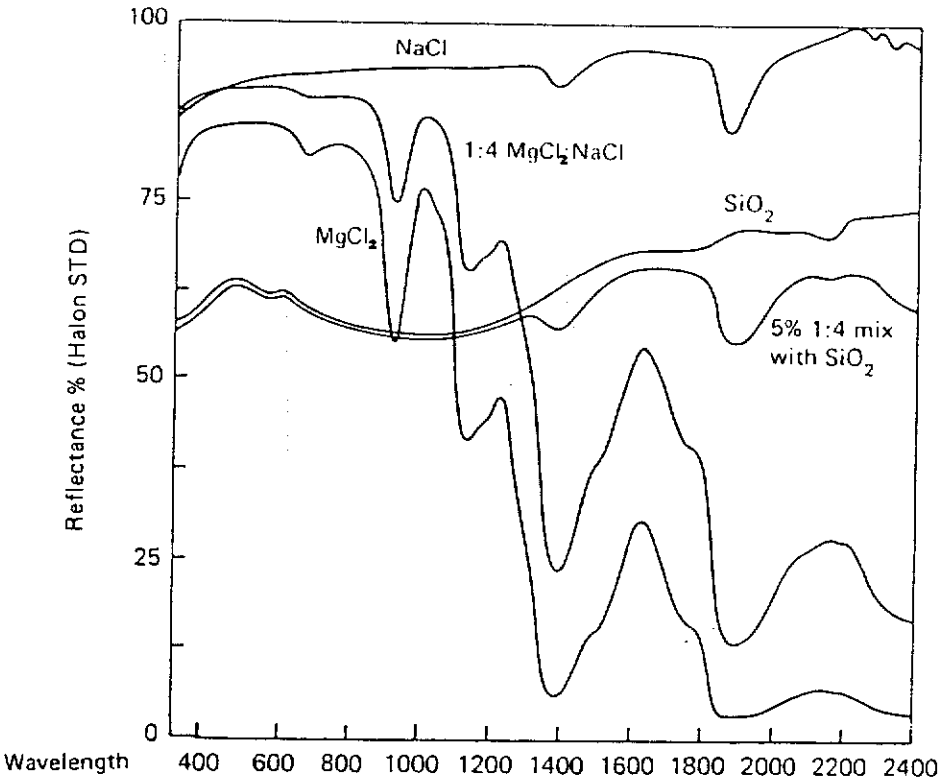

Figure Ten. Laboratory Spectra of Sodium and Magnesium Chloride with silica mixtures measured by the Hitachi Spectrophotometer.

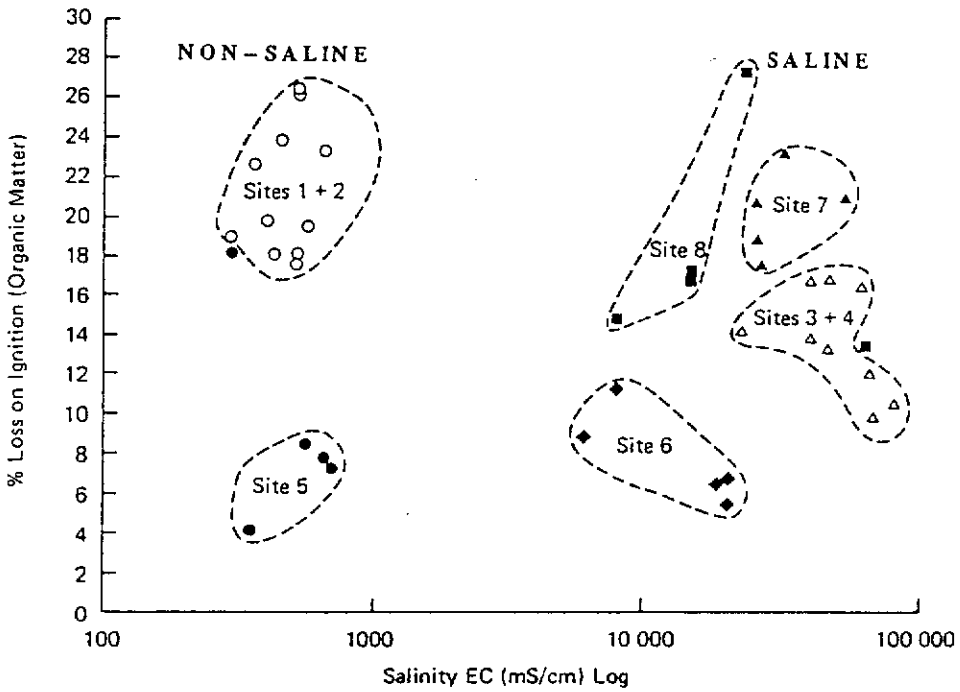

Figure Eleven. Plot of Organic Matter derived from Loss On Ignition (LOI) against surface Electrical Conductivity (EC) shows no relationship between salinity and organic matter. ($r = -.1$).

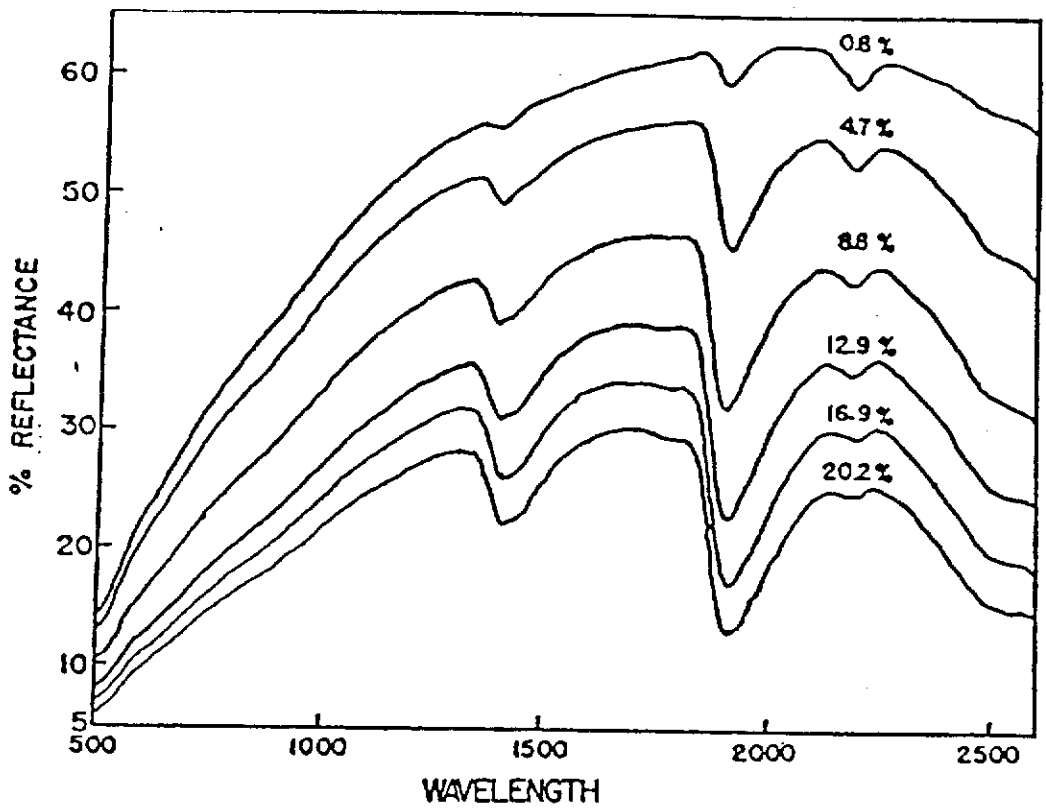

Figure Twelve. Soil Spectra showing effect of moisture. Note change in slope beyond 1900 nm and the decreasing absorption at 2200 nm, and refer to the cellulose absorptions in Figure Thirteen.

3.2.2 Spectral Analysis of Vegetation

Vegetation covers a significant proportion of the ground surface of most of the study sites. Figure thirteen shows examples of vegetation spectra with the typical green peak (point B, centred at 550 nm) reflectance characteristics for photosynthetically active vegetation dominated by carotenoid pigment absorption (centered at 480 nm) and chlorophyll absorption (point A, centered at 680 nm). The sharp rise in reflectance above 700 nm (point C) marks the change from chlorophyll absorption to cellular reflectance (the red edge). This near-infrared reflectance from 700 nm to 1300 nm is dominated by cell wall and airspace interfaces and, to a lesser extent, by the specific characteristics of those cells. It is often referred to as the Reflected Infrared Plateau (point D). A minor water absorption occurs at 1200 nm (point F) and then beyond 1300 nm, reflectance is primarily controlled by leaf water content with major absorptions near 1400 nm and 1900 nm; these are all marked on Figure Thirteen with point E.

During the vegetative cycle, reflectance decreases in the visible regions and increases in the near-infrared wavelengths until maximum canopy density is reached. Then, with senescence, a reversal occurs. Figure thirteen also shows significant cellulose peaks at 1923 nm, 2086 nm, 2145 nm, 2307 nm and 2338 nm with corresponding absorptions between, as recorded by the IRIS Spectrophotometer (CSIRO Spectral Library). These are evident both on the dry grass and on the cellulose powder which was prepared to highlight these features.

Field spectra recorded with the Geoscan Portable Field Spectroradiometer showed these characteristic absorptions and peaks of reflectance, either as a function of degradation of vegetation due to salinity or through senescence of annual pasture or crop species (See Figures Sixteen and Seventeen).

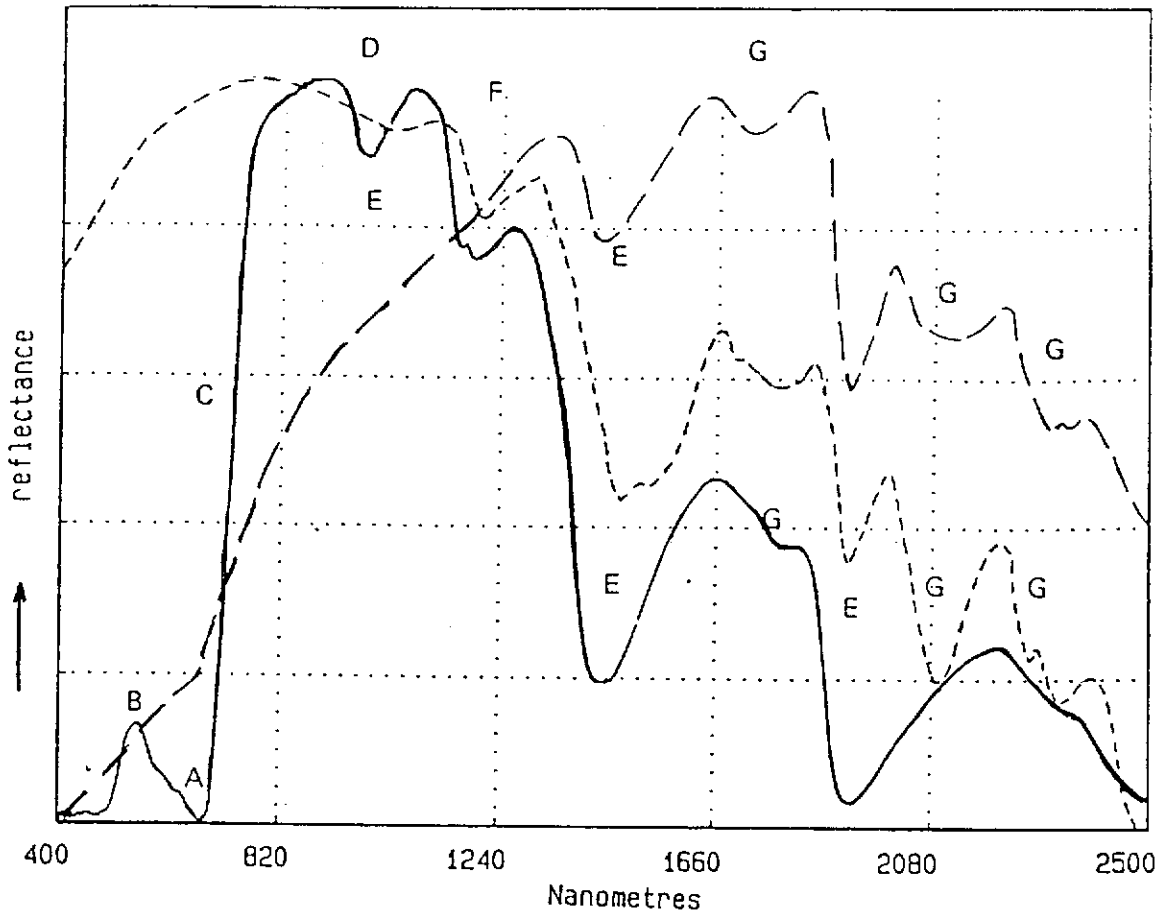

GREEN GRASS (KIKUYU)

DRY GRASS (KIKUYU)

CELLULOSE POWDER

A Chlorophyll Absorption

B Green Peak

C Red—Infrared Edge

D Reflected Infrared Plateau

E Water Absorption

F Cellular Water

G Cellulose Absorption

Figure Thirteen. Spectra of Vegetation. These typical reflectance spectral curves, for vegetation components, have clear spectral responses for materials common on the study sites. Soil spectra, as shown in Figure Twelve, will influence these spectra as vegetation degrades.

3.2.3 Laboratory Spectral Analysis

Figure Ten shows spectra, measured on the spectrophotometer, for sodium and magnesium chlorides. Baseline data for preliminary estimation of the absorptions which relate to salt are contained in Figure Ten. The proportions of magnesium (Mg^{2+}) to sodium (Na^{+}) ions to chloride vary, but a generally accepted figure for the samples from Yalanbee and other places in Western Australia (Johnson et al. 1982, p.4) appears to be between 1:3 and 1:8 (see Table Two).

Table Two

Chemical Analysis of Salts.

Sample type	Cl^{-}	Na^{+}	K^{+}	Mg^{++}	Ca^{++}	pH	Mg:Na
Surf. Water nr 1,2&3	36.2	27.1	0.5	9.4	3.2	7.7	2.9:1
" " nr 6,7&8	118.4	66.0	0.2	20.7	5.8	7.7	3.1:1
Grdwater nr site 4	280.1	206.4	0.8	45.3	15.0	3.5	4.5:1
Grdwater (York)	254.1	256.9	1.3	35.4	1.5	8.8	7.3:1
Grdwater (Dangin)	6.9	5.5	0.2	1.1	0.6	8.1	5.0:1

Laboratory-grade dry NaCl, $MgCl_2$ and SiO_2 were used to prepare mixtures for spectral comparisons. In the case of $MgCl_2$, considering the hygroscopic nature of this material, the sample preparation time was less than one minute, with 5 grams being presented to the spectrophotometer, and the run time being 6 minutes starting from the longer wavelength. This spectra shows "deep" water absorptions when compared with NaCl. A 1:4 mixture of $MgCl_2$ and NaCl shows similar, but not as "deep", water absorptions. The mixture was then added to pure silica contributing 5% of the total. This spectrum closely resembles many of the saline field spectra (Figure Nine) in the region between 1400 and 2400 nm.

The deliquescence of $MgCl_2$ is responsible for the characteristic water absorptions even when present in small amounts. This may be

further accounted for when the assumptions of Goldschmidt (1954, p.590) are considered. He concludes that the dispersion of marine salts throughout the atmosphere are not exclusively NaCl crystals, as previously thought, but include very hygroscopic salts as hydrated chlorides of magnesium. These nuclei, probably in many cases, form an extremely hygroscopic solid or deliquescent surface layer upon the NaCl crystals. It is reasonable to assume that this atmospheric state would translate well to the top few millimetres of the soil surface as measured spectrally; the similarity of spectra from field sites is due in part to the moisture contained in these coatings of $MgCl_2$.

The examples taken from the eight Yalanbee sites (Figure Nine) clearly show this pattern. The samples in each case are a mixed bulk sample combined from the top one centimetre of four profiles. The samples were analysed on the spectrophotometer in oven-dried (105°C), air dried (at 40°C) and moist condition. The bottom spectra in each case from Figure Nine represents "moist", the centre spectra the oven-dry and the top spectra the air-dry. The pattern in the air-dry and oven-dry spectra is fairly predictable until the water absorption region at 1900 nm, at which point anomalies occur. The low salinity sites, e.g. 1, 2 and 5, show a decrease between 2000 nm and 2150 nm in both air-dry and oven-dry samples. The more saline sites show a different trend, with an increase in reflectance of the air-dry sample over the same region. The oven-dry measurement reverses this trend. This appears to be independent of organic matter (Figure Eleven).

The explanation offered for this is that moisture locked into the salts of the high salinity samples is extending the slope from the 1900 nm water absorption region out towards 2200 nm. This moisture, which would remain in all seasonal conditions, is then removed by oven-drying at 105^{o}C. Such soil temperatures would not occur in the field, and thus the effect would persist.

The explanation for the generally higher overall reflectance for the air-dry over the oven-dry is more difficult. If the Loss On Ignition (LOI) organic carbon figures are compared, the difference in reflectance is generally much less, especially between 1,400 nm and 1,900 nm, for the sites with lower organic matter.
Figure Eleven is a plot of LOI against log EC (1:5); over the eight sample sites, and shows a poor relationship between salinity and organic matter ($r = -.1$).

3.2.4 Portable Field Spectroradiometer (PFS) Analysis

The use of the PFS, coinciding where possible with overflights with the airborne scanner, enabled detailed spectral comparisons, under solar-illuminated conditions, of soil and vegetation components. PFS data were recorded on the following dates:-

16 May 1985

7 October 1985
15 October 1985
30 October 1985
6 December 1985
25 February 1986
26 March 1986
29 April 1986
1 September 1986
21 November 1986
30 January 1987
26 March 1987

During 1986 an intermittent, but increasingly frequent, instrument malfunction rendered some sampling dates unreliable for analysis. It took some time to determine that there was a fault and then to rectify the problem, delaying important samplings in the spring-flush. This was an unavoidable circumstance, inherent when evaluating prototype instruments.

Figures Fourteen and Fifteen are examples (non-saline and saline) of the plotted raw output from the PFS. It shows the spectral reflectance between 400-2500 nm (.4-2.5μm), including filter changes as described in the specifications of the circular-variable filter wheel (Appendix Five). These spectral plots are the individual spectra of replicate samplings of saline and non-saline sites and include the wavelength overlap near 700 nm (A) and the gap between 1200 and 1300 nm (B). The spikes associated with the water

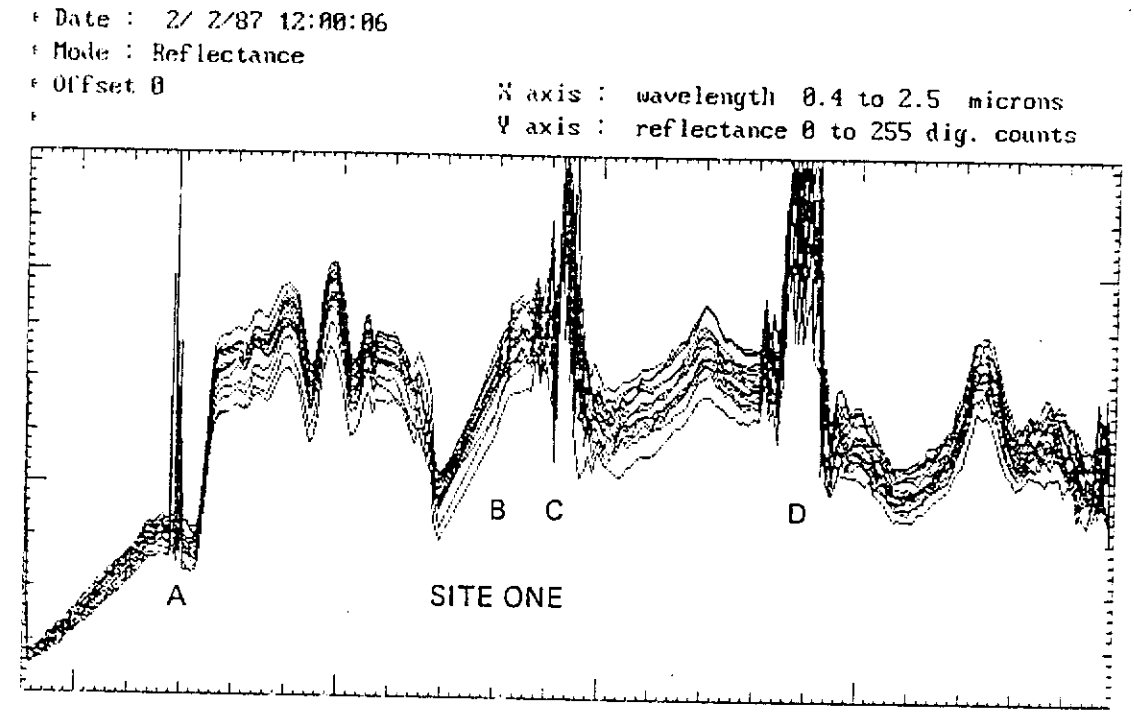

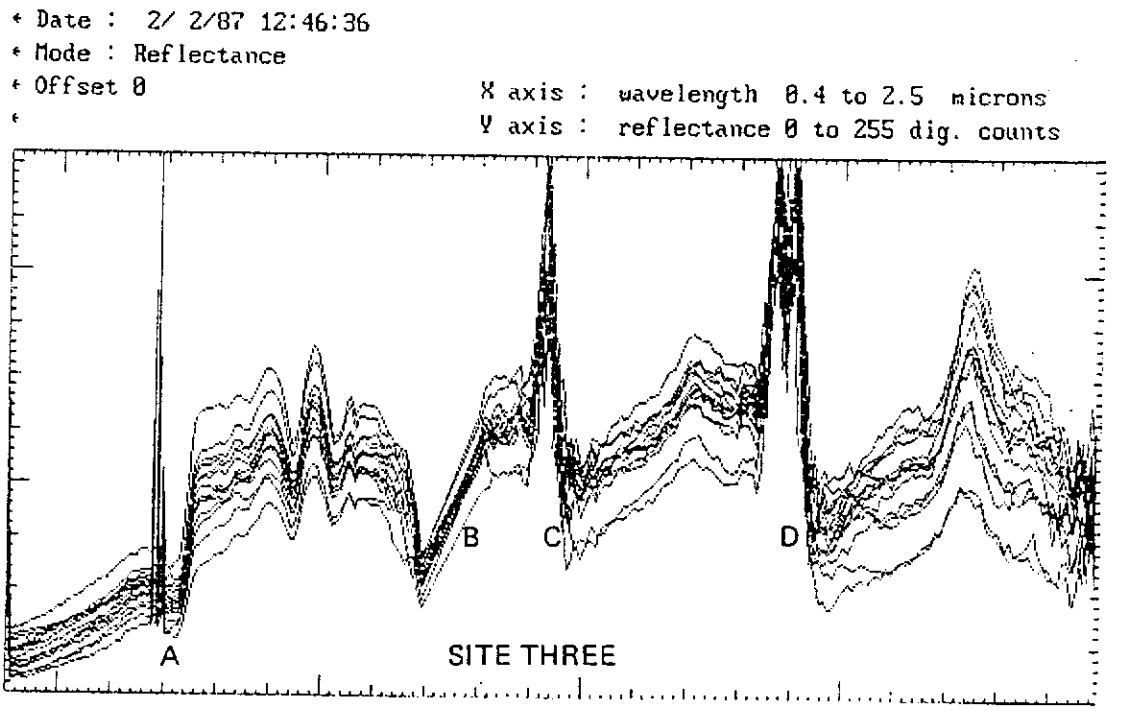

Figures Fourteen and Fifteen. Raw PFS data from site 1 (non-saline) top, and 3 (saline) bottom, in February 1987. These are examples of the actual display output produced in the field, and shows the variability of aproximately 30 spectra on each site. The horizontal scale represents the fully non-linear range of the instrument and the vertical scale is reflectance as a proportion of a $BaSO_4$ plate. A,B,C,+D are regions to be omitted from analysis.

absorption regions (C + D) are an instrumental artefact and have been masked from Figures Sixteen & Seventeen and also from the statistical analysis.

Figures Sixteen and Seventeen are of the mean spectra with a boundary on either side representing a confidence level of 95% around the mean(i.e. ± 2 std error). These masked spectra now have four discrete regions, and for the purpose of discussion here can be considered as the "visible", " the vegetative infrared", "1600 nm shortwave infrared (SWIR) Window" and the "2200 nm SWIR Window". Appendix Seven includes further examples of these spectra. These appendix figures have been photo-reduced and all dates for each site plotted together to enable visual comparison of seasonal trends as a function of wavelength.

The MKII Geoscan Scanner currently [1987] under construction will have wavebands as narrow as 15 nm in the visible and near infrared and 30 nm in the SWIR. The practical minimum bandwidth is determined by detector technology and optical constraints. The PFS samples 256, equally-spaced points on each rotation of the filter wheel which represents slightly over-or under-lapping parts of the spectrum between 400-2400 nm. Each segment of the wheel represents samples which range between 5 and 10 nm (see Appendix Five). The fine spectral structure, necessary to provide diagnostic information (see Figure Thirteen), can be accommodated with bandwidths of 30 nm and this figure was chosen to reduce the enormous dimensionality of the spectral data before analysis. Further data reduction was achieved with the omission, or masking, of instrumental artefacts and water absorption regions. This left 46 channels, each 30 nm wide, to be statistically analysed (see Table Three). These are referred to as "PFS bands".

		λ
1	1	0.400
	2	0.404
	3	0.409
	4	0.414
	5	0.418
	6	0.423
	7	0.428
2	8	0.432
	9	0.437
	10	0.442
	11	0.446
	12	0.451
	13	0.456
	14	0.460
3	15	0.465
	16	0.470
	17	0.475
	18	0.479
	19	0.484
	20	0.489
	21	0.493
4	22	0.498
	23	0.503
	24	0.507
	25	0.512
	26	0.517
	27	0.521
	28	0.526
5	29	0.531
	30	0.535
	31	0.540
	32	0.545
	33	0.550
	34	0.554
	35	0.559
6	36	0.564
	37	0.568
	38	0.573
	39	0.578
	40	0.582
	41	0.587
	42	0.592
7	43	0.596
	44	0.601
	45	0.606
	46	0.610
	47	0.615
	48	0.620
	49	0.625
	50	0.629

		λ
8	51	0.634
	52	0.639
	53	0.643
	54	0.648
	55	0.653
	56	0.657
	57	0.662
	58	0.667
	59	0.671
	60	0.676
	61	0.681
	62	0.685
	63	0.690
	64	0.695
	65	0.680
	66	0.685
	67	0.696
9	68	0.704
	69	0.712
	70	0.720
	71	0.728
10	72	0.736
	73	0.745
	74	0.753
	75	0.761
11	76	0.769
	77	0.777
	78	0.785
	79	0.793
12	80	0.801
	81	0.810
	82	0.818
	83	0.826
13	84	0.834
	85	0.842
	86	0.850
	87	0.858
14	88	0.866
	89	0.875
	90	0.883
	91	0.891
15	92	0.899
	93	0.907
	94	0.915
	95	0.923
16	96	0.931
	97	0.940
	98	0.948
	99	0.956
17	100	0.964

		λ
17	101	0.972
	102	0.980
	103	0.988
18	104	0.996
	105	1.005
	106	1.013
	107	1.021
19	108	1.029
	109	1.037
	110	1.045
	111	1.053
20	112	1.061
	113	1.070
	114	1.078
	115	1.086
	116	1.094
	117	1.102
	118	1.110
	119	1.118
	120	1.126
	121	1.135
	122	1.143
	123	1.151
	124	1.159
	125	1.167
	126	1.175
	127	1.183
	128	1.191
	129	1.200
	130	1.208
	131	1.216
	132	1.224
	133	1.232
	134	1.240
	135	1.248
	136	1.256
	137	1.265
	138	1.273
	139	1.281
	140	1.289
	141	1.297
	142	1.305
	143	1.313
	144	1.322
	145	1.330
	146	1.338
	147	1.346
	148	1.354
	149	1.362
	150	1.370

		λ
21	151	1.379
	152	1.387
	153	1.395
22	154	1.403
	155	1.411
	156	1.419
23	157	1.428
	158	1.436
	159	1.444
24	160	1.452
	161	1.460
	162	1.468
25	163	1.477
	164	1.485
	165	1.493
26	166	1.501
	167	1.509
	168	1.517
27	169	1.526
	170	1.534
	171	1.542
28	172	1.550
	173	1.558
	174	1.566
29	175	1.575
	176	1.583
	177	1.591
30	178	1.599
	179	1.607
	180	1.615
31	181	1.624
	182	1.632
	183	1.640
	184	1.648
	185	1.656
	186	1.664
	187	1.673
	188	1.681
	189	1.689
	190	1.697
	191	1.705
	192	1.713
	193	1.722
	194	1.730
	195	1.738
	196	1.746
	197	1.754
	198	1.762
	199	1.771
	200	1.779

		λ
32	201	1.787
	202	1.795
	203	1.803
33	204	1.811
	205	1.819
	206	1.828
34	207	1.836
	208	1.844
	209	1.852
35	210	1.860
	211	1.868
	212	1.876
36	213	1.885
	214	1.893
	215	1.901
37	216	1.909
	217	1.917
	218	1.925
38	219	1.933
	220	1.942
	221	1.950
39	222	1.958
	223	1.966
	224	1.974
40	225	1.982
	226	1.990
	227	1.998
41	228	2.007
	229	2.015
	230	2.023
42	231	2.031
	232	2.039
	233	2.047
43	234	2.056
	235	2.064
	236	2.072
44	237	2.080
	238	2.088
	239	2.096
45	240	2.104
	241	2.113
	242	2.121
46	243	2.129
	244	2.137
	245	2.145
	246	2.153
	247	2.162
	248	2.170
	249	2.178
	250	2.186

Table Three. The Portable Field Spectroradiometer samples 250 channels. These have been subdivided into 46 bands, 30 nm wide, "PFS bands". They cover the regions which are free from instrumental problems or absorption features and were the basis of the statistical analysis.

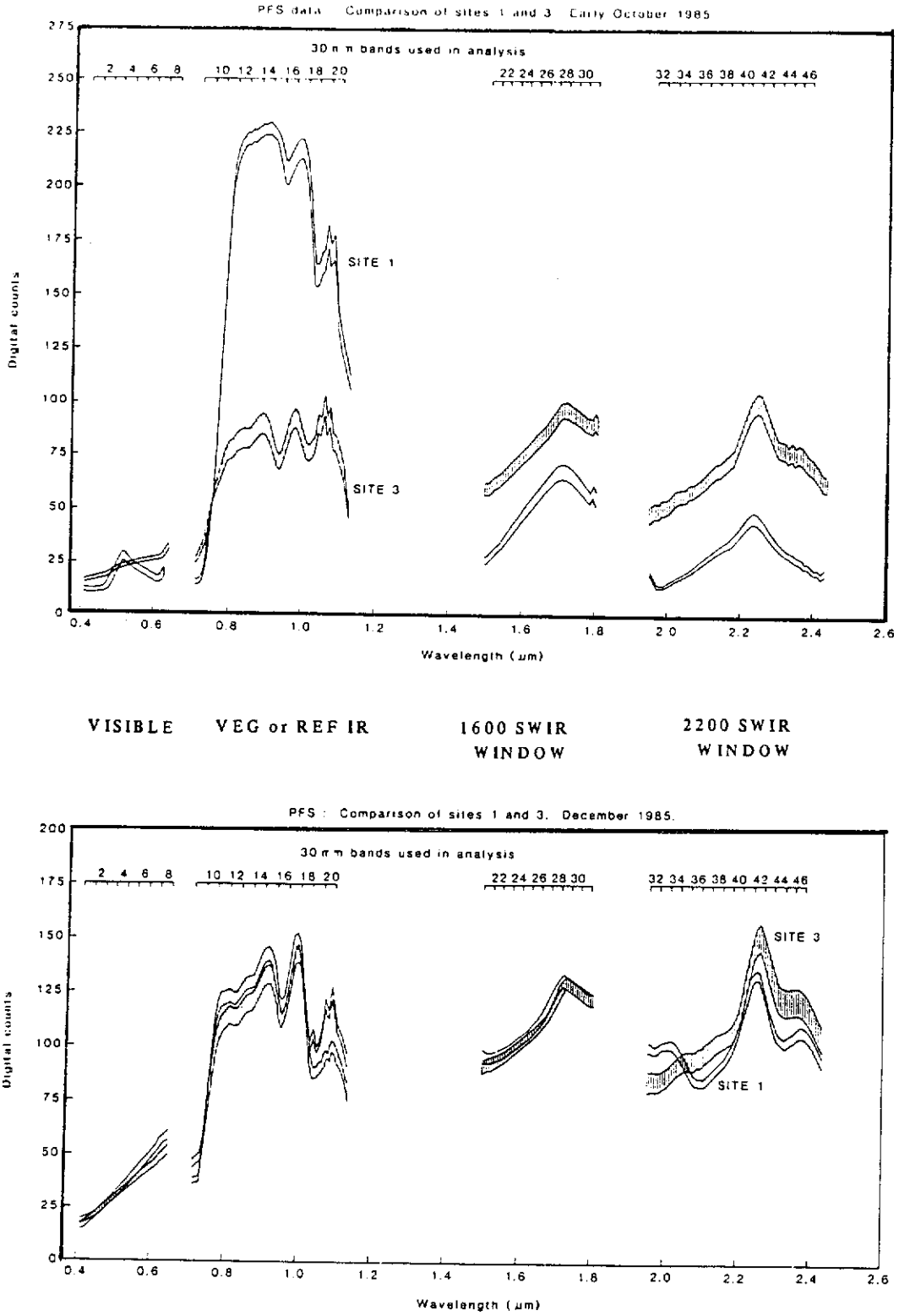

Figures Sixteen and Seventeen. Masked mean PFS data, and constructed "PFS bands", for October and December for sites 1 (non-saline) and 3 (saline). Note "green" (PFS band 4) peak and large difference between saline and non saline in the reflected infrared (PFS bands 10-20) in early October compared with small visible-near IR differences by December, and the inversely correlated bands in the SWIR region (PFS bands 32 and 36).

Using Figures Sixteen & Seventeen and Table Three as examples and with reference to Figure Thirteen, each of the regions was considered in the analysis of the PFS data as follows:

The "visible" (PFS bands 1-8, 400-660 nm) in "Early October" has a maxima relating to green and minima at blue and red. Following this region over all dates shows an increase in red as the vegetation "hays-off" over the summer which corresponds well with the visual appearance of the sites. The change being from vigorous lush green plant material in October, haying-off and exposing more underlying soil as the season progresses.

The second region of interest in the spectra show this phenology trend even more significantly. This region, "the vegetative infrared", or reflected infrared plateau, (PFS bands 9-20, 700-1086 nm) includes two absorptions which relate to moisture, and one which relates to chlorophyll, but the overall maxima, or plateau (Figure Thirteen) can be considered in three parts. The first is the start point of the region (PFS band 9, 700-730 nm) which is in a chlorophyll absorption region but still reflects a significant amount of visible red (red-edge). The other two parts are the maxima on either side of the central water absorption minima (PFS band 16, 930-960 nm). These relate to reflectance from chlorophyll on the left (PFS bands 10-15, 730-920 nm), and cellulose on the right (PFS bands 17-20, 960-1186 nm). The responses of these three parts of this region over time provides a descriptive analysis of the sites. Again, using Figures Sixteen & Seventeen as examples, the increase in visible red and cellulose and the relative decrease in chlorophyll also relates well to haying-off after the spring-flush, a feature not present on the saline sites.

3.2.4 Portable Field Spectroradiometer (PFS) Analysis

The use of the PFS, coinciding where possible with overflights with the airborne scanner, enabled detailed spectral comparisons, under solar-illuminated conditions, of soil and vegetation components. PFS data were recorded on the following dates:-

16 May 1985

7 October 1985
15 October 1985
30 October 1985
6 December 1985
25 February 1986
26 March 1986
29 April 1986
1 September 1986
21 November 1986
30 January 1987
26 March 1987

During 1986 an intermittent, but increasingly frequent, instrument malfunction rendered some sampling dates unreliable for analysis. It took some time to determine that there was a fault and then to rectify the problem, delaying important samplings in the spring-flush. This was an unavoidable circumstance, inherent when evaluating prototype instruments.

Figures Fourteen and Fifteen are examples (non-saline and saline) of the plotted raw output from the PFS. It shows the spectral reflectance between 400-2500 nm (.4-2.5μm), including filter changes as described in the specifications of the circular-variable filter wheel (Appendix Five). These spectral plots are the individual spectra of replicate samplings of saline and non-saline sites and include the wavelength overlap near 700 nm (A) and the gap between 1200 and 1300 nm (B). The spikes associated with the water

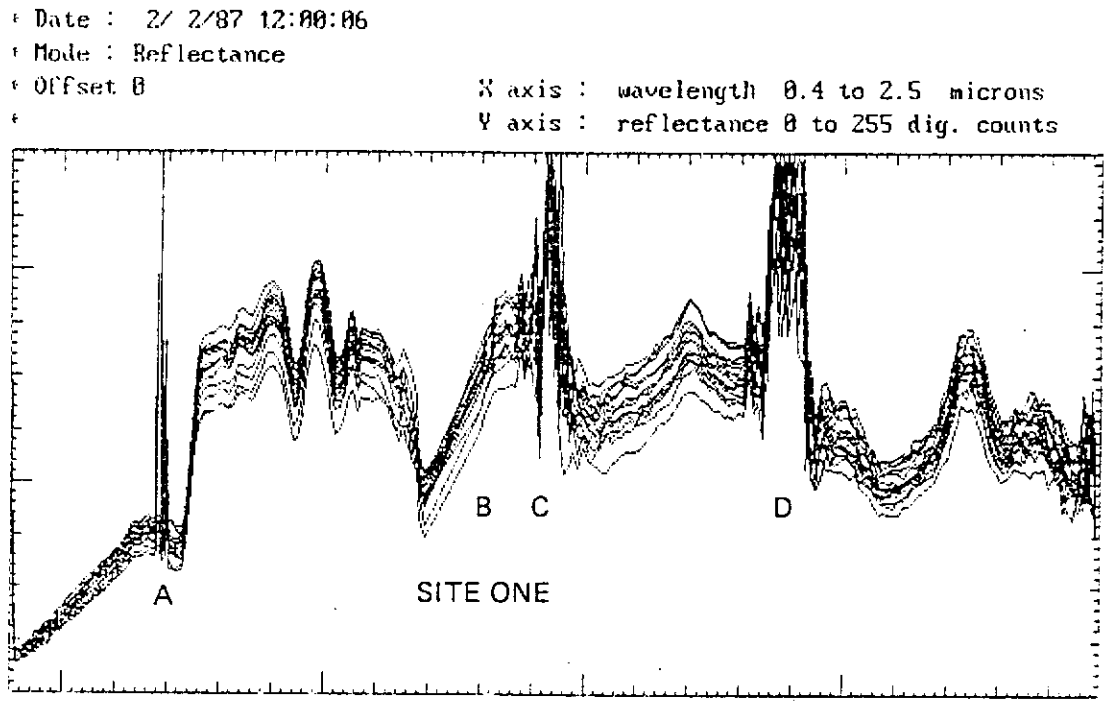

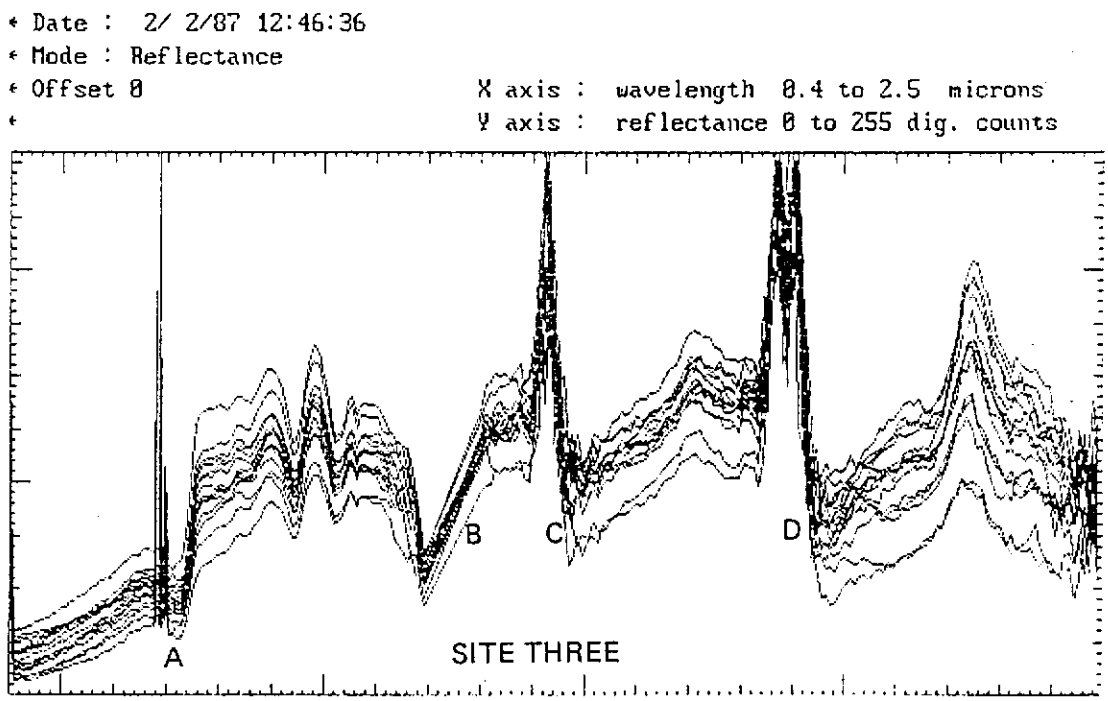

Figures Fourteen and Fifteen. Raw PFS data from site 1 (non-saline) top, and 3 (saline) bottom, in February 1987. These are examples of the actual display output produced in the field, and shows the variability of aproximately 30 spectra on each site. The horizontal scale represents the fully non-linear range of the instrument and the vertical scale is reflectance as a proportion of a $BaSO_4$ plate. A,B,C,+D are regions to be omitted from analysis.

absorption regions (C + D) are an instrumental artefact and have been masked from Figures Sixteen & Seventeen and also from the statistical analysis.

Figures Sixteen and Seventeen are of the mean spectra with a boundary on either side representing a confidence level of 95% around the mean(i.e. ± 2 std error). These masked spectra now have four discrete regions, and for the purpose of discussion here can be considered as the "visible", " the vegetative infrared", "1600 nm shortwave infrared (SWIR) Window" and the "2200 nm SWIR Window". Appendix Seven includes further examples of these spectra. These appendix figures have been photo-reduced and all dates for each site plotted together to enable visual comparison of seasonal trends as a function of wavelength.

The MKII Geoscan Scanner currently [1987] under construction will have wavebands as narrow as 15 nm in the visible and near infrared and 30 nm in the SWIR. The practical minimum bandwidth is determined by detector technology and optical constraints. The PFS samples 256, equally-spaced points on each rotation of the filter wheel which represents slightly over-or under-lapping parts of the spectrum between 400-2400 nm. Each segment of the wheel represents samples which range between 5 and 10 nm (see Appendix Five). The fine spectral structure, necessary to provide diagnostic information (see Figure Thirteen), can be accommodated with bandwidths of 30 nm and this figure was chosen to reduce the enormous dimensionality of the spectral data before analysis. Further data reduction was achieved with the omission, or masking, of instrumental artefacts and water absorption regions. This left 46 channels, each 30 nm wide, to be statistically analysed (see Table Three). These are referred to as "PFS bands".

		λ			λ			λ			λ			λ
1	1	0.400	8	57	0.652	17	101	0.972	21	151	1.506	32	201	1.975
	2	0.404		58	0.657		102	0.980		152	1.515		202	1.984
	3	0.409		59	0.662		103	0.988		153	1.525		203	1.993
	4	0.414		60	0.648	18	104	0.996	22	154	1.534	33	204	2.002
	5	0.418		61	0.653		105	1.005		155	1.543		205	2.012
	6	0.423		62	0.657		106	1.013		156	1.553		206	2.021
	7	0.428		63	0.662		107	1.021	23	157	1.562	34	207	2.031
2	8	0.432		64	0.667		108	1.029		158	1.571		208	2.040
	9	0.437		65	0.671	19	109	1.037		159	1.581		209	2.050
	10	0.442		66	0.676		110	1.045	24	160	1.590	35	210	2.059
	11	0.446		67	0.681		111	1.053		161	1.600		211	2.069
	12	0.451		68	0.685	20	112	1.061		162	1.609		212	2.078
	13	0.456		69	0.690		113	1.070	25	163	1.618	36	213	2.087
	14	0.460		70	0.695		114	1.078		164	1.628		214	2.096
3	15	0.465		71	0.680		115	1.086		165	1.637		215	2.106
	16	0.470		72	0.688		116	1.094		166	1.646		216	2.115
	17	0.475		73	0.696		117	1.102	26	167	1.656	37	217	2.125
	18	0.479	9	74	0.704		118	1.110		168	1.665		218	2.134
	19	0.484		75	0.712		119	1.118		169	1.675		219	2.143
	20	0.489		76	0.720		120	1.126	27	170	1.684	38	220	2.153
	21	0.493		77	0.728		121	1.135		171	1.693		221	2.162
4	22	0.498		78	0.736		122	1.143		172	1.703		222	2.171
	23	0.503	10	79	0.745		123	1.151	28	173	1.712	39	223	2.181
	24	0.507		80	0.753		124	1.159		174	1.721		224	2.190
	25	0.512		81	0.761		125	1.167		175	1.731		225	2.200
	26	0.517		82	0.769		126	1.175	29	176	1.740	40	226	2.209
	27	0.521	11	83	0.777		127	1.183		177	1.750		227	2.218
	28	0.526		84	0.785		128	1.191		178	1.759		228	2.228
5	29	0.531		85	0.793		129	1.200	30	179	1.768	41	229	2.237
	30	0.535		86	0.801		130	1.207		180	1.778		230	2.246
	31	0.540	12	87	0.810		131	1.216		181	1.787		231	2.256
	32	0.545		88	0.818		132	1.224	31	182	1.796	42	232	2.265
	33	0.550		89	0.826		133	1.232		183	1.806		233	2.275
	34	0.554		90	0.834		134	1.240		184	1.815		234	2.284
	35	0.559	13	91	0.842		135	1.248		185	1.825	43	235	2.293
6	36	0.564		92	0.850		136	1.256		186	1.834		236	2.303
	37	0.568		93	0.858		137	1.265		187	1.843		237	2.312
	38	0.573		94	0.866		138	1.273		188	1.853	44	238	2.321
	39	0.578	14	95	0.875		139	1.281		189	1.862		239	2.331
	40	0.582		96	0.883		140	1.289		190	1.871		240	2.340
	41	0.587		97	0.891		141	1.297		191	1.881	45	241	2.350
	42	0.592		98	0.899		142	1.306		192	1.890		242	2.359
7	43	0.596	15	99	0.907		143	1.314		193	1.900		243	2.368
	44	0.601		100	0.915		144	1.322		194	1.909	46	244	2.378
	45	0.606		101	0.923		145	1.330		195	1.918		245	2.387
	46	0.610		102	0.931		146	1.339		196	1.928		246	2.396
	47	0.615	16	103	0.940		147	1.347		197	1.937		247	2.406
	48	0.620		104	0.948		148	1.355		198	1.946		248	2.415
	49	0.625		105	0.956		149	1.487		199	1.956		249	2.425
	50	0.629	17	106	0.964		150	1.496		200	1.965		250	2.434

Table Three. The Portable Field Spectroradiometer samples 250 channels. These have been subdivided into 46 bands, 30 nm wide, "PFS bands". They cover the regions which are free from instrumental problems or absorption features and were the basis of the statistical analysis.

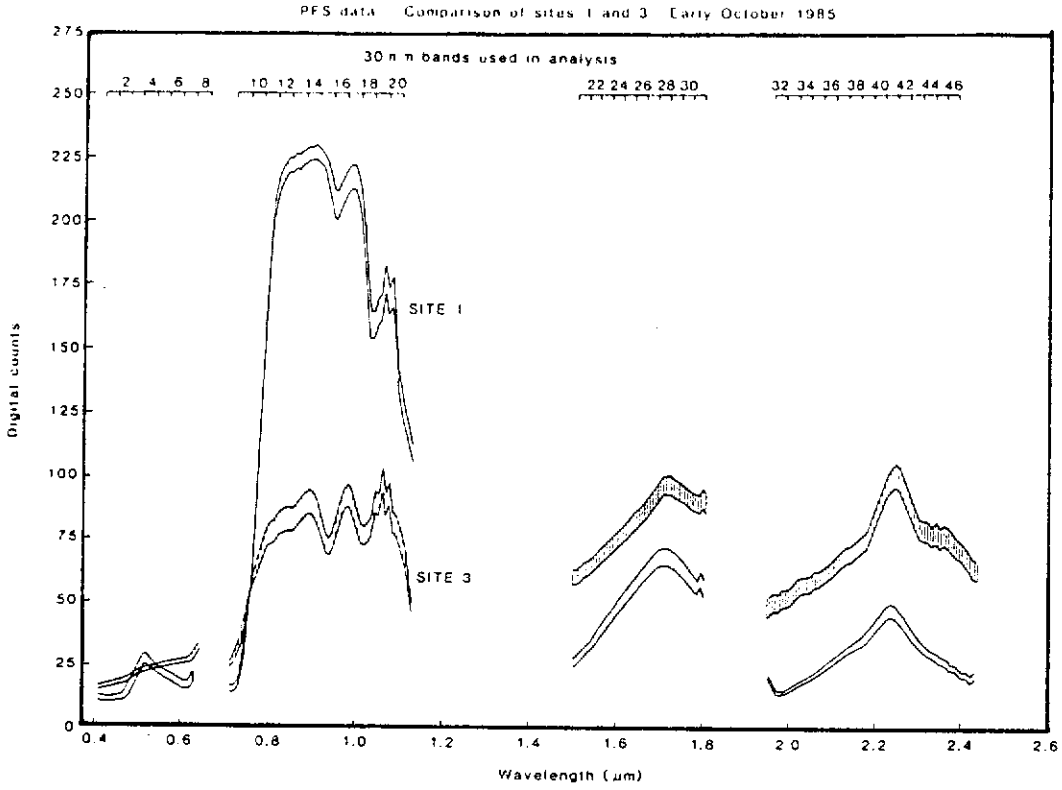

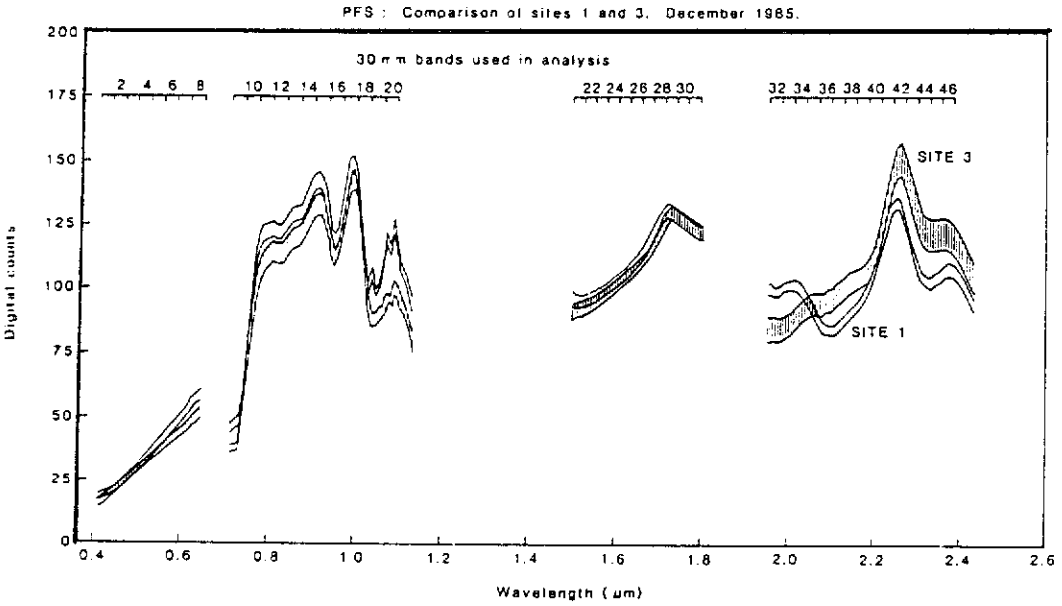

Figures Sixteen and Seventeen. Masked mean PFS data, and constructed "PFS bands", for October and December for sites 1 (non-saline) and 3 (saline). Note "green" (PFS band 4) peak and large difference between saline and non saline in the reflected infrared (PFS bands 10-20) in early October compared with small visible-near IR differences by December, and the inversely correlated bands in the SWIR region (PFS bands 32 and 36).

Using Figures Sixteen & Seventeen and Table Three as examples and with reference to Figure Thirteen, each of the regions was considered in the analysis of the PFS data as follows:

The "visible" (PFS bands 1-8, 400-660 nm) in "Early October" has a maxima relating to green and minima at blue and red. Following this region over all dates shows an increase in red as the vegetation "hays-off" over the summer which corresponds well with the visual appearance of the sites. The change being from vigorous lush green plant material in October, haying-off and exposing more underlying soil as the season progresses.

The second region of interest in the spectra show this phenology trend even more significantly. This region, "the vegetative infrared", or reflected infrared plateau, (PFS bands 9-20, 700-1086 nm) includes two absorptions which relate to moisture, and one which relates to chlorophyll, but the overall maxima, or plateau (Figure Thirteen) can be considered in three parts. The first is the start point of the region (PFS band 9, 700-730 nm) which is in a chlorophyll absorption region but still reflects a significant amount of visible red (red-edge). The other two parts are the maxima on either side of the central water absorption minima (PFS band 16, 930-960 nm). These relate to reflectance from chlorophyll on the left (PFS bands 10-15, 730-920 nm), and cellulose on the right (PFS bands 17-20, 960-1186 nm). The responses of these three parts of this region over time provides a descriptive analysis of the sites. Again, using Figures Sixteen & Seventeen as examples, the increase in visible red and cellulose and the relative decrease in chlorophyll also relates well to haying-off after the spring-flush, a feature not present on the saline sites.

The third region, the 1600 nm SWIR window (PFS bands 21-31, 1500-1800 nm), has changes in its overall reflectance but its relative shape does not appear to change significantly between dates or between sites.

The fourth region, "the short-wave infrared" (PFS bands 32-46, 1970-2390 nm) also has an increase in overall brightness between saline and non-saline, but of much more significance is the relative change of shape. Again using Figures Sixteen & Seventeen as an example, this region has a roughly central maxima (PFS band 41, 2220-2250 nm) with minima tapering down on either side. The changes to these minima can be explained by moisture content and cellulose (Figures Twelve and thirteen). Comparison of the spectral trends between dates for Figures Sixteen & Seventeen indicates the significance of this region for salinity studies.

The seasonal differences described in the site details for each date reflect well in the PFS data. The major differences in the late spring relate to vegetation vigour and greenness (i.e. PFS bands 12-20, 800-1180 nm), although the influence of the "haying-off" region increases in importance (PFS bands 36-41, 2080-2250 nm) by November. The PFS Band 32 (1970-2000 nm), which adjoins the 1900 nm water absorption, contributes throughout most dates. Its prominence in site separation is enforced in the summer and autumn.

Table Four compares all dates for the 8 Yalanbee sites and shows the best band combinations to discriminate between saline and non-saline sites. The canonical root, [bracketed], gives an indication of the degree of separation between sites. The statistical technique used produces linear combinations of the 46 bands which are uncorrelated within groups, and which maximise the ratio of the between to within group variability (Campbell 1982).

EARLY OCT [15.24]	20	2	32	35	33	9	12
16	17	15	36	41	19	40	27	30
23	5	13	3					
LATE OCT [7.31]	17	20	18	43	10	9	41
37	24	15	16	14	13	12	42	27
29	28	31	19					
NOVEMBER [11.05]	2	5	10	14	17	18	19
20	23	27	28	29	31	32	36	37
39	41	14	26					
DECEMBER [21.09]	9	43	32	36	11	31	21
22	34	40	42	12	33	39	23	18
17	19	20	16					
FEBRUARY [28.11]	10	43	32	21	4	37	23
31	26	17	19	18	20	28	24	36
42	27	46	7					
MARCH [38.76]	13	11	32	44	12	28	36
33	22	20	39	46	29	26	31	34
35	43	15	19					
*APRIL (4) [64.37]	32	35	21	20	17	33	34
18	16	15	19	9	31	28	27	26
30	45	40	42					
APRIL (8) [37.81] a	32	21	23	25	27	26	44
39	42	45	24	29	30	17	16	19
20	15	18	5					
**APRIL [55.12] b	32	21	9	7	46	11	16
17	15	19	20	35	5	2	39	37
14	44	8	30					
* JUNE [15.12]	13	10	32	35	12	2	9
20	6	30	23	46	34	33	36	26
5	25	18	15					

Table Four. Best 20 subsets of PFS bands, ranked on the best band, followed by the next best excluding the former, and so on.

There has been some down weighting of atypical variables. Due to computing limitations, a forward stepwise variable selection procedure was used to reduce the variables to the best subset of 20. This technique does not guarantee that the absolute "best" 20 variables are chosen but fixes the best variable followed by the next "best" two variables and so on to the "best" 20. From this reduced "best-subset", the procedure produces a linear combination of bands which is uncorrelated within-groups. A trade-off is then calculated involving the number of bands against the usefulness of that set of bands. This technique uses the Akaike Information Criteria (AIC) (Fujikoshi Y. 1985). These bands are then grouped to maximise the ratio of between-to-within group variability, and the analysis of this subset is subsequently presented in Table Five.

The high value for the canonical root in *April [(64.37)] in Table Four relates to the limited number of sites, only two saline and two non-saline sites. Data for April is also in two parts, (a & b), which represent different contrasts. In (a), a one dimensional contrast, some sites were well separated but site 5, a non-saline site, was included with the saline sites. In (b), a second one-dimensional contrast enabled strong separation of the errant site. The explanation was provided by reference to the field data. Site 5, the capeweed site, by its nature has little vegetative debris and by April the soil surface is exposed, similar to many saline sites. The second analysis showed that the separation does come from PFS band 32, further supporting the value of this short-wave infrared region.

The June analysis includes test sites other than Yalanbee and, although not ideal, is included to cover the shortfall of data due to instrument failure.

Table Five is a summary of the bands selected using the Akaike Information Criterion (AIC) to determine the minimum number of bands to achieve the maximum separation between sites. The minimum number varies between dates, with some cases as few as three bands providing the separation (i.e. November), and other dates when up to twelve bands are required to enable a similar degree of separation (i.e. April). The combination of bands with the minimum AIC is identified in Table Five, and graphically represented in Figure Eighteen. The contribution of each band to the coefficient is marked positively or negatively indicating the relationship of near or contiguous bands to one another. This shows whether such bands are correlated, or not, and whether they should be used as ratios or could be added together to provide broader bands. For example, useful bands displayed in Figure Eighteen for November are 15,16 and 17, but band 16 would be only of use if ratioed with 15 or 17. Conversely, in December, bands 16,17 and 18 could be combined as a single broad band. Band 32 would normally be used in a ratio with band 36 which is highlighted in Figure Seventeen for the PFS data and supports the laboratory data in Figure Nine.

The AIC calculation is based on the log of the band and the log power of each band is summarised as a standardised vector (Table Six) and graphically represented with the AIC selected band combination (Table Five) in Figure Eighteen.

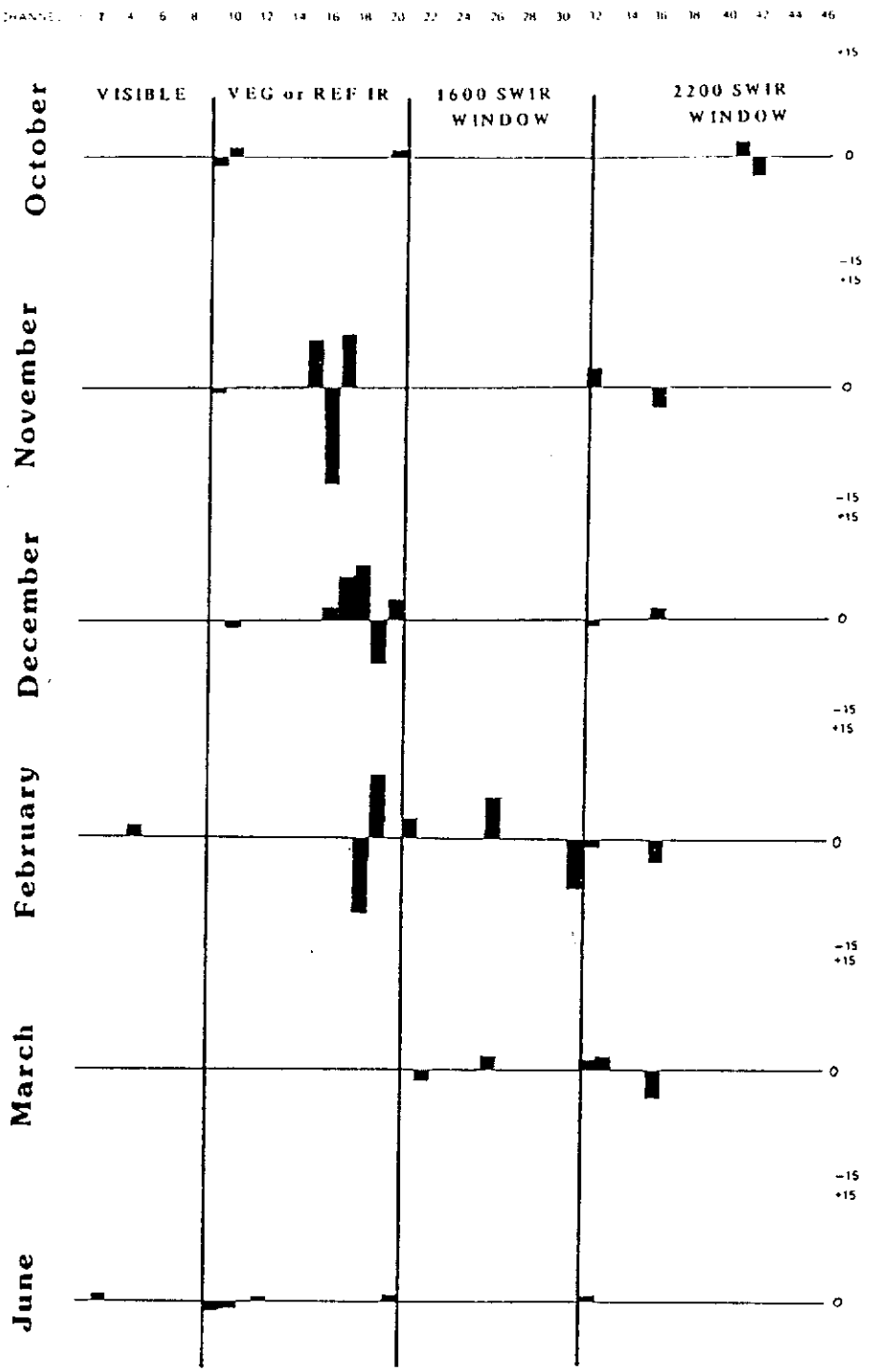

Figure Eighteen. Graphical representation of best combination of bands with Standardised Vectors for some of the dates. - This figure shows which bands, used either as combinations or as ratios depending on positive or negative vectors, best separated the sites on each date (also see Table Five). The vector illustrates the relative contribution of that band. These are fully documented in Table Six.

MONTH/ SEASON	MIN AIC(*)		PFS BANDS										
EARLY OCT	9-11	*(9)	+2		-10	+19	-20		+27	-28	-29	+31	-32
		(9)	2		10	19	20	23	27	28	29	31	
		(10)	2	5	10	19	20	23	27	28	29	31	
		(11)	2	5	10	19	20	23	27	28	29	31	32
LATE OCT.	5-6	(*5)	-9	+10		+20	+41	-42					
		(6)	9	10	17	20	41	42					
		(5)	9	10		20	41		43				
		(5)	9	10	17	20			43				
NOVEMBER	3-6	(3)						20	32	35			
		(4)	9	12					32	35			
		(5)			15	16	17		32		36		
		*(6)	-9		+15	-16	+17		+32		-36		
DECEMBER	8-10	*(8)	-9		+16	+17	+18	-19	+20	-32	+36		
		(9)	9		16	17	18	19	20	32	36	42	
		(10)	9	11	16	17	18	19	20	32	36	42	
FEBRUARY	7-9	*(8)	+4	-18	+19		+21		+26	-31	-32	-36	
		(8)	4	18	19		21		26	31	32		37
		(8)	4	18	19	20		24		31	32		37
		(8)	4	18	19	20	21	24		31			37
MARCH	3-6	(3)	12					32		36			
		(4)	12				28		33	36			
		*(5)			-22	+26		+32	+33	-36			
		(6)		20	22	26		32	33	36			
APRIL (1)	5-7	*(5)		+16	-17	+19	-20		+32				
		(6)		16	17	19	20			39	42		
		(6)	15	16	17	19	20		32				
		(7)	15	16	17	19	20	21	32				
APRIL (2)	10-12	*(12)	-9	+15	-16	+17	-18	+19	-20	+31	-33	+34	-40 +42
		(11)	9	15	16	17	18	19	20		33	34	40 42
		(12)	9	15	16	17	18	19	20	30	33	34	40 42
		(10)		15	16	17	18	19	20		33	34	40 42
JUNE	6-7	*(6)	+2		-9	-10	+12			+20	+32		
		(7)	2	6	9	10	12			20	32		
		(7)	2		9	10	12	13		20	32		
		(7)	2		9	10	12		18	20	32		

Table Five. Minimum band subsets from the "Best-20" analysis. The * indicates the minimum AIC score used to prepare Figure Eighteen. The + or- indicates the positive or negative relationship of bands to one another.

Month/ Season	Min AIC	Standardised Vector					
October(E)	(9)	+.64	-.78	+5.89	-4.96	+6.54	-1.63
		-9.54	+5.52	-.87			
October(L)	(5)	-1.07	+1.38	+.81	+2.05	-2.35	
November	(6)	-.69	5.91	-11.92	+6.73	+2.59	-2.26
December	(8)	-.81	+1.55	+4.62	+6.42	-5.58	+2.52
		-.85	+1.25				
February	(8)	+1.68	-9.07	+7.81	+2.34	+5.11	-5.88
		-.84	-2.72				
March	(5)	-1.2	+1.83	+1.62	+1.83	-3.53	
April [1]	(5)	+10.0	-19.24	+15.87	-7.12	+.74	
April [2]	(12)	-.34	+5.03	-11.76	+15.51	-13.28	+6.88
		-2.22	+.54	-3.49	+3.34	-2.56	+1.97
June	(6)	+.72	-1.2	-.83	+.55	+.87	+.47

Table Six. Standardised vectors of minimum AIC number of bands. Examples of these are graphically produced in Figure Eighteen, which also shows the location of these PFS bands.

3.2.5 AIRCRAFT SCANNER DATA

As mentioned in the methodology section, eleven sets of data were analysed from Yalanbee Experiment station. These data sets were collected from Geoscan airborne scanning missions over the eight sites between December 1984 and March 1987. The sites were displayed on an image processing system (IPS) using an enhancement which gave good visual discrimination between sites (see Figure Four). The site centres were located using the zooming capabilities of the IPS, and the pixel values for a 3x3 area and their coordinates were extracted for statistical analysis using robust canonical variate analysis (Campbell 1982). This procedure, as used to analyse the "best 20" subset of PFS data, produces linear combinations of spectral bands which are uncorrelated within groups and which maximize the ratio of between to within group variability. Atypical pixels are also identified and downweighted. The aim of the procedure is to produce a lower dimensional representation of the data which can be plotted to reveal group differences.

At each date the eight 3x3 pixel sites were supplemented by additional training sites of cover types and land surfaces surrounding the study sites to improve the estimation of the within-groups variation. The between-groups variability was computed from the means of the eight training sites only and also for a contrast of the non-saline sites 1,2,5 and the saline sites 3,4,6.

Table Seven gives the canonical root (ratio of between-to-withingroup variability) for the contrast between the

saline and non-saline sites. In this table the higher the canonical root the greater the separability between saline and non-saline sites on that date.

Since the within-group variability is estimated using different additional training sites at different dates, the canonical root may show some variability due to these different training sites. However, the general conclusions drawn from the table are unaffected.

	1984	1985	1986	1987
JAN	N/A*			9.624
FEB			2.665	
MAR		3.190	4.192	14.06
JUN			2.918*	
AUG			17.08	
SEP			19.14	
NOV		15.09	1.972	
DEC	5.16			

Table Seven. Canonical roots for the saline versus non-saline contrast for each data using Geoscan bands 1 to 9. * Limited no. of variables.

Table Seven shows that the best discrimination in the Yalanbee sites occurs in August/September [heights canonical roots of 17.08 and 19.14]. This is also supported by plots of the canonical variates for the eight group analysis and the saline/ nonsaline contrast. This supports previous assumptions that the "spring-flush" (refer to Section 1.2.3) enables separation between sites given that there is little or no growth on the saline sites at this time. Good separation between sites persists into March 1987, but February and November 1986 stand out as not showing these differences. Heavy cyclonic rain resulted in early germination in February 1986.

These canonical roots in Table Seven are based on using Geoscan bands 1 to 9 (Figure Two) for each date. All possible subsets calculations were made at each date to determine the best single

band, followed by the best two bands in combination, etc., up to the best five bands for discriminating between saline and non-saline sites. Table Eight includes these results.

	1984	1985	1986	1987
JAN				(3)(2,4)(2,3,4) (2,3,4,8)(2,3,4,7,8) MCR 9.283
FEB			(3)(3,5)(3,6,8) (3,4,6,8)(2,3,4,6,8) MCR 2.634	
MAR		(3)(1,3)(1,3,9) (1,3,8,9)(1,3,5,8,9) MCR 2.858	(4)(3,4)(3,4,8) (3,4,8,9)(1,3,4,8,9) MCR 3.899	(3)(3,6)(3,6,8) (2,3,6,8)(2,3,5,6,8) MCR 13.504
JUN		(4)(4,5)(3,4,5) (1,3,4,5)(1,2,3,4,5) MCR 2.918*		
AUG		(4)(4,8)(4,6,7) (4,5,6,7)(4,5,6,7,8)		MCR 16.721
SEP			(4)(3,4)(3,4,6) (3,4,5,6)(1,3,4,6,9) MCR 18.224	
NOV		(9)(3,9)(3,7,9) (3,4,7,9)(1,3,4,7,9) MCR 14.440	(4)(1,4)(4,7,8) (4,6,7,8)(1,4,6,7,8) MCR 1.942	
DEC	(6)(1,6)(4,6,9) (4,5,6,9)(4,5,6,7,9) MCR 5.131			

* ONLY 5 VARIABLES

Table Eight. Best subsets of band combinations when 1,2,3,4 or 5 bands are used for discrimination between saline and non saline sites. The maximum canonical root (MCR) for subsets of size 5 is also given.

Before conclusions can be drawn from these data, it is important to not only consider which band, or combination of bands, is giving the available separation, but also the magnitude of the separation as measured by the maximum canonical root (MCR).

As mentioned earlier, and displayed in Figure Nineteen, the maximum separability appears to occur in August-September. In each case the best single band was band four (Table Eight), a reflected infrared band between 830-870 nm. In September, the visible-red band (Geoscan band three, between 650-770 nm) with Geoscan band four gave the best two-band combination and this is further improved by the near infrared Geoscan band six, between 1980-2080 nm. In August, the best three Geoscan bands included the highly correlated short wave infrared Geoscan bands six (1980-2080 nm), seven (2160-2190 nm) and eight (2205-2234 nm) as they all figured prominently. The explanation probably lies in the vigorous vegetation on the non-saline sites and the very strong water absorption effect on the saline sites. At the sampling time there was free water seeping from the surface of sites three, four and from part of six.

By November, the importance of Geoscan band four remains but is diminished, especially in 1985 which was a dryer finishing year than 1986. Also in November, the importance of the infrared Geoscan bands seven, eight and nine, and band six by December, has increased significantly. This is probably a result of "haying-off" of the vegetation on the non-saline sites, persistent thin green halophytic vegetation on the saline sites which still display some bare but now dryer soil. Dry vegetation has specific cellulose absorption characteristics (refer Figure Thirteen).

In January 1987, heavy pasture residue persisted on non-saline sites leaving a highly reflective surface when compared with the

non-saline areas, and this would explain the high contribution toward the separation from Geoscan band three, the visible red, followed by visible yellow-green and reflected infrared from bands two and four. This persisted into February, although the inclusion of bands six and eight could be attributed to the increasing appearance of bare saline soil. Continued grazing of the sites, especially in 1987, continued that trend until the break of season.

Figure Nineteen graphs the effectiveness of three-band combinations for discrimination between sites. It is compiled from all Geoscan imaging dates and orders the significance of the three-band combinations on the basis of the maximum canonical root (MCR) as chosen in Table Eight. The relative effectiveness of other three-band combinations is almost as significant as the highest scoring combination.

The significance of Figure Nineteen therefore lies not in the best band combination on a specified date, but more importantly the trend indicated by those dates with an MCR above or below a figure of about five on the canonical root axis.

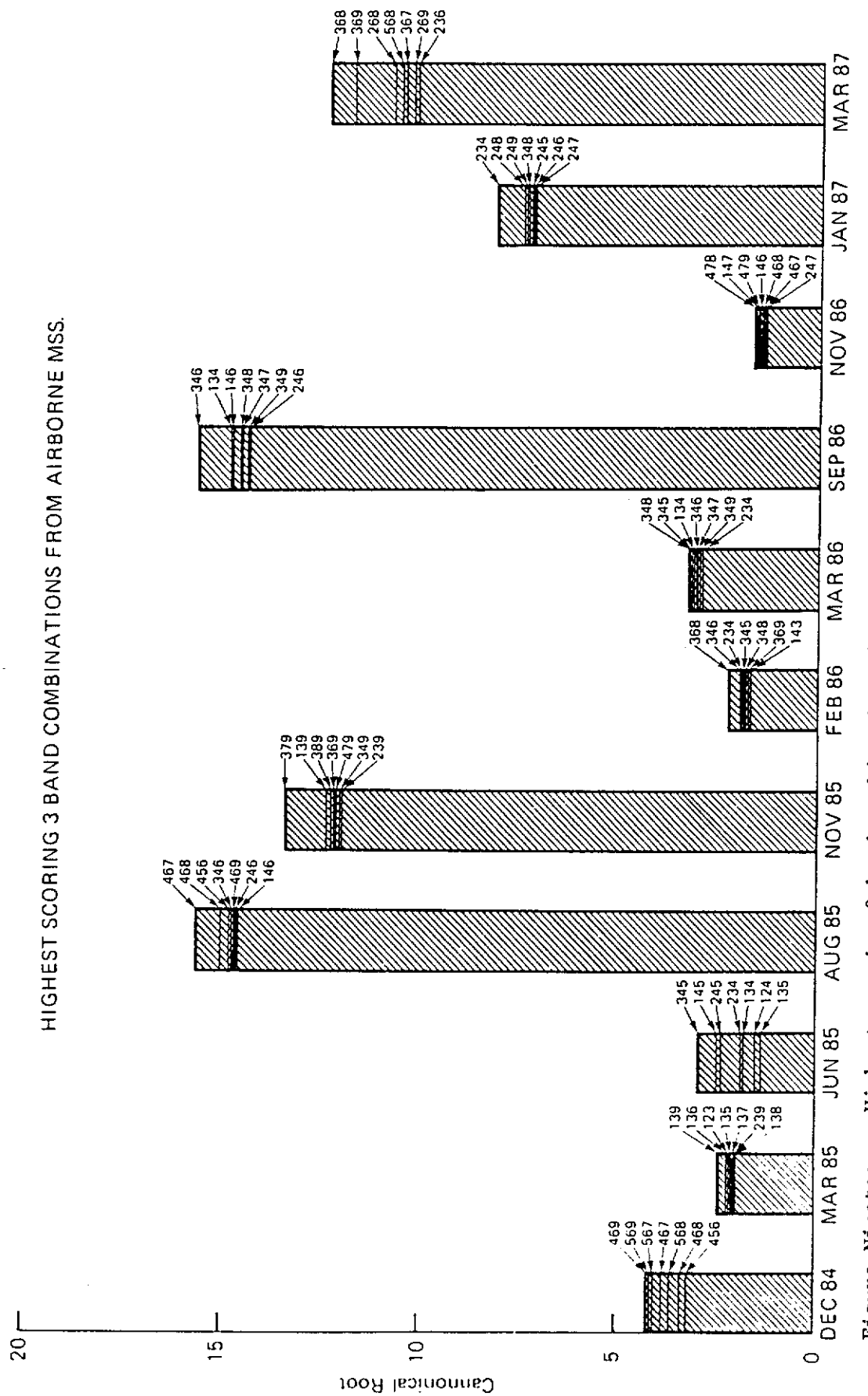

Figure Nineteen. Highest scoring 3 band combination of airborne MSS data.

3.2.6 Lowtran Plots

Initial laboratory analysis of spectra, as discussed in Section 3.2.1, and supported by analysis of the PFS data, indicated that discrimination of the saline sites could come from spectral bands near the major water absorption regions, especially beyond 1900 nanometers (Section 3.2.4).

To obtain a quantitative analysis of the atmospheric absorption, the Lowtran 6 computer code was used (see Section 1.2.7). This program was installed on a microcomputer and was run using the following range of atmospheres and configurations.

1. Tropical (moist)
2. Mid latitude summer
3. Mid latitude winter
4. Sub arctic summer
5. Sub arctic winter (dry)
6. Low altitude (1220 m)
7. Medium altitude (2220 m)
8. High altitude (3050 m)
9. High altitude off nadir (45°)

Figure Twenty represents two hypothetical 30 nm bands centred at 1985 nm and 2100 nm for a range of atmospheres. The selection was based on a minimum transmittance of 60%. Calculations for off-nadir and different altitudes were made using the mid-latitude summer model with low aerosol contamination, based on a "rural" atmosphere between 100-300 km from the coast (refer Table Ten). Consideration was made of the conditions under which satellite imagery or airborne scanner acquisitions are generally made.

In the Agricultural belt of W.A., cloud free conditions mostly occur when dry easterly (continental) winds prevail. Most scanner flights were flown when winds were from the SE, E or NE.

The use of the mid-latitude summer model atmosphere may have been conservative, and the summer Geoscan imagery may have been acquired with dryer atmospheres than used in the calculations. Unfortunately no meteorological data, which could have been incorporated into the calculations, were available for the atmosphere near the sites.

Tables Ten - Thirteen are extracts from the Lowtran 6 calculations and are presented as examples of data input and output. Table Ten includes the 4 parameter cards for atmosphere model, aerosol model, slant path, and frequency and range respectively, as adjusted for mid-latitude summer, at 2.2 km height for a clear atmosphere. Table Eleven is a summary of the atmospheric parameters used in the calculation and the geometry selected to represent the sub-nadir viewing of the scanner at 2.2 km (7000 ft approx. AGL)

Table Twelve gives an example of the output, with a 30 nm band, centred on 1985 nm delineated. A band in this region is proposed in the conclusions as being useful in this exercise. Signal to noise ratios of better than 50:1 are normal under most flying conditions for the MKI Scanner (N Andronis, Geoscan Pty Ltd pers. comm.). Total transmission (refer to column in Table Twelve) averaged over the band is .6127 or of the order of greater than 60%+ reflectance return to an airborne detector. The majority of the absorption is due to H_2O (column 4), with a lesser contribution from the more uniformly mixed CO_2 (column 5) which has absorptions at 1960 nm and 2000 nm (La Rocca 1978, p.5-57). Other atmospheric gases and

aerosols have minor influence at this wavelength. By comparison, Table Thirteen, with a 30 nm band centred at 2100 nm, has a total transmission average of .9008. The absorptions over this band are about the same for the aerosols but significantly less from H_2O and CO_2.

```
1                        ***** LOWTRAN 6 *****
0 CARD 1  *****    2    2    0    0    0    0    0    0      .000      .000
0 CARD 2  *****    1    0    0    3    0    0   23.000      .000      .000      .000
0 CARD 3  *****       .000     2.200       .000       .000      .000      .000    0
0 CARD 4  *****  4165.000  8335.000     5.000
0 PROGRAM WILL COMPUTE TRANSMITTANCE
0 ATMOSPHERIC MODEL
          TEMPERATURE =    2     MIDLATITUDE SUMMER
          WATER VAPOR =    2     MIDLATITUDE SUMMER
          OZONE       =    2     MIDLATITUDE SUMMER
0 AEROSOL MODEL
          REGIME                    AEROSOL TYPE            PROFILE                    SEASON

          BOUNDARY LAYER (0-2 KM) RURAL                     23.0 KM VIS AT SEA LEVEL
          TROPOSPHERE  (2-10KM)   TROPOSPHERIC              TROPOSPHERIC               SPRING-SUMMER
          STRATOSPHERE (10-30KM)  BACKGROUND STRATO         BACKGROUND STRATO          SPRING-SUMMER
          UPPER ATMOS (30-100KM)  METEORIC DUST             NORMAL
0 SLANT PATH, H1 TO H2
          H1    =       .000 KM
          H2    =     2.200 KM
          ANGLE =       .000 DEG
          RANGE =       .000 KM
          BETA  =       .000 DEG
          LEN   =    0
0 FREQUENCY RANGE
           V1 =      4165.0 CM-1  (      2.40 MICROMETERS)
           V2 =      8335.0 CM-1  (      1.20 MICROMETERS)
           DV =         5.0 CM-1
1
```

Table Ten. Parameters used for Lowtran 6 model for Midlatitude Summer, Midaltitude which represents conditions occurring during scanner flights over Yalanbee Experiment Station.

SLANT PATH PARAMETERS IN STANDARD FORM

H1	=	.000 KM
H2	=	2.200 KM
ANGLE	=	.000 DEG
PHI	=	180.000 DEG
HMIN	=	.000 KM
LEN	=	0

1CALCULATION OF THE REFRACTED PATH THROUGH THE ATMOSPHERE

I	ALTITUDE FROM (KM)	TO (KM)	THETA (DEG)	DRANGE (KM)	RANGE (KM)	DBETA (DEG)	BETA (DEG)	PHI (DEG)	DBEND (DEG)	BENDING (DEG)	FBA (ME
	H1 TO H2										
1	.000	1.000	.000	1.000	1.000	.000	.000	180.000	.000	.000	957.3
2	1.000	2.000	.000	1.000	2.000	.000	.000	180.000	.000	.000	851.5
3	2.000	2.200	.000	.200	2.200	.000	.000	180.000	.000	.000	792.3

CUMULATIVE ABSORBER AMOUNTS FOR THE PATH FROM H1 TO Z

J	Z (KM)	TBAR (K)	H2O	CO2+ (SCALED LOWTRAN UNITS)	O3	HNO3 (ATM CM)	O3 UV (ATM CM)	CNTMSLF1 (MOL CM-2)	CNT (MOL
1	1.000	291.98	1.062E+00	8.252E-01	2.700E-03	.000E+00	2.800E-03	8.033E+20	6.73
2	2.000	287.48	1.688E+00	1.512E+00	5.284E-03	.000E+00	5.600E-03	9.593E+20	1.27
3	2.200	284.60	1.776E+00	1.636E+00	5.789E-03	.000E+00	6.162E-03	8.873E+20	1.36

J	Z (KM)	N2 CONT	MOL SCAT	AER 1	AER 2	AER 3	AER 4	CIRRUS
1	1.000	6.455E-01	8.830E-01	1.263E-01	.000E+00	.000E+00	.000E+00	.000E+00
2	2.000	1.169E+00	1.691E+00	2.054E-01	.000E+00	.000E+00	.000E+00	.000E+00
3	2.200	1.261E+00	1.831E+00	2.166E-01	6.927E-04	.000E+00	.000E+00	.000E+00

Table Eleven. Atmospheric and Geometric parameter summary used in Lowtran 6 calculation.

FREQ CM-1	WAVELENGTH MICRONS	TOTAL TRANS	H2O TRANS	CO2+ TRANS	OZONE TRANS	N2 CONT TRANS	H2O CONT TRANS	MOL SCAT TRANS	AEROSOL TRANS	HNO3 TRANS	AEROSOL ABS	INTEGRATED ABSORPTION
4915.	2.035	.8642	.9427	.9751	1.0000	1.0000	.9710	.9999	.9683	1.0000	.0040	111.837
4920.	2.033	.8472	.9330	.9662	1.0000	1.0000	.9707	.9999	.9683	1.0000	.0040	112.591
4925.	2.030	.8214	.9240	.9463	1.0000	1.0000	.9703	.9999	.9682	1.0000	.0040	113.464
4930.	2.028	.7980	.9184	.9254	1.0000	1.0000	.9699	.9999	.9682	1.0000	.0040	114.494
4935.	2.026	.7733	.9184	.8972	1.0000	1.0000	.9695	.9999	.9682	1.0000	.0040	115.627
4940.	2.024	.7273	.9093	.8527	1.0000	1.0000	.9691	.9999	.9682	1.0000	.0040	116.991
4945.	2.022	.6770	.8964	.8055	1.0000	1.0000	.9687	.9999	.9681	1.0000	.0040	118.606
4950.	2.020	.6090	.8667	.7497	1.0000	1.0000	.9682	.9999	.9681	1.0000	.0040	120.561
4955.	2.018	.5413	.8480	.6816	1.0000	1.0000	.9676	.9999	.9681	1.0000	.0040	122.854
4960.	2.016	.5205	.8498	.6544	1.0000	1.0000	.9669	.9999	.9680	1.0000	.0040	125.252
4965.	2.014	.5149	.8667	.6353	1.0000	1.0000	.9662	.9999	.9680	1.0000	.0040	127.677
4970.	2.012	.5197	.8806	.6317	1.0000	1.0000	.9654	.9999	.9680	1.0000	.0040	130.078
4975.	2.010	.5170	.8819	.6280	1.0000	1.0000	.9646	.9999	.9680	1.0000	.0040	132.493
4980.	2.008	.5083	.8729	.6243	1.0000	1.0000	.9637	.9999	.9679	1.0000	.0040	134.951
4985.	2.006	.4125	.8445	.5243	1.0000	1.0000	.9628	.9999	.9679	1.0000	.0040	137.889
4990.	2.004	.3759	.8252	.4894	1.0000	1.0000	.9619	.9999	.9679	1.0000	.0040	141.009
4995.	2.002	.3982	.8107	.5284	1.0000	1.0000	.9606	.9999	.9679	1.0000	.0040	144.018
5000.	2.000	.4634	.8042	.6207	1.0000	1.0000	.9594	.9999	.9678	1.0000	.0040	146.701
5005.	1.998	.5850	.7900	.7989	1.0000	1.0000	.9578	.9999	.9678	1.0000	.0040	148.776
5010.	1.996	.6504	.7801	.9010	1.0000	1.0000	.9563	.9999	.9677	1.0000	.0040	150.524
5015.	1.994	.6665	.7675	.9401	1.0000	1.0000	.9549	.9999	.9676	1.0000	.0041	152.191
5020.	1.992	.6772	.7599	.9662	1.0000	1.0000	.9534	.9999	.9675	1.0000	.0041	153.805
5025.	1.990	.6855	.7539	.9877	1.0000	1.0000	.9516	.9999	.9674	1.0000	.0041	155.378
5030.	1.988	.6822	.7480	.9929	1.0000	1.0000	.9497	.9999	.9673	1.0000	.0041	156.967
5035.	1.986	.6721	.7390	.9925	1.0000	1.0000	.9475	.9999	.9673	1.0000	.0042	158.607
5040.	1.984	.6606	.7299	.9901	1.0000	1.0000	.9452	.9999	.9672	1.0000	.0042	160.304
5045.	1.982	.6336	.7064	.9844	1.0000	1.0000	.9422	.9999	.9671	1.0000	.0042	162.136
5050.	1.980	.6144	.6927	.9767	1.0000	1.0000	.9391	.9999	.9670	1.0000	.0042	164.064
5055.	1.978	.5704	.6560	.9617	1.0000	1.0000	.9352	.9999	.9669	1.0000	.0043	166.212
5060.	1.976	.5323	.6295	.9391	1.0000	1.0000	.9313	.9999	.9669	1.0000	.0043	168.551
5065.	1.974	.4856	.5903	.9201	1.0000	1.0000	.9249	.9999	.9668	1.0000	.0043	171.123
5070.	1.972	.4626	.5941	.8769	1.0000	1.0000	.9185	.9999	.9667	1.0000	.0043	173.810
5075.	1.970	.4302	.5903	.8283	1.0000	1.0000	.9102	.9999	.9666	1.0000	.0044	176.659
5080.	1.969	.4059	.5865	.7939	1.0000	1.0000	.9019	.9999	.9665	1.0000	.0044	179.630
5085.	1.967	.3343	.5219	.7437	1.0000	1.0000	.8914	.9999	.9664	1.0000	.0044	182.956
5090.	1.965	.2563	.3920	.7740	1.0000	1.0000	.8809	.9999	.9664	1.0000	.0044	186.667
5095.	1.963	.2348	.3526	.7939	1.0000	1.0000	.8681	.9999	.9663	1.0000	.0045	190.493
5100.	1.961	.1854	.2880	.7791	1.0000	1.0000	.8555	.9999	.9662	1.0000	.0045	194.566
5105.	1.959	.1984	.3287	.7467	1.0000	1.0000	.8366	.9999	.9661	1.0000	.0045	198.574
5110.	1.957	.2021	.3573	.7158	1.0000	1.0000	.8182	.9999	.9660	1.0000	.0045	202.563
5115.	1.955	.1861	.3431	.7086	1.0000	1.0000	.7924	.9999	.9660	1.0000	.0046	206.633
5120.	1.953	.1841	.3287	.7557	1.0000	1.0000	.7674	.9999	.9659	1.0000	.0046	210.712
5125.	1.951	.1690	.3004	.7964	1.0000	1.0000	.7313	.9999	.9658	1.0000	.0046	214.869
5130.	1.949	.1536	.2797	.8162	1.0000	1.0000	.6968	.9999	.9657	1.0000	.0046	219.099
5135.	1.947	.0750	.1364	.8630	1.0000	1.0000	.6602	.9999	.9656	1.0000	.0047	223.724
5140.	1.946	.0896	.1650	.8998	1.0000	1.0000	.6254	.9999	.9656	1.0000	.0047	228.276
5145.	1.944	.0569	.1080	.9335	1.0000	1.0000	.5847	.9999	.9655	1.0000	.0047	232.991

Table Twelve. Lowtran 6 calculation for 1945-2035 nanometres. The 30 nm wide, centered on 1985 nm is outlined.

FREQ CM-1	WAVELENGTH MICRONS	TOTAL TRANS	H2O TRANS	CO2 TRANS	OZONE TRANS	N2 CONT TRANS	H2O CONT TRANS	MOL SCAT TRANS	AEROSOL TRANS	HNO3 TRANS	AEROSOL ABS	INTEGRATED ABSORPTION
4665.	2.144	.9361	.9920	.9995	1.0000	1.0000	.9737	.9999	.9696	1.0000	.0041	78.022
4670.	2.141	.9387	.9946	.9997	1.0000	1.0000	.9738	.9999	.9696	1.0000	.0041	78.329
4675.	2.139	.9373	.9931	.9998	1.0000	1.0000	.9738	.9999	.9696	1.0000	.0041	78.642
4680.	2.137	.9355	.9911	.9998	1.0000	1.0000	.9738	.9999	.9696	1.0000	.0041	78.965
4685.	2.134	.9321	.9876	.9997	1.0000	1.0000	.9738	.9999	.9695	1.0000	.0041	79.304
4690.	2.132	.9284	.9838	.9997	1.0000	1.0000	.9738	.9999	.9695	1.0000	.0041	79.662
4695.	2.130	.9242	.9795	.9995	1.0000	1.0000	.9738	.9999	.9695	1.0000	.0041	80.041
4700.	2.128	.9190	.9741	.9994	1.0000	1.0000	.9738	.9999	.9694	1.0000	.0041	80.446
4705.	2.125	.9089	.9636	.9993	1.0000	1.0000	.9738	.9999	.9694	1.0000	.0041	80.901
4710.	2.123	.9081	.9631	.9990	1.0000	1.0000	.9738	.9999	.9694	1.0000	.0041	81.361
4715.	2.121	.9067	.9619	.9987	1.0000	1.0000	.9737	.9999	.9694	1.0000	.0041	81.827
4720.	2.119	.9058	.9613	.9983	1.0000	1.0000	.9737	.9999	.9693	1.0000	.0041	82.298
4725.	2.116	.9076	.9636	.9981	1.0000	1.0000	.9737	.9999	.9693	1.0000	.0041	82.760
4730.	2.114	.9110	.9676	.9977	1.0000	1.0000	.9737	.9999	.9693	1.0000	.0041	83.205
4735.	2.112	.9135	.9707	.9973	1.0000	1.0000	.9736	.9999	.9693	1.0000	.0041	83.638
4740.	2.110	.9163	.9741	.9969	1.0000	1.0000	.9736	.9999	.9692	1.0000	.0041	84.056
4745.	2.107	.9146	.9726	.9966	1.0000	1.0000	.9736	.9999	.9692	1.0000	.0041	84.483
4750.	2.105	.9079	.9659	.9963	1.0000	1.0000	.9736	.9999	.9692	1.0000	.0040	84.944
4755.	2.103	.9015	.9596	.9957	1.0000	1.0000	.9736	.9999	.9691	1.0000	.0040	85.436
4760.	2.101	.8906	.9490	.9948	1.0000	1.0000	.9736	.9999	.9691	1.0000	.0040	85.983
4765.	2.099	.8862	.9458	.9932	1.0000	1.0000	.9736	.9999	.9691	1.0000	.0040	86.552
4770.	2.096	.8911	.9537	.9904	1.0000	1.0000	.9736	.9999	.9691	1.0000	.0040	87.097
4775.	2.094	.8950	.9608	.9875	1.0000	1.0000	.9736	.9999	.9690	1.0000	.0040	87.622
4780.	2.092	.8994	.9682	.9849	1.0000	1.0000	.9736	.9999	.9690	1.0000	.0040	88.124
4785.	2.090	.8991	.9707	.9820	1.0000	1.0000	.9735	.9999	.9690	1.0000	.0040	88.629
4790.	2.088	.8954	.9693	.9794	1.0000	1.0000	.9735	.9999	.9689	1.0000	.0040	89.152
4795.	2.086	.8903	.9653	.9778	1.0000	1.0000	.9735	.9999	.9689	1.0000	.0040	89.701
4800.	2.083	.8838	.9613	.9748	1.0000	1.0000	.9735	.9999	.9689	1.0000	.0040	90.281
4805.	2.081	.8787	.9596	.9709	1.0000	1.0000	.9735	.9999	.9689	1.0000	.0040	90.888
4810.	2.079	.8622	.9550	.9574	1.0000	1.0000	.9735	.9999	.9688	1.0000	.0040	91.577
4815.	2.077	.8464	.9524	.9424	1.0000	1.0000	.9734	.9999	.9688	1.0000	.0040	92.345
4820.	2.075	.8279	.9524	.9219	1.0000	1.0000	.9734	.9999	.9688	1.0000	.0040	93.206
4825.	2.073	.8032	.9482	.8985	1.0000	1.0000	.9733	.9999	.9688	1.0000	.0040	94.190
4830.	2.070	.7805	.9458	.8754	1.0000	1.0000	.9732	.9999	.9687	1.0000	.0040	95.287
4835.	2.068	.7702	.9451	.8645	1.0000	1.0000	.9732	.9999	.9687	1.0000	.0040	96.436
4840.	2.066	.7683	.9412	.8661	1.0000	1.0000	.9731	.9999	.9687	1.0000	.0040	97.595
4845.	2.064	.7654	.9377	.8661	1.0000	1.0000	.9731	.9999	.9686	1.0000	.0040	98.768
4850.	2.062	.7644	.9349	.8676	1.0000	1.0000	.9730	.9999	.9686	1.0000	.0040	99.946
4855.	2.060	.7620	.9320	.8676	1.0000	1.0000	.9730	.9999	.9686	1.0000	.0040	101.136
4860.	2.058	.7557	.9311	.8614	1.0000	1.0000	.9729	.9999	.9686	1.0000	.0040	102.358
4865.	2.055	.7493	.9367	.8491	1.0000	1.0000	.9728	.9999	.9685	1.0000	.0040	103.611
4870.	2.053	.7521	.9443	.8455	1.0000	1.0000	.9727	.9999	.9685	1.0000	.0040	104.851
4875.	2.051	.7707	.9537	.8581	1.0000	1.0000	.9726	.9999	.9685	1.0000	.0040	105.997
4880.	2.049	.8005	.9602	.8853	1.0000	1.0000	.9725	.9999	.9685	1.0000	.0040	106.995
4885.	2.047	.8335	.9602	.9219	1.0000	1.0000	.9723	.9999	.9684	1.0000	.0040	107.827
4890.	2.045	.8516	.9544	.9479	1.0000	1.0000	.9722	.9999	.9684	1.0000	.0040	108.570

Table Thirteen. Lowtran 6 calculation for 2045-2145 nanometres. The 30 nm wide band centered on 2100 nm is outlined.

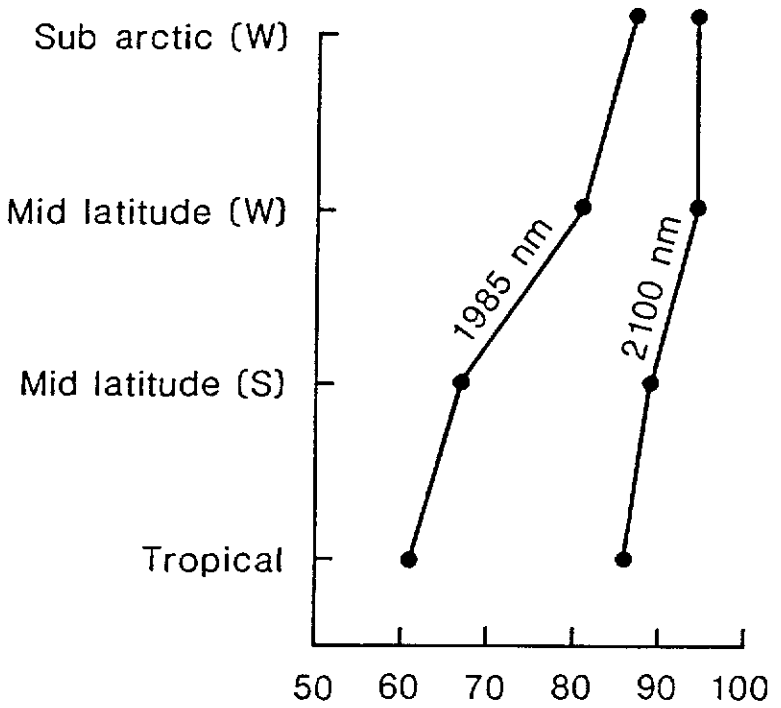

Figure Twenty. Transmission at 1985 nm and 2100 nm for a range of atmospheric conditions - calculated from Lowtran 6 model.

3.3.1 Geophysical Electromagnetic Techniques

The measurements made with the EM-38 are incorporated in Appendix Two B and show the general relationship of electrical conductivity (EC 1:5) to the electromagnetic (EM) response. Further analysis of these data is presented in Table Fourteen. These are compiled from the field data and represent an averaged EC and an averaged EM.

The EC readings were summed for the whole profile, for all dates and may not accurately represent the total salt in the profile as the sampling is weighted toward the surface, i.e. the sampling method is based upon 0-1, 1-5 and 5-10 cm, then a sample from between 20-30 and 40-50 etc. It does, however, provide descriptive differences between sites.

The EM data are meaned for all dates for both vertical and horizontal measurements, with standard deviations also shown. The ratio of vertical over horizontal is calculated, and when compared with EC, show a value greater than one for the non-saline sites and values less than one for the saline sites.

The relationship with EC is not strong but the groups separate well. This also applies when both the vertical and horizontal data are plotted separately against EC. The limited number of sites precludes a definitive statistical interpretation beyond the presentation of these trends. The variability between dates is shown in the large standard deviations. This variability is greater, proportionally, on the non-saline sites and this may be partly due to instrumental calibration between dates.

	Ave bulk EC (mS/cm)	Vertical Em(sd) Em(sd)	Horizontal Em(sd) Em(sd)	Ratio V/H
Site 5	111.9	29(8)	15(9)	1.93
1	113.6	22(26)	11(6)	2.00
2	141.6	23(11)	22(8)	1.04
6	2203.1	105(22)	140(23)	0.75
8	3870.5	44(1)	60(5)	0.73
3	5398.9	128(11)	150(33)	0.85
7	5801.2	81(16)	140(11)	0.57
4	6583.6	154(26)	225(61)	0.68

Table Fourteen. The average figures for Electrical Conductivity, with standard deviations (sd) and Electromagnetic Conductivity for all sites on all dates.

When the sites were chosen at Yalanbee, the most significant factor influencing selection was vegetation, followed by the uniformity of the soil profile (see site description in Appendix Two). At that time EM-38 readings were also recorded over the chosen sites. Initial EM anomalies could not always be reconciled with vegetation variation, although most sites produced EM values which were fairly consistent within sites and significantly different between sites. The higher readings related well to the visible signs of increased salinity. One exception, site 6, which had a uniform stand of Cotula sp. gave different EM readings on the northern half of the site to those recorded on the southern side. During the study this difference has been noted to correspond to

vegetation and salinity readings. In hindsight, site 6 could have had its position adjusted on the evidence of the initial EM-38 readings.

The EM values presented in Appendix Two are for both vertical and horizontal configurations of the instrument. The relative responses reflected in the V/H readings is due to differences in conductance between surface and subsoil materials. The horizontal dipole is more sensitive to near surface materials whereas the vertical dipole is less-sensitive to those materials. High ratios then represent areas where salts are concentrated at the surface relative to the subsoil salinity.

This has application at Yalanbee as some seeps are forming from groundwaters which have low salinities but, due to high evaporation and poor drainage, the surfaces may develop high salt concentrations. In other instances, due to free drainage, the lower soil horizons can be the site for salt accumulation with minimal surface expression.

3.4 CONCLUSIONS

3.4.1 Conclusions - Restatement of Aims

The aim of the study was to provide a scientific basis for the design of a remote sensing system which would be of maximum benefit for the early identification of land affected by salinisation. From the work, it has been possible to assess the relative usefulness of current and future spaceborne and airborne land sensor packages covering the visible, reflected and shortwave infrared regions, using examples from Yalanbee, but with conclusions which should be more widely applicable.

Concisely, the aims were:-

1) to optimise maximum spectral discrimination at useable wavelengths, or multiple wavebands, which describe the characteristics of saline and non-saline lands;

2) to determine those times in a normal year's agricultural cycle at which maximum discrimination can be made; and

3) to determine the most appropriate ground spatial resolution to discriminate saline affected targets from the surrounding land.

Based on these aims, conclusions are categorised under spectral, spatial and temporal aspects.

3.4.2 Spectral Aspects

Spectral analysis applied to a range of saline and non-saline soils under controlled laboratory conditions gave the first indications that existing spectral bands incorporated in current sensors are not optimal for the delineation of salinity. The modification to infrared spectra by moisture is well documented, but the effects of the minor saline constituent, $MgCl_2$, in otherwise apparently air dry soil samples had not been previously documented

in this context. The hygroscopic nature of $MgCl_2$ slightly modified the spectra of soils by extending the effect of the water absorption over the region of 1970-2000 nm.

The importance of the $MgCl_2$ effect on the infrared spectrum for salinity studies was initially thought to be only where field conditions were as close as possible to bare dry soil, as would be the case in summer fallow, or post-cropping with heavy grazing, but this proved not to be so. Bands from both the Portable Field Spectroradiometer (PFS) and the Geoscan Airborne Scanner, located close to the 1900 nm water absorption band, proved to have significant value for the discrimination between saline and non-saline sites, even when relatively well vegetated, as is the case at Yalanbee. This would be applicable only when the ground surface was relatively dry (ie.no recent rain or dew).

This study did show, however, that the volunteer vegetation was the best indicator of phenological impact from increasing salinity. On well-vegetated pasture sites the effects of salinity were most noticeable in the spring-flush, the period of maximum growth. Unfortunately, confusion could exist between sites which had degraded vegetation vigour but were not saline. Such degradation could come from cultural, nutritional or grazing pressures.

The statistical analysis of the Geoscan Airborne Multispectral Scanner data demonstrated that the discrimination between saline and non-saline sites was a result of the effects of salt on vegetation. The examples given in Figure Nineteen demonstrated that maximum discrimination occurred in months of maximum vegetation growth. Also of note is the very significant contribution of Geoscan band 6 (1980-2080 nm) toward the maximum three-band combinations which are dominated by the reflected infrared Geoscan band 4 (830-870 nm) and red Geoscan band 3 (650-700 nm). Other high scoring, three-band

combinations, as illustrated in Figure Nineteen, invariably featured combinations of the reflected and shortwave infrared with specific emphasis on Geoscan band 6 (1980-2080 nm).

The spectral data analysed from the Portable Field Spectroradiometer (PFS) included narrower bands throughout the visible reflected and shortwave infrared. This instrument includes the 1600 nm window region where Landsat Thematic Mapper has a band (band Five 1550-1750 nm) which is not covered by the MKI Geoscan Scanner. If the scanner included all the bands analysed from the PFS data it most certainly would reflect more closely the PFS results, especially in the SWIR region. This study is not trying to establish which existing scanner band is optimum but whether there are better bands which could be used.

Unfortunately, instrument problems occurred with the PFS during the August-September period in 1986 and extensive cloud coverage affected the same period in 1985. As a consequence, the PFS data were not available to coincide with aircraft scanner data for that period.

The PFS data did show the value of narrow bands, used as ratios, in the reflected infrared regions (Figure Eighteen), specifically between 900-1100 nm. The data also showed that those bands (PFS bands 15-20) provided maximum information between November and February (Summer). The PFS data also showed the value of the shortwave infrared region (SWIR), especially PFS bands 32 and 36, when used as ratios over the same summer period.

Spectra from laboratory prepared samples (Figure Ten, Section 3.2.1) and field spectra (Figure Seventeen, Section 3.2.4) suggest that the moisture effect correlates with salinity in the spectral region of 1970-2000 nm.

Figure Thirteen, Section 3.2.2, the spectra of vegetation, clearly shows increased reflectance due to cellulose (1923 nm), before the major cellulose absorption near 2080 nm. Dry plant material was plentiful on most saline sites, but unfortunately its salinity level was never measured. This appears to be an oversight. It may be reasonable to assume that salt crystals, through "rainsplash", wind, dust, etc., were on the surfaces of dry plant material on the saline sites, and probably in similar proportions to the amount on the soil surface.

The combined effect of greater amounts of cellulose, from plant debris, on non-saline sites and the moisture absorption effect on the saline sites, even though significant cellulose occurs on them, probably are the contributing factors to the salt-related trend which occurs between 1970-2000 nm. Put simply, there is a compounding effect of both absorption due to moisture and reflectance due to cellulose in this region.

In order to put the relative usefulness of these results into perspective, comparison with alternative sensing systems is appropriate. The visible scanner bands one, two and three are covered by panchromatic and colour photography and some of the Landsat MSS and TM bands (Figure Two). Infrared photography, and both Landsat systems, in a broad band, cover the Geoscan airborne scanner bands four and five. The Landsat TM also has a broad band which covers scanner bands seven and eight. Assuming that the best three band combinations were chosen (this being the practical minimum number of bands for colour display when using an image processing system for semi-automated digital image analysis), maximum information needed to discriminate the sites would rarely be available using existing satellite sensors.

The Thematic Mapper (TM) instrument on the Landsat series of satellites has seven bands, six fall within the range of the PFS.

TM Band	Band Range (nm)		PFS Band(s)	Band Range (nm)
1	(450- 520)	-	2 - 4	(430- 530)
2	(520- 600)	-	4 - 6	(500- 600)
3	(630- 690)	-	8	(630- 660)
4	(760- 900)	-	11 - 14	(770- 890)
5	(1550-1750)	-	23 - 29	(1560-1750)
6	(2080-2350)	-	36 - 45	(2080-2350)

Comparison of these bands with the best combinations determined from Table Five (Section 3.2.4) shows two major deficiencies in the TM instrument for the detection of salinity: firstly, the omission of bands in the (700-730 nm), (730-760 nm), (900-1100 nm) and (1970-2070) region; secondly, broader bands lose the diagnostic value of the narrow bands which make up the broad structure, (refer to Figure Eighteen, Section 3.2.4).

3.4.3 Temporal Aspects

It is not possible to give a precise answer to which is the best time of the year for salinity mapping. Geoscan Scanner data indicated that excellent discrimination was possible in September 1986. Data from August and November 1985 also scored highly (Figure Nineteen, Section 3.2.5). On the basis of visual observations the sites had maximum floristic differences during the period of maximum growth or the "spring-flush" (September-November). Unfortunately, the airborne data from November 1986 did not support this. It is apparent that there is high variability relating to seasonal conditions. The variability for the three March flights can be

explained by unseasonal rainfall in two of the three years. Generally, spring appears to offer most chance of success for spectral separation of sites based on the vegetation's response to salinity. But, there are significant factors which will detract from this conclusion. The high probability of cloud makes large-scale operations unreliable, low sun angles limit the hours of the day when sensing is possible, high soil moisture status would negate the value of a shortwave infrared band, and cropping practices detract from the diagnostic value of volunteer plant successions.

For these reasons, it is suggested that a later time in the year be considered. This would be December to February, which is supported by the PFS data analysis. Figure Eighteen (Section 3.2.4) suggests that the inclusion of a shortwave infrared band centred on 1985 nm would permit a wider time window available for optimum discrimination between saline and non-saline sites. This could span September through to February/March. The use of this band has the added advantage of discrimination on land surfaces which are devoid of vegetation.

3.4.4 Spatial Aspects

It is not possible to be definitive on what spatial resolution is optimum for salinity studies. This study concentrated on image pixels which ranged from approximately 5 metres to 80 metres. Examples were presented of Landsat MSS nominal 80 metre (57x79 sample size) which did show the major saline components of the Crocodile Creek catchments, Figure Six, (Section 3.1.1) but was of little or no use for describing the active saline encroachment occurring on the study sites. Figure Seven A,B,C, and D, are enhancements of Geoscan Airborne Scanner images. With the nominal 5 metre resolution, the region of active encroachment and individual tree mortalities can be seen. The precise area of salt-affected land could be measured, at this spatial resolution, as well as any ground-based system. Intermediate resolutions of 10,15 and 20 metres were synthesised by pixel merging and demonstrate the image degradation.

Landsat Thematic Mapper, with 30 metre resolution (Figure Seven), shows the major saline components and is also capable of resolving the features of saline encroachment which were the basis of the study sites. The French satellite SPOT-Image has a 3 band multispectral scanner with nominal 20 metre resolution.

Points made in Section 1.2.5 indicated that the effects of salinity, in dryland agriculture areas, can range in their appearance from subtle changes in vegetation to high contrast, often linear, features. These features reflect the level of severity of the salinisation which is somewhat arbitrary depending on the specific land use. The impact of the severity would be quite different in, for example, a high value horticultural crop, but this study has concentrated on dryland agriculture; therefore the

determination of spatial resolution is based upon that land use and its economic management.

From the examples given the spatial resolution by SPOT (20 m) and Thematic Mapper (30 m) would appear to be satisfactory for most regional or management scale determinations. Any less definition of ground features would result in errors of omission and any more would become prohibitively expensive in both data collection and processing.

There is possibly a case for variable spatial resolution if a long-term monitoring program is to be implemented. Infrequent, but strategically timed, high resolution imaging could provide details of specific changes resulting from salinity; this would then complement mapping of forest clearing or land use changes which are often the cause of salinity and would be generally evident on lower resolution acquisitions.

REFERENCES

Australian Bureau of Statistics (1974). Condnsed. Biometric Section WA Department of Agriculture Bulletin 3999 pp.1-9 Malcolm C.V. and Stoneman T.C.

Bettenay, E., Blackmore, A.V. and Hingston, f.J. (1962). Salinity investigations in the Belka Valley, Western Australia. CSIRO Division of Soils Divisional Report 10/62.

Bettenay, E., (1986). Salt affected soils in Australia. Reclamation and Revegetation Research, 5: 167-179.

Bowers, S.A. and Hanks, R.J. (1965). Reflection of Radiant Energy from soils. Soil Science, 100 (2) pp.130-138.

Bowker, D.E., Davis, R.E., Myrick, D.L., Stacy, K. and Jones, W.T. (1985). Spectral reflectances of natural targets for use in remote sensing studies. NASA Reference Publication 1139, p 3.

Bunnik, N.J.J. (1981). Fundamentals of Remote Sensing, Beug, A. (ed.) Applications of Remote Sensing for Agriculture Proc. Forecasting, p.47.

Burvill, G.H. (1947). Soil salinity in the agricultural area of Western Australia. Journal Australian Institute of Agricultural Science, 13, 9-19.

Campbell, N.A. (1982). Robust Procedures in Multivariate Analysis I. Robust Canonical Variate Analysis. Journal of the Royal Statistical Society, 31 (1) pp.1-8.

Carver, K.R. and Bush, T.F. (1979). Airborne multispectral remote sensing of saline seeps: The 1978 Harding County South Dakota Sth Dakota experiment. New Mexico State University, Las Cruces New Mexico, NASA-NA59-15421.

Chaturvedi, L., Carver, K.R., Harlan, J.C., Hancock, G.D., Small, F.V., and Dalstead, K.J. (1983). Multispectral remote sensing of saline seeps. IEEE. Geoscience and Remote Sensing Vol. GE21 no.3 pp.239-251.

CSIRO Spectral Library (1987). EGRU Workshop - Remote Sensing in Mineral Exploration CSIRO Division Exporation Geosciences Australia.

Dalstead, K. J. The use of remote sensing technology to detect saline seeps. MSc thesis North Dakota State University, N.D.

DeJong, E., Ballantyne, A.K., Cameron, D.R. and Read, D.W.L. (1979). Measurement of apparent electrical conductivity of soils by an EM induction probe to aid salinity surveys. Journal of the Soil Science Society of America No. 43, 810-813.

Dimmock, G.M., Bettenay, E. and Mulcahy, M.J. (1974). Salt content of lateritic profiles in the Darling Range Western Australia. Australian Journal of Soil Research 12, pp.63-69.

Estes, J.E. and Simonette, D.S. (1978). Remote sensing detection of perched water tables, a pilot study. Contribution No. 175, California Water Resources Centre, University of California, Davis, California, USA.

Fujikoshi, Y., 1985. Multivariate Analysis, Ch. 6 pp.219-236. Ed. Krishnaiah. Elsevier Science Publication.

Henschke, C.J. (1980). Saltland in statistics - the 1979 saltland survey. Journal Agriculture of Western Australia 21, 116-119.

Hick, P.T. and Tapley, I.J. (1982). Window mount for acquisition of small format aerial photography from high wing aircraft. RPS Aeronewsletter of the Royal Photographic Society of Great Britian p.6 Vol. 26

Hick, P.T., Davies, J.R. and Steckis, R.A. (1984). Mapping of dryland salinity in Western Australia using remotely sensed data. Satellite Remote Sensing, Proceedings of the 10th International Conference Remote Sensing Society Reading U.K. 1984. pp.343-350.

Hick, P.T. and Macham, W. (1986). Modifications to a spectrophotometer to enable presentation of soils and unconsolidated materials. Paper No. 86-036 Photogrammetric Engineering and Remote Sensing (submitted).

Hingston, F.J. and Gailitis, V. (1976). The variation of salt precipitated over W.A. Australian Journal Soil Research, 14, 319-335.

Hirschfeld, T (1985). Salinity determination using NIRA. Applied Spectroscopy Vol.39, No.4, p.740.

Honey, F.R., Hick, P.T., Steckis, R.A. and McCulloch, L.M. (1984). Mapping dryland salinity using remotely sensed data. Proceedings of the Third Australasian Remote Sensing Conference, Queensland, pp.44-47.

Honey, F.R. and Daniels, J. (1984). Mapping mineralization in Australia with a new high resolution scanner and spectroradiometer data. Proc. of ERIM 3rd Thematic Conference Remote Sensing for Geology, Colorado.

Honigs, D.E., Freelin, J.M., Hieftje, G.M., Hirschfeld, T.B. (1983). NIR Reflectance analysis by Gauss-Jordan Linear Algebra. Applied Spectroscopy 37, 6, p.491.

Johnston, C.D., Williamson, D.R. and Trotter, C.L. (1982). Ionic composition and electrical conductivity relationships of soil water relationships from south Western Australia. CSIRO Land Resources Management Tech. Pap. No. 12, 1-10.

Kneizys, F.X., Chetwynd Jr, J.H., Clough, S.A., Shettle, A.P., Abreu, L.W. Fenn, R.W., Gallery, W.O. and Selby, J.E.A. (1983). Atmospheric Transmittance/Radiance Computer Code Lowtran 6 Report No. AFGL-TR-83 0187 Air Force Geophysics Laboratory, Massachusetts 01731.

Krishnan, P., Alexander, J.D., Butler, B.J. and Hummel, J.W. (1980). Reflectance technique for predicting soil organic matter. Journal of the Soil Science Society of America pp.44: 1282-1285.

La Rocca, A.J. (1978). Atmospheric Absorption. Chap. 5, Fig 5-13 in The Infrared Handbook, Wolfe and Zissis eds. Env. Res. Inst. of Michigan, Ann Arbor.

McNeill, J.D. (1980). Survey Interpretation Techniques EM38 p.1-15. Geonics Company Report, Ontario, Canada.

Malcolm, C.V. and Stoneman, T.C. (1976). Salt encroachment, the 1974 saltland survey. Journal of Agriculture Western Australia 17, pp.42-49.

May, G.A. and Petersen, G.W. (1975). Spectral signature selection for mapping unvegetated soils. Remote Sensing of Environment. 4: 211-220.

May, G.A. and Peterson, G.W. (1976). Use of Landsat-1 data for the detection and mapping of saline seeps in Montana. Space & Science Engineering Laboratory Pennsylvania State Univ. ORSEL-SSEL Technical Report 4.76.

Murphy, J.T. and Smoot, R.C. (1982). Physics, Principles and Problems. pp. 267. Pub. Merrill Colomb. Ohio

Northcote, K.H. (1960). Fourth Edit 1979) A Factual key for the recognition of Australian soils. CSIRO Pub. Rellim Technical Publications Adelaide South Australia.

Northcote, K.H. and Skene, J.K.H. (1972). Australian soils with saline and sodic properties. Soil Publication No. 27, CSIRO Melbourne.

Nulsen, R.A. (1981). Salt affected land in the Shire of Wongan-Ballidu, Western Australia. Australian Journal Soil Research 19, 87-91.

Peck, A.J., Thomas, J.F. and Williamson, D.R. (1983). Effects of man on salinity in Australia. Water 2000 Consultants Report Vol. 8. Dept of National Development and Energy, Canberra pp. 1-78.

Piper, C.S. (1944). Soil and Plant Analysis. Loss of Ignition. pp.59. University of Adelaide Press. Adelaide.

Schaper, P.W. (1976). Infrared Sensing Methods. Ch. 3, pp. 84-109. Remote Sensing for Environmental Sciences. Ed. E. Schanda. Springer-Verlag (Publ.)

Stoner, E.R. and Baumgardner, M.F. (1981). Soil spectral characterization 1981 International Geoscience and Remote Sensing Symposium, Vol II, 1426-1436.

Stoner, E.R., Baumgardner, M.F., Weismiller, R.A., Biehl, L.L. and Robinson, B.F. (1980b). Extension of laboratory-measured soil spectra to field conditions. Journal of Soil Science and Society of America 44: 572-574.

Teakle, L.J.H. (1938). Soil salinity in Western Australia. Journal of Agriculture Western Australia (2nd series), 15, 434-452.

Williams, B.G. (1983). Electromagnetic induction as an aid to salinity investigations in N.E. Thailand. Tech. Memo. 83/27 CSIRO Inst. of Biological Resources, DLWR Canberra.

Williamson, D.R. (1984). Salinization. Vol. 2, 1-45 pp. Eighth Groundwater School. Australian Mineral Foundation.

Wolfe, W.L. (1965). (ed.) Handbook of Military Infrared Technology. Dept of Navy. Office of Naval Research.

APPENDIX ONE

SENSOR	SPACECRAFT	CHANNELS	BANDPASSES (um)	SPATIAL RESOLUTION AT NADIR (GROUND IFOV)	REPEAT CYCLE	SWATH WIDTH
AVHRR	NOAA series polar orbiting	2 in VNIR 3 in MIR	0.58-0.68 VIS 0.72-1.1 NIR 3.55-3.93 MIR 10.3-11.3 MIR 11.5-12.5 MIR	1100 m	twice daily 10-day cycle	2400 km
HCMR	HCMM	1 in VNIR 1 in MIR	0.5-1.1 10.5-12.5	500 m 600 m	16 days	700 km
MSS	LANDSAT 1,2,3	4 IN VNIR	0.5-0.6 VIS 0.6-0.7 VIS 0.7-0.8 NIR 0.8-1.1 NIR	79 m (bands 4-7)	18 days	185 km
TM	LANDSAT	TM 1 TM 2 TM 3 TM 4 TM 5 TM 7 TM 6	0.45-0.52 VIS 0.52-0.60 VIS 0.63-0.69 VIS 0.76-0.90 NIR 1.55-1.75 SWIR 2.08-2.35 SWIR 10.4-12.5 MIR	30 m 120 m	16 days	185 km
SIR-A RADAR	SPACE SHUTTLE	1	L band 23.5 cm HH Polarization	40 m approx	Experiment only	50 km
SIR-B RADAR	SPACE SHUTTLE	1	L band 23.5 cm HH Polarization	14-46 m variable	Experiment only	50 km
HRV	SPOT	3 in VNIR 1 panch-romatic	0.5-0.59 VIS 0.61-0.68 VIS 0.79-0.89 VIS 0.51-0.73 VIS	20 m 10 m	26 days 1 and 4-5 days off nadir	60 km + 60 km off nadir stereo capability
LFC	SPACE SHUTTLE	Colour/ CIR		20 m (height resoln + 9 m)	Experiment only	208 km

Appendix One (a) Some important spaceborne sensors used in Australia - compiled by the CSIRO Division of Mineral Physics and Mineralogy.

SENSOR	CHANNELS	BANDPASSES (μm)	SPATIAL RESOLUTION AT NADIR (GROUND IFOV)	SWATH WIDTH
SAR and SLAR	1	X band 2.5–4.0 cm L band 13–30 cm	Variable	Variable
ATM	8 in VNIR 2 in SWIR 1 in MIR	0.42–0.45 0.45–0.52 (TM1) 0.52–0.60 (TM2) 0.605–0.625 0.63–0.69 (TM3) 0.695–0.75 0.76–0.90 (TM4) 0.91–1.05 1.55–1.75 (TM5) 2.08–2.35 (TM7) 8.5–13.0 (TM6)	5 m or 2.5 m at 2000 m AGL (2.5 mrads and 1.25 mrads)	3 km at 2000 m AGL
GEOSCAN MSS Mk-I	5 in VNIR 4 in SWIR 4 in MIR	0.45–0.50 0.55–0.60 0.65–0.70 0.83–0.87 0.93–0.97 1.98–2.08 2.16–2.19 2.205–2.235 2.30–2.40 8.5–8.9 9.7–10.1 10.8–11.2 11.5–12.0	5 mrads (10 m at 2000 m AGL)	5.12 km at 2000 m AGL
MEIS-II	8 in VNIR	Range .38–1.1 μm Bands selected by front-mounted filters	Variable, typically 5 to 10 metres	39.66°
AIS	128 in SWIR	Range 1.2–2.4 μm Sampling interval 9.6 nm	1.91 mrad/pixel (5.7 m at 3000 m AGL)	183.3 m at 3000 m AGL
TIMS	6 in MIR	8.2–8.6 μm 8.6–9.0 9.0–9.4 9.4–10.2 10.2–11.2 11.2–12.2	2.5 mrad/pixel (5 m at 2000 m AGL)	3.4 km at 200 m AGL
COLLINS SPECTRO-RADIOMETER	512 in VNIR 64 in SWIR	Range 0.35–1.0 μm Range 1.9–2.5 μm	20 m at 610 m AGL	20 m profile at 610 m AGL
CSIRO POD SPECTRO-RADIOMETER	512 in VNIR 128 in SWIR	Range 0.4–1.1 Range 1.3–2.5 Sampling interval 5 nm	35 mrads	-
DAEDALUS SCANNER	10 in VNIR	Range 0.4–1.1 μm 10 channels selected from 32 minimum channel width 20 nm	2.5 mrads (5 m at 2000 m AGL)	-

Appendix One (b) Some important airborne sensors used in Australia - compiled by the CSIRO Division of Mineral Physics and Mineralogy.

APPENDIX TWO

Site Descriptions at Selection 15.10.85

(see Species List, Appendix Three, and Methodology Section)

SITE ONE.

This is the non saline site and is in a midslope position in a discrete minor valley. At the time of selection, it carried a very dense pasture stand. Its composition by volume was 40% subterranean clover, 40% capeweed, the remainder being an even mixture of grasses including hordeum (H. lep), soft brome and winter grass.

Horizon	Depth - cms	Description Dy 3.62
A1	0-1	Very dark greyish brown (10 YR 3/2) organic sandy loam, few small Fe gravels pH 6.0, clear change to
A2	1-40	brown (10 YR 3/3) gritty clayey sand, moderate Fe gravel, clear change to
B	40 -	brownish yellow (10 YR 6/8) mottled yellow (10 YR 7/8) gritty medium clay, abundant Fe gravel, pH 6.5.

SITE 1 DATE	DEPTH (CMS)	EC (1:5) ms/cm	AIR DRY % MOISTURE	EM V/H	RAINFALL SINCE PREV. SAMPLING	VEGETATION
15/10/85	0-1	71.3	13.5	18/9	4.6 mm	C/weed 40% H. lep 5% Cover 35% Vulpia 5% Brome 10% Poa 5% Lush vigorous pasture 15-20 cm deep uniform mixtures some capeweed in flower.
	1-5	36.6	9.0			
	5-10	32.2	8.3			
	20-30	34.2	7.8			
	40-50	24.4	5.7			
28/10/85	0-1	377	13.0	81/4	7.6	C/weed 10% H. lep 10% Clover 60% Vulpia 10% Brome 10% Wimera Tr + Other Grasses. Dense mat of drying vegetation. C/weed collapsing, horizontal heads beginning to "Hay-off".
	1-5	64.6	5.5			
	5-10	26.7	2.2			
	20-30	21.3	2.0			
	40-50	17.3	2.3			
13/11/85	0-1	169	4.4	17/20	9.0	Completey "Hayed-off" - Brown/Grey/Yellow litter. No bare ground
	1-5	39	3.3			
	5-10	22	3.3			
	20-30	13	3.1			
	40-50	10	3.1			
16/1/86	0-1	379	0.6		12.9	6.12.85 dense dry vegetation. No bare ground.
	1-5	163	0.1			
	5-10	36.9	0.6			
	20-30	29.6	1.1			
	40-50					
6/2/86	0-1	422	0.0	6/10	0.0	Yellow grey "Hay" all dead. 60% flattened 40% standing. pH 6.02 (mean of 5 surface samples)
	1-5	855	0.2			
	5-10	134	1.3			
	20-30	49	1.2			
	40-50	50	6.9			
26/3/86	0-1	22.3	3.6	1/4	115.4	Rainfall caused good germination. Clover c/weed and grasses.
	1-5	24.1	2.7			
	5-10	23.6	2.4			
	20-30	45.4	2.6			
	40-50	101.6	2.8			
28/4/86	0-1	313	0.8	17/16	4.8	Some early germination still surviving - Heavily grazed. Clover and grasses.
	1-5	96	1.1			
	5-10	34	0.9			
	20-30	38	2.1			
	40-50	21	1.6			
5/6/86	0-1	406	24.3	20/17	84.4	Good clover and some c/weed germination some residual grass stubble remaining.
	1-5	114	10.7			
	5-10	59	7.2			
	20-30	33	5.3			
	40-50	30	8.8			
19/8/86	0-1	353	48.6	18/17	282.6	Good clover + c/weed cover - some grasses
	1-5	43.5	16.0			
	5-10	28.7	12.8			
	20-30	36.1	13.1			
	40-50	31.3	13.3			
16/10/96	0-1	434	38.7	8/9	57.0	Clover 70% C/weed 20% H. lep+Vulpia+Wimera 10% Clover dom. grazed. Sparse c/weed flowers dense swath. Grasses flowering.
	1-5	48.4	12.9			
	5-10	32.8	8.9			
	20-30	29.4	7.1			
	40-50	34.9	10.0			
2/2/87	0-1	273	.1	16/15	53.0	Ungrazed dense dry clover/grass pasture, uniformly hayed off.
	1-5	80.8	.4			
	5-10	31.7	.8			
	20-30	25.3	2.7			
	40-50	24.7	4.1			
3/4/87	0-1	450	20.5*	17/14	15.5	Dry grazed clover and grass debris. 100% clover.
	1-5	170	4.7			
	5-10	96.5	4.9			
	20-30	35.0	4.1			
	40-50	18.2	4.8			

*light rain affected

SITE TWO.

This non-saline site carried a good pasture stand on a gravelly midslope position with a well drained A horizon. There was a mixture of 25% subterranean clover, 25% capeweed, 25% hordeum (H. lep), with the remainder being soft brome and other minor grass species.

Horizon	Depth - cms	Description - Ks Dy 5.62
A1	0-5	Very dark greyish brown (10 YR 3/2) organic sandy loam, moderate Fe gravel, pH 6.5, clear change to
A2	5-50	dark brown (10 YR 4/3) gritty clayey sand, abundant Fe gravel, clear change to
B	50 -	brownish yellow (10 YR 6/8) mottled yellow (10 YR 7/8) gritty medium clay, abundant Fe gravel, pH 6.5.

SITE 2 DATE	DEPTH (CMS)	EC (1:5) ms/cm	AIR DRY % MOISTURE	EM V/H	RAINFALL SINCE PREV. SAMPLING	VEGETATION
15/10/85	0-1	152	6.6	33/19	4.6 mm	C/weed 25% H. lep 25%
	1-5	92.6	5.2			Clover 25% Brome 20%
	5-10	58.8	4.0			Erodium Tr Vulpia 5%
	20-30	54.3	4.3			
	40-50					
					7.6	
28/10/85	0-1	322	4.0	22/23		C/weed 10% H. lep 35%
	1-5	56	2.0			Clover 25% Brome 30%
	5-10	51	2.6			Erodium Tr Vulpia Tr
	20-30	41	2.4			Rapidly haying-off.
	40-50	58	2.8			
					9.0	
13/11/85	0-1	140	1.5	25/30		Almost completey "Hayed-off"
	1-5	52	3.8			
	5-10	29	5.5			
	20-30	39	5.2			
	40-50	64	.8			
					12.9	
16/1/86	0-1	313	0.1			(6.12.85) dense dry vege-
	1-5	94	0.3			tation, other grey litter,
	5-10	59	0.6			some bare areas
	20-30	52	0.8			
	40-50					
					0.0	
6/2/86	0-1	851	0.0	6/10		Dense dry vegetation.
	1-5	195	0.2			Dry c/weed holding.
	5-10	78	0.8			pH 6.37 (mean of 5 surface
	20-30	58	1.7			samples)
	40-50	204	4.6			
					115.4	
26/3/86	0-1	193	2.3	12/15		Germination of c/weed.
	1-5	66.9	2.5			
	5-10	61.6	3.2			
	20-30	68.3	3.5			
	40-50	131	6.2			
					4.8	
28/4/86	0-1	297	0.5	30/29		Faint tinge of green
	1-5	105	1.1			vegetation. Mostly dry
	5-10	41	1.7			grass on gravelly surface.
	20-30	39	2.6			
	40-50	49	2.2			
					84.4	
5/6/86	0-1	478	21.0	36/30		Good c/weed and clover
	1-5	166	10.6			germination some grass
	5-10	115	8.8			stubble residue.
	20-30	89	8.5			
	40-50	336	15.5			
					282.6	
19/8/86	0-1	376	42.6	26/25		Clover + c/weed with
	1-5	75.9	15.4			some fine grasses.
	5-10	45.5	11.3			
	20-30	82.5	9.9			
	40-50	160	15.0			
					57.0	
16/10/86	0-1	559	26.7	19/20		Clover 85% C/weed 10%
	1-5	201	12.4			Vulpia + Wimera 5%
	5-10	89.5	12.3			Heavily grazed, clover dom.
	20-30	106.3	8.8			Sparse flowering of c/weed.
	40-50	218	16.8			
					53.0	
2/2/87	0-1	265	.2	41/38		Lightly grazed clover,
	1-5	71.2	.5			c/weed, grass pasture
	5-10	35.1	1.1			patches at bare soil.
	20-30	95.2	3.4			
	40-50	195	7.3			
					15.5	
3/4/87	0-1	402	12.7*	40/37		Dry grass, clover + c/weed
	1-5	247	4.6			debris some soil showing
	5-10	349	4.9			with gravel.
	20-30	180	6.6			
	40-50	368	12.1			*light rain affect

SITE THREE.

This site is adjacent to sites one and two and is at the head of an expanding saline scald. Although carrying some vegetation, its biomass productivity is very severely impaired. This site is considered to be becoming increasingly saline.

The site consisted of a mixture of 40% sedge and 40% Hordeum (H. gen), with the remainder comprising wintergrass, wimera and other minor grasses.

Horizon	Depth - cms	Description - Dy 5.81
A1	0-8	Very dark (10 YR 3/1) organic sandy loam, few small Fe gravels, pH 5.5, sharp break to
A2 1	8-20	dark greyish brown (10 YR 6/3) gritty loamy sand, few small Fe gravels, clear break to
A2 2	20-30	pale brown (10 YR 6/3) gritty loamy sand (bleach), few small Fe gravels, clear change to
B1	30-40	very pale brown (10 YR 7/3) gritty light clay, few small Fe gravels, gradual change to
B2	40 -	brownish yellow (10 YR 6/6) mottled red (10 R 4/6) slightly gritty medium clay, few small Fe gravels, pH 5.5.

SITE 3 DATE	DEPTH (CMS)	EC (1:5) ms/cm	AIR DRY % MOISTURE	EM V/H	RAINFALL SINCE PREV. SAMPLING	VEGETATION
15/10/85	0-1	8140	18.9	125/135	4.6 mm	H. gen 5)% Cyperus 5)%
	1-5	1510	19.1			P. vag 10%
	5-10	315	12.9			Wimera 10%
	20-30	432	11.1			
	40-50	877	14.1			
					7.6	
28/10/85	0-1	5580	20.1	120/120		H. gen 35% Cyperus 45
	1-5	890	12.9			P. vag 20%
	5-10	389	10.5			Wimera Tr
	20-30	307	8.0			
	40-50	800	15.4			
					9.0	
13/11/85	0-1	7790	17.6	115/112		Mixture persists.
	1-5	840	13.4			
	5-10	312	9.2			
	20-30	227	8.0			
	40-50	256	8.1			
					12.9	
16/1/86	0-1	17400	10.0			6.12.85 Mixture of H. gen
	1-5	2010	13.7			and Polydogon. Other dry
	5-10	948	11.9			veg. (Wimera).
	20-30	1079	13.1			
	40-50	1018	13.5			
					0.0	
6/2/86	0-1	66200	1.0	140/205		Sparse H. gen salt crystals
	1-5	15500	11.2			at the surface. Mostly
	5-10	6380	7.2			bare ground.
	20-30	536	8.8			pH 5.74 (mean of 5 surface
	40-50	850	12.0			samples).
					115.4	
26/3/86	0-1	22500	13.3	137/175		Little or no Germination.
	1-5	2880	13.1			Moisture at or near
	5-10	1190	15.3			surface.
	20-30	776	13.2			
	40-50	624	11.6			
					4.8	
28/4/86	0-1	24200	7.6	143/171		50% bare. Salty crusts
	1-5	4660	16.0			and dry plant material
	5-10	684	13.0			- no germination.
	20-30	552	13.9			
	40-50	714	15.3			
					84.4	
5/6/86	0-1	8560	28.4	118/136		50% bare dark soil 25% dry
	1-5	3160	12.1			grass stubble with some
	5-10	3180	10.8			germination of grasses.
	20-30	811	8.7			
	40-50	855	12.6			
					282.6	
19/8/86	0-1	932	38.2	103/94		Variable surface, sparse
	1-5	432	40.6			vegetation to bare some
	5-10	560	20.2			salt tolerant species.
	20-30	376	13.9			
	40-50	428	14.7			
					57.0	
16/10/86	0-1	1670	23.6	120/125		Bare soil 50% of surface
	1-5	1207	17.5			Cyperus 75% H. gen 20%
	5-10	1217	15.3			Polypagon 5%. Sheep tracks
	20-30	635	13.4			breaking up site. Nth side
	40-50	596	12.9			of plot increase salinity
						and pasture loss.
					53.0	
2/2/87	0-1	75,100	4.2	170/235		Remnants of polypogon
	1-5	7320	12.2			H. lep H. gen - bare
	5-10	550	9.3			with salt crust in
	20-30	529	10.4			places.
	40-50	629	11.0			
					15.5	
3/4/87	0-1	20,900	15.4*	166/277		Mostly bare with some
	1-5	9,050	11.1			poly. H. lep/gen
	5-10	2,350	11.6			
	20-30	500	9.8			
	40-50	417	10.0			*light rain affect

SITE FOUR.

This site, further downslope from site 3, had the highest surface salinity of all sites at the time of selection. The sparse vegetation comprised 60% cotula, 35% hordeum (H. gen) with 5% introduced perennial puccinellia.

Horizon	Depth - cms	Description - Dy 5.82
A1 1	0-5	Very dark grey (10 YR 3/1) organic sandy loam, pH 5.5, clear change to
A1 2	5-10	dark grey (10 YR 4/1) gritty loamy sand, clear change to
A2 1	10-20	greyish-brown (10 YR 5/2) gritty loamy sand, clear change to
A2 2	20-40	pale brown (10 YR 6/5) gritty loamy sand (bleach), gradual change to
B1	40-50	light grey (10 YR 7/2) gritty light clay, clear change to
B2	50 -	very pale brown (10 YR 7/3) mottled yellow (10 YR 7/6) and red (2.5 YR 5/8) gritty medium clay, pH 7.0.

SITE 4 DATE	DEPTH (CMS)	EC (1:5) ms/cm	AIR DRY % MOISTURE	EM V/H	RAINFALL SINCE PREV. SAMPLING	VEGETATION
15/10/85	0-1	26000	25.1	130/185	4.6 mm	H. gen 35% Cotula 60%
	1-5	1200	22.6			Pucc 5%
	5-10	1220	10.6			Poa Tr
	20-30	768	7.5			
	40-50	648	8.8			
					7.6	
28/10/85	0-1	21900	19.7	140/180		H. gen 40% Cotula 30%
	1-5	1350	8.5			P. vag 5%
	5-10	806	7.1			Polypogon 25%
	20-30	626	8.1			
	40-50	684	8.7			
					9.0	
13/11/85	0-1	24370	18.9	121/173		Mixture persists.
	1-5	3570	13.9			
	5-10	888	9.5			
	20-30	488	7.5			
	40-50	432	7.9			
					12.9	
16/1/86	0-1	41900	1.4			6.12.85 Dominance of
	1-5	4680	5.2			standing Polypogon and dry
	5-10	712	4.2			standing Cotula. Green
	20-30	418	4.5			tinge in places (Pucc)
	40-50	427	6.0			and some Polypogon.
					0.0	
6/2/86	0-1	38700	2.9	150/180		Sparse H. gen Cotula.
	1-5	10490	14.1			Salt crystals and bare
	5-10	982	7.			surface.
	20-30	728	8.3			pH 5.68 (mean of 5 surface
	40-50	430	7.9			samples).
					115.4	
26/3/86	0-1	29300	16.0	165/330		
	1-5	4280	12.2			
	5-10	910	9.2			
	20-30	869	11.9			
	40-50	1089	12.6			
					4.8	
28/4/86	0-1	30000	12.1	182/277		Mostly bare. Some remnant
	1-5	3000	9.5			dry vegetation. Pale
	5-10	685	9.1			crusting. Small patches
	20-30	955	12.5			Polypogon and well grazed
	40-50	613	10.3			Pucc.
					84.4	
5/6/86	0-1	3480	28.6	192/251		Patchy some bare patches
	1-5	705	11.6			mostly dry residual stubble
	5-10	667	10.1			with small amount
	20-30	1292	12.0			germination.
	40-50	1084	12.1			
					282.6	
19/8/86	0-1	2840	39.2	148/168		Sparse to patchy vegetation
	1-5	1350	21.4			some cotula + H. gen.
	5-10	1078	16.7			
	20-30	991	16.2			
	40-50	642				
					57.0	
16/10/86	0-1	6420	41.5	158/200		Cotula 50% H. gen 45%
	1-5	4360	16.1			Pucc 5% Vegetation is
	5-10	1700	12.2			only surviving on remnants
	20-30	1036	15.4			of top soil, 50% bare
	40-50	-	-	Too wet		western side 30% bare
						eastern side pale bare
						patches with pockets dark
						organic.
					53.0	
2/2/87	0-1	48,800	2.6	162/207		Grazed leaving bare patches,
	1-5	7,750	7.7			some pucc. Cotula dry
	5-10	578	6.5			H. lep/H. gen.
	20-30	668	7.9			
	40-50	585	9.6			
					15.5	
3/4/87	0-1	50,700	26.5*			Bare with organic stains
	1-5	25,400	21.8			some poly. H. gen in
	5-10	6,070	8.5			in patches.
	20-30	829	13.2			
	40-50	605	11.1			*light rain affect

SITE FIVE.

This site is located on a grey sandy "spillway" in a midslope position and is characterised by an almost pure capeweed stand with less than 5% mixed grasses. This is considered a non-saline site.

Horizon	Depth - cms	Description
A1 1	0-3	Very dark greyish brown (10 YR 3/2) sandy loam with few Fe gravels, pH 7.0, clear change to
A1 2	3-20	brown (10 YR 5/3 clayey sand with few Fe gravels, gradual change to
A2	20 - 60	pale brown (10 YR 6/3) clayey sand (bleach) with moderate Fe gravels, clear change to
B1	60 - 70	yellowish brown (10 YR 5/8) sandy light clay with few Fe gravels, clear change to
B2	70 -	brownish yellow (10 YR 5/8) mottled, light yellowish brown (10 YR 6/4) and red (2.5 YR 5/8) sandy medium clay with few Fe gravels, pH 6.5.

SITE 5 DATE	DEPTH (CMS)	EC (1:5) ms/cm	AIR DRY % MOISTURE	EM V/H	RAINFALL SINCE PREV. SAMPLING	VEGETATION
15/10/85	0-1	121	3.3	32/8	4.6 mm	C/weed 95% H. lep 5%
	1-5	45.4	4.5			Wimera +
	5-10	36.9	4.6			Vulpia +
	20-30	17.1	5.2			Brome = 5%
	40-50	23.3	8.9			Many flowers.
					7.6	
28/10/85	0-1	234	5.6	20/8		C/weed 85% H. lep 15%
	1-5	80	4.3			Wimera +
	5-10	26.3	2.8			Vulpia +
	20-30	13.6	3.4			Brome = 15%
	40-50	17.1	6.1			Rapidly haying-off - flowering nearly finished.
					9.0	
13/11/85	0-1	247	1.2	34/25		Haying-off, flowering finished
	1-5	85	3.3			
	5-10	61	3.3			
	20-30	21	3.0			
	40-50	20.5	5.2			
					12.9	
16/1/86	0-1	396	0.2			6.12.85 All dry litter.
	1-5	240	1.0			Some still standing.
	5-10	45	2.4			Remaining barley grass
	20-30	22.5	2.9			drying off. 10% bare
	40-50					grey sandy soil surface.
					0.0	
6/2/86	0-1	422	0.1			Abundant dead c/weed.
	1-5	196	0.2			Some bare surface.
	5-10	33	2.4			pH 5.88 (mean of 5 surface
	20-30	27	3.4			samples).
	40-50					
					115.4	
26/3/86	0-1	323	0.6	19/4		Germination of c/weed,
	1-5	173	2.5			some bare soil.
	5-10	44	3.1			
	20-30	25.3	3.7			
	40-50	19.6	5.0			
					4.8	
28/4/86	0-1	366	0.3	35/23		C/weed holding, not
	1-5	210	0.3			much bare ground - uniform.
	5-10	25	1.1			
	20-30	35	2.4			
	40-50	45	3.9			
					84.4	
5/6/86	0-1	133	6.7	35/22		90% uniform germination
	1-5	93	3.6			of c/weed.
	5-10	139	3.9			
	20-30	97	4.6			
	40-50	100	5.2			
					282.6	
19/8/86	0-1	158	25.6	34/23		80% c/weed with clover
	1-5	35.8	12.1			+ grasses
	5-10	24.5	14.0			
	20-30	27.3	17.4			
	40-50	52.6	20.0			
					57.0	
16/10/86	0-1	189	18.2	25/17		Dense swath.
	1-5	39.2	8.6			C/weed 50% Clover 10%
	5-10	34.8	6.8			Wimera 20% Vulpia 15%
	20-30	17.7	6.7			H. lep 5% Brome Tr
	40-50	27.8	11.1			C/weed flowering.
						Dense patches clover.
					53.0	
2/2/87	0-1	202	.03	44/30		Collapsed c/weed residue
	1-5	59.3	.2			with Wimera etc standing
	5-10	64.3	.9			rank.
	20-30	153	8.1			
	40-50	104	6.6			
					15.5	
3/4/87	0-1	216	10.8*	42/28		Dry Wimera. C/weed Dock
	1-5	117	2.2			(Slight hint of c/weed
	5-10	208	2.3			germination.)
	20-30	52	4.8			
	40-50	48	4.6			*light rain affect

SITE SIX.

This site is in a mid to lower slope and has well-developed salinity with an extensive, uniform, cotula stand (80%) with 10% succulents, the remainder being minor grasses and puccinellia.

This Dy 3.81 profile is variable at the surface and is now considered in 2 parts as free moisture seeps across the site giving variability of surface salinity. (see note regarding this point in Section 3.4, Electromagnetic Techniques).

Horizon	Depth - cms	Description - Dy 3.81
A1 1	0-5	Very dark grey brown (2.5 YR 3/2) organic sandy clay loam, pH 5.5, gradual change to
A1 2	5-15	light olive brown (2.5 Y 5/4) slightly organic sandy clay loam, clear change to
A2	15-40	pale yellow (5 Y 7/3) sandy clay loam (bleach) with some coarse Fe gravels, gradual change to
B1	40-50	pale yellow (5 Y 7/3) sandy clay with few Fe gravels, gradual change to
B2	50 -	pale yellow (5 Y 7/3) mottled, brownish yellow (10 YR 6/6) and red (2.5 YR 5/6) sandy medium clay, pH 5.5.

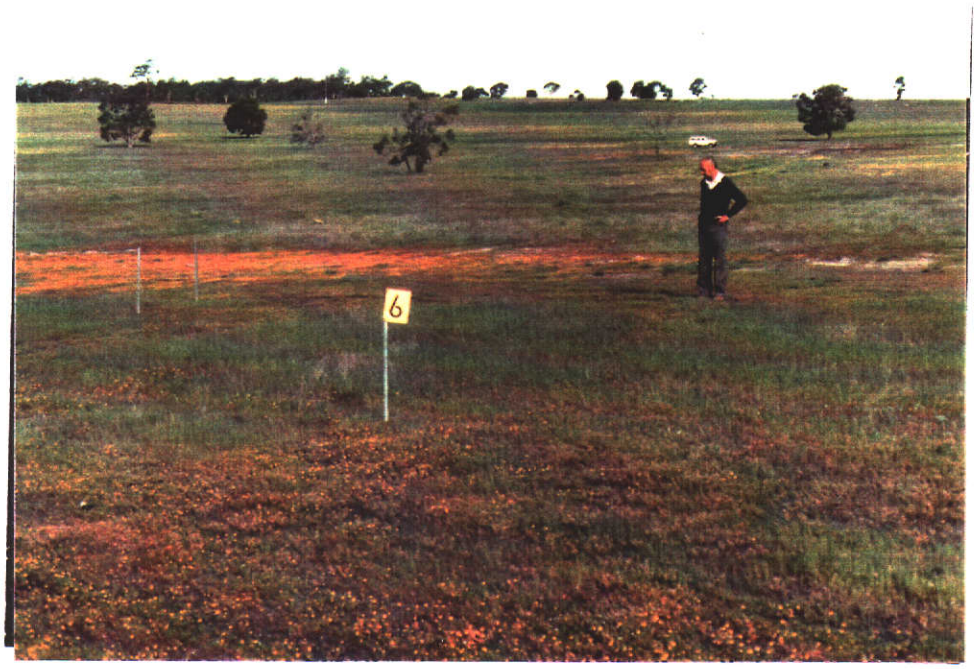

SITE 6 DATE	DEPTH (CMS)	EC (1:5) ms/cm	AIR DRY % MOISTURE	EM V/H	RAINFALL SINCE PREV. SAMPLING	VEGETATION
15/10/85	0-1	2790	21.3	72/98	4.6 mm	Cotula 80% H. gen 10%
	1-5	1360	15.1			Poa Tr Puccs 5%
	5-10	326	16.0			Sperg 5%
	20-30	411	12.3			
	40-50	310	10.9			
					7.6	
28/10/85	0-1	5760	22.9	101/128		Cotula 65% H. gen 5%
	1-5	1193	15.1			Polypogon 25% Pucc + 5%
	5-10	434	13.7			Sperg. 5%
	20-30	334	13.6			
	40-50	228	9.9			
					9.0	
13/11/85	0-1	7320	17.4	115/145		Mixture persists.
	1-5	1326	12.5			
	5-10	606	11.6			
	20-30	410	11.2			
	40-50	392	9.0			
					12.9	
16/1/86	0-1	8600	0.2	90/15		6.12.85 Cotula finished
	1-5	1430	2.3			flowering - still part
	5-10	214	3.9			green . Polypogon now
	20-30	254	4.7			dominant on north side.
	40-50					South side - sparse. 40%
						veg, 60% bare. Some
						Cotula in flower + Puccs.
					0.0	
6/2/86	0-1	6240	0.1			Sparse mixture of Cotula
	1-5	1630	0.9			and Polypogon. Part bare,
	5-10	215	2.6			dry surface.
	20-30	195	4.0			pH 5.25 (mean of 5 surface
	40-50	186	4.0			samples).
					115.4	
26/3/86	0-1	14500	21.5			Variable, very moist.
	1-5	1510	15.9			
	5-10	491	11.1			
	20-30	437	10.3			
	40-50	534	9.6			
					4.8	
28/4/86	0-1	17600	12.6	121/156		Still shows marked differ-
	1-5	1730	14.0			ence between northern and
	5-10	397	11.2			southern parts. South-bare
	20-30	435	11.5			north-organic surface with
	40-50	424	11.7			uniform germiantion of
						Cotula.
					84.4	
5/6/86	0-1	2170	30.0	134/164		+ 50% bare, patchy Cotula
	1-5	992	17.8			germination - very wet.
	5-10	969	17.8			
	20-30	964	17.2			
	40-50	490	12.1			
					282.6	
19/8/86	0-1	1086	38.5	110/110		Cotula and H. gen patch
	1-5	407	20.9			+ some bare areas.
	5-10	458	20.7			
	20-30	413	15.7			
	40-50	339	13.9			
					57.0	
16/10/86	0-1	1232	37.6	110/127		Site inundated.
	1-5	712	19.5			Polypogon 45% Cyperus 30%
	5-10	561	18.2			Cotula 15% Sperg. 10%
	20-30	528	16.4			40% of surface bare. Cotula
	40-50	-	Too wet			dominant on south side.
					53.0	
2/2/87	0-1	22,300	12.3	100/86		Patch dry Cotula and
	1-5	726	2.7			polypogon bare areas
	5-10	294	4.0			mixed.
	20-30	169	4.5			
	40-50	218	6.5			
					15.5	
3/4/87	0-1	25,000	18.0*	127/153		Mixed polypogon, B grass
	1-5	7,650	11.1			some dry Cotula.
	5-10	3,450	10.7			
	20-30	540	10.8			
	40-50	1,096	12.3			*light rain

SITE SEVEN.

This site is located in a 'high-risk' valley line below an earth tank which is rapidly becoming too saline for stock water. This site has an extensive stand of the perennial grass paspalum (75%); the remainder is mainly sedges and minor annual grasses. This site remains moist throughout the year.

Horizon	Depth - cms	Description - Dy 5.82
02	0-2	very dark greyish brown (10 YR 3/2) organic loam, pH 6.0, sharp change to
A1	2-15	dark grey brown (2.5 Y 4/2) sandy loam, pH 6.0, clear change to
A2	15-50	pale yellow (2.5 Y 7/4) few mottles, brownish yellow (10 YR 6/8) sandy light clay with few Fe gravels, clear change to
B1	50-60	pale yellow (2.5 Y 7/4) few mottles, brownish yellow (10 YR 6/8) sandy light clay with few Fe gravels, clear change to
B2	60 -	light grey (2.5 Y 7/2) mottled, yellowish brown (10 YR 5/8) and red (2.5 YR 5/6) sandy medium clay with few Fe gravels, pH 6.5.

SITE 7 DATE	DEPTH (CMS)	EC (1:5) ms/cm	AIR DRY % MOISTURE	EM V/H	RAINFALL SINCE PREV. SAMPLING	VEGETATION
15/10/85	0-1	16500	26.2	68/138	4.6 mm	P. vag 75% Cyperus 20%
	1-5	1460	14.4			H. gen 5% Sperg Tr
	5-10	812	13.6			Polypogon Tr Cotula Tr
	20-30	422	10.9			
	40-50	446	12.2			
					7.6	
28/10/85	0-1	10830	31.1	70/130		P. vag 70% Cyperus 15%
	1-5	919	12.4			H. gen Tr Sperg 15%
	5-10	398	9.9			Poa Tr Cotula Tr
	20-30	270	8.9			
	40-50	308	11.2			
					9.0	
13/11/85	0-1	11460	32.5	83/128		Mixture persists.
	1-5	1957	19.6			Flowering nearly finished.
	5-10	736	12.0			Haying off.
	20-30	330	8.2			
	40-50	346	11.3			
					12.9	
16/1/86	0-1	27300	2.0			6.12.85 Greem P. vag
	1-5	4150	3.6			Polypogon in seed.
	5-10	768	3.5			Cotula browning off.
	20-30	319	3.0			75% veg. cover. Light
	40-50					and dark grey/brown
						soil surface.
					0.0	
6/2/86	0-1	29600	0.0			Little or not green
	1-5	4980	.5			vegetation. Perennials
	5-10	284	1.3			Heavily grazed. Dry
	20-30	212	2.2			surface (dark in appearance)
	40-50	186	2.5			pH 5.27 (mean of 5 surface
						samples).
					115.4	
26/3/86	0-1	50100	27.8	65/160		Responsed to rainfall. Some
	1-5	13900	17.6			germination - heavily grazed.
	5-10	845	12.1			surface.
	20-30	796	15.4			
	40-50	628	14.1			
					4.8	
28/4/86	0-1	23800	16.7	96/144		Good response to rain
	1-5	5330	16.5			persisting heavilly grazed
	5-10	397	9.7			annuals and perennials -
	20-30	383	10.0			some bare soil.
	40-50	362	11.0			
					84.4	
5/6/86	0-1	6150	46.1	104/142		50% bare, very wet P. vag
	1-5	1330	23.5			regrowth some algal
	5-10	766	16.0			mat.
	20-30	666	16.1			
	40-50	Too wet to sample				
					282.6	
19/8/86	0-1	1820	49.8	81/110		Very wet - variable cover
	1-5	678	29.1			P. vag H.gen Cotula
	5-10	603	22.5			
	20-30	549	17.3			
	40-50	-	-	Too wet		
					57.0	
16/10/86	0-1	1790	40.5	89/127		Site inundated.
	1-5	933	20.5			Polypogon 40% Cyperus 20%
	5-10	980	19.9			Cotula 15% P. vag 25%
	20-30	-	-	Too wet		Ground cover extends over
	40-50	-	-	Too wet		80-90% of surface.
						Cotula flowering.
					53.0	
2/2/87	0-1	24,400	13.2	77/106		Some green P. vag,
	1-5	1,610	7.4			Polypogon and Cotula.
	5-10	412	5.8			
	20-30	301	4.6			
	40-50	281	4.7			
					15.5	
3/4/87	0-1	34,000	28.5*	911/151		Grazed (artif.) regrowth
	1-5	15,000	13.7			of P. vag.
	5-10	5,000	9.5			
	20-30	363	6.5			
	40-50	312	8.7			*light rain affect

SITE EIGHT.

This site is in an upper-slope, tributary valley saline seep position adjacent to site 7 and although fairly saline still supports a moderate grass pasture. There was mostly hordeum (85%) (H. gen) dominance, with the remainder being cotula and minor succulents. 40% of the surface material is organic matter.

Horizon	Depth - cms	Description - Dy 5.82
A1 1	0-5	Very dark grey (10 YR 3/1) organic sandy loam, pH 5.5, clear change to
A1 2	5-10	dark grey (10 YR 4/1) gritty loamy sand, sharp change to
A2	10-60	light grey (10 YR 7/2) slightly clayey sand (bleach) with few small Fe gravels, sharp change to
B	60 -	light brownish grey (10 YR 6/2) mottled brownish yellow (10 YR 6/8) gritty medium clay with few small Fe gravels, pH 6.5.

SITE 8 DATE	DEPTH (CMS)	EC (1:5) ms/cm	AIR DRY % MOISTURE	EM V/H	RAINFALL SINCE PREV. SAMPLING	VEGETATION
15/10/85	0-1	2440	34.0	43/69	4.6 mm	H. gen 85% Cotula 5%
	1-5	1600	24.6			Polypogon Tr Lythrum 10%
	5-10	307	12.5			Wimera Tr
	20-30	242	12.2			
	40-50	213	10.0			
28/10/85	0-1	4480	36.8	45/55	7.6	H. gen 40% Cotula Tr
	1-5	624	16.6			Polypogon 40% Lythrum 10%
	5-10	322	13.3			Wimera 10%
	20-30	286	12.1			
	40-50	166	11.8			
13/11/85	0-1	6175	30.6	45/56	9.0	Mixture persists.
	1-5	1115	16.1			Flowering finishing.
	5-10	410	9.0			
	20-30	217	6.5			
	40-50	163	8.7			
16/1/86	0-1	12100	19.1		12.9	6.12.85 Dense, tall stand-
	1-5	3430	24.7			ing rank dry grass. Polydogon
	5-10	107	5.1			+ Hordeum sp. slightly
	20-30	235	5.2			green tinge still remains.
	40-50					
6/2/86	0-1	61700	3.8		0.0	Dense dry hayed off grass
	1-5	11740	5.6			pH 5.59 (mean of 5 surface
	5-10	192	4.9			samples).
	20-30	115	5.5			
	40-50	104	6.5			
26/3/86	0-1	16200	31.9	44/60	115.4	Dense mat of ungrazed
	1-5	2150	15.6			grasses. Some germination.
	5-10	223	8.0			
	20-30	256	9.3			
	40-50	243	11.3			
28/4/86	0-1	13300	20.3	44/59	4.8	Dense residual vegetation
	1-5	1330	16.2			with good germination.
	5-10	191	6.9			- no germination.
	20-30	151	8.8			
	40-50	186	10.6			
5/6/86	0-1	2740	46.6		84.4	Dense residual rank headed
	1-5	647	22.1			grass with good new growth
	5-10	536	17.1			of grasses. No bare soil.
	20-30	442	16.6			
	40-50	Too wet to sample				
19/8/86	0-1	1600	68.5	59/75	282.6	Very wet - some patchiness
	1-5	606	31.5			residula grass - H. gen,
	5-10	408	26.4			Cotula
	20-30	-	-	Too wet		
	40-50	-	-	Too wet		
16/10/86	0-1	1120	60.6	63/79	57.0	Site inundated.
	1-5	498	25.8			H. gen 95% Wimera 5%
	5-10	400	23.4			Lithrum Tr.
	20-30	-	-	Too wet		H. gen in seed. Dense
	40-50	-	-	Too wet		ungrazed matt of veg.
2/2/87	0-1	34,600	10.1	38/44	53.0	Dense dry hayed-off
	1-5	1,029	5.8			pasture - ungrazed.
	5-10	137	4.4			Grass and succulents
	20-30	122	5.6			mixed.
	40-50	139	7.0			
3/4/87	0-1	19,700	21.5*	44/50	15.5	Dense grass debris.
	1-5	4,600	7.4			Grazed (artif.). Some
	5-10	379	4.8			per succulents on north
	20-30	78.2	4.8			end.
	40-50	93.3	6.5			* light rain affect

APPENDIX THREE

Species List for Yalanbee Sites 1985

Common name	Genus, Species	ref. in tables
Soft Brome	Bromus mollis	Brome
Cotula	Cotula australis	Cot
Capeweed	Cryptostemma calendula	C/weed
Sedges	Cyperus Spp	Cyp
Geranium	Erodium botrys	Erod
Barley Grass	Hordeum geniculatum	H. gen
Barley Grass	Hordeum leporinum	H. lep
Wimera Rye Grass	Lolium rigidum	Wimera
Wild Oats	Aristida spp	Aris
Salt water couch	Paspalum vaginatum	P. vag
Wintergrass	Poa annua	Poa
Annual Beard grass	Polypogon monspeliensis	Poly
Puccinellia	Puccinellia ciliata	Pucc
Spurry	Spergularia Spp	Sperg
Sub-clover	Trifolium subterraneum	Clov
Haresfoot Clover	Trifolium avense	Hfc
Silver grass	Vulpia Spp	Vulp

APPENDIX FOUR

OPTICAL LAYOUT OF SPECTROPHOTOMETER

Figure 4 shows an optical layout of the Model 340 Recording Spectrophotometer. Light emitted from the light source (W or D_2) is reflected by mirror M_1, and forms an image on entrance slit S_1. After passing through entrance slit s_1, the light beam is reflected by plane mirror M_2, and made almost parallel by collimator M_3, and directed to prism P serving as the first monochromator. The beam dispersed by the prism is converged by collimator M_3, reflected by plane mirrors M_4 and M_5, and then focused on intermediate slit S_2. The second monochromator is composed of collimator M_5 and diffraction grating G_1 or G_2, and the desired monochromatic light is obtained at slit S_3.

Two diffraction gratings are employed according to the wavelength region, one of 1440 lines/mm for ultraviolet to visible regions (190 - 850 nm), and the other of 600 lines/mm for near infrared region (800 - 2600 nm). The one quartz prism covers a wavelength range of 190 to 2600 nm. For driving these dispersing elements, a feed screw and a sine bar are employed for the diffraction gratings, and two cams are employed for the prism.

The monochromator from exit slit S_3 is alternately reflected to plane mirror M_7 or continues straight to plane mirror M_8 by the rotating sector mirror Se_1. The beam which alternately passes through the sample side and reference side repeats reflection and straight advance by sector mirror Se_2 which rotates synchronized with sector mirror M_9 and then focuses onto the detector by condenser mirror M_{10}. The detectors are a photomultiplier for ultra-violet to visible regions, and a PbS cell for near infrared region.

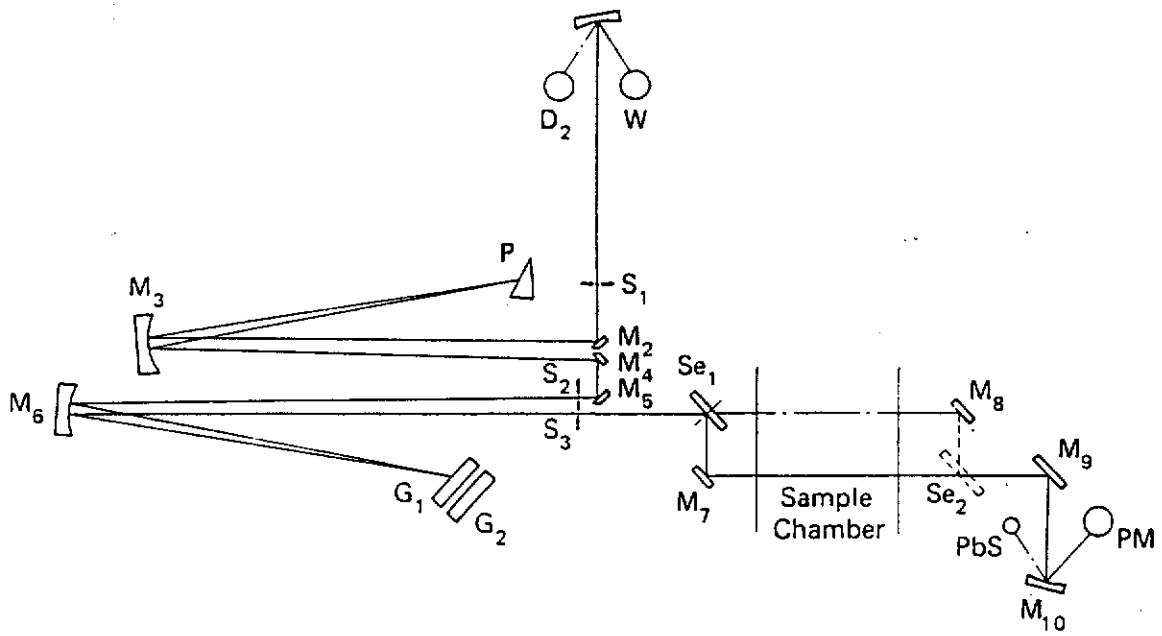

Figure Twenty-one. Optical layout of the Hitachi 340 Spectrophotometer.

APPENDIX FIVE

SPECIFICATIONS OF PORTABLE FIELD SPECTRORADIOMETER

(per Geoscan Pty Ltd)

Wavelength range: 3 segment OCLI filter wheel. Segment ranges (nanometers) and resolution (delta lambda over lambda) are:

Segment	Range	Resolution
1	400 - 700	3 per cent
2	680 - 1200	3 per cent
3	1300 - 2500	1.5 per cent

Detectors: Two colour (Silicon over Lead Sulfide.)

Field of View: 2 degrees

Samples per Spectrum: 256

Time per Spectrum: 3 seconds

Modes of Operation: (i) Radiance. Digital voltages represent uncalibrated radiance.

(ii) Reflectance. Digital voltages represent reflectance of target, relative to either a barium sulphate target, or to a PTFE translucent screen.

Telescope module: The telescope is an F/2 Newtonian telescope, with a 15 cm focal length spherical primary.

Scanning module: Focused radiation from the telescope module passes into the scanning module, through a 1000 Hz chopper and the OCLI circular variable filter (CVF) onto the two colour silicon over lead sulphide detector. Signals from the two

detector elements are preamplified in separate amplifiers and then second stage amplified through amplifiers whose gains and offsets are digitally selectable. The CVF is driven by a stepping motor geared to an annular gear around the CVF. One spectrum consists of 256 steps.

Controller module: The controller module, immediately below the scan module, contains the Z80-based microprocessor controller, the bubble memory, the controller for the liquid crystal display, and the second-stage amplifiers and analogue-to-digital converter board. On the back end of the controller module, a customized keyboard allows entry of commands for recording, displaying and storing spectra. The liquid crystal display module on the back of the combined unit functions as a display unit for the processor, and as a graphical display for spectra.

APPENDIX SIX

THE MODULES AND SPECIFICATIONS FOR THE GEOSCAN MULTISPECTRAL SCANNER

(i) The scan mirror module, which has a 150 mm aperture, 45 degree mirror which can be rotated at speeds between 0 and 10 cps. This variable-scan speed, which is controlled by the system processor, allows imagery to be acquired between altitudes of 3,000 and 10,000 feet (approx. 1000-3000 m) above terrain.

(ii) An f/2.3 Dall-Kirkham telescope, with a dichroic beamsplitter for separation of the short-wave infrared (SWIR), and the thermal infrared (TIR). The visible portion of the energy is reflected from a 45 degree mirror prior to the telescope, using the "dead space" due to the telescope secondary mirror.

(iii) Three dispersion/detection modules, consisting of strings of dichroics and induced transmission filters for dispersion, and discrete detectors. The detectors for the visible region are silicon photodiodes; for the SWIR region, Judson Infrared Indium Antimonide (InSb); and for the thermal IR, Judson Infrared Mercury Cadmium Telluride (MCT). The InSb and MCT detectors are cooled using Joule Thomson generated liquid nitrogen. Preamplifiers for the detectors are built into their respective modules.

(iv) The stabilizing ring, which corrects the system for pitch and yaw variations, up to 15 degrees in each axis. Any roll variations are corrected by varying the sampling times

for each scan line. Attitude reference for the pitch and roll axes is provided by a vertical gyro. For the yaw axis an integrating gyroscope is used.

(v) The electronics console, which consists of a rack with a bank of gain/offset amplifiers, a rack containing the system processor (a Motorola 68010 microprocessor), interfaces to the scan and attitude systems, a disk interface, a streaming tape drive interface, an analogue-to-digital converter bank, memory boards, an image processing controller, and a system status display. Analogue electronics, controlling the pitch and yaw servo systems, and the mirror speed control, are mounted in the third rack in the console, with all system power switching and fuses in a separate panel. Stabilized power is provided using switching power supplies mounted on the back of the electronics console.

(vi) The Priam 168 megabyte Winchester disk.

(vii) A Cypher streaming tape drive, for backing up the data onto 1600 bpi computer compatible tapes.

(viii) A 14-inch Mitsubishi high resolution monitor for real-time interactive display.

(ix) A customized 24 volt to 240 volt AC inverter.

This scanner is considered as a prototype for future scanners. The planning of the MK2 scanner is already well advanced and has significant improvements incorporated into its design which will be relevant research into spectral band selection. The new scanner will record any 8 of 32 narrow bands evenly spaced between 400 and 1000 nanometers, it has 8 strategically-placed bands, for

mineralogical discrimination, in the SWIR between 1980 and 2600 nanometers, and 4 bands in the thermal region. It also has the capability to record bands, with interchangeable modules, between 1400 - 1800 nanometers and between 3000 - 5000 nm. The scanner will be fitted into a pressurised aircraft enabling flying heights up to 10,000 metres, giving a spatial resolution between 3 and 20 metres, and field of view of 92^{o}. This is accomplished with 2.95 milliradian I.F.O.V. with 2.1 milliradian pixel spacing, covering a ground swath 768 pixels wide. The data will be recorded onto two, 330 megabyte winchester disks giving 540 megabytes of useable storage. This is backed-up onto two, 400 megabyte laser disks, thus doing away with the tape drive.

Pitch and yaw will be compensated stabilized mechanical gyro mount, and roll is removed electronically. A Doppler navigation system linked to the recording system will provide location as well as ground speed and drift.

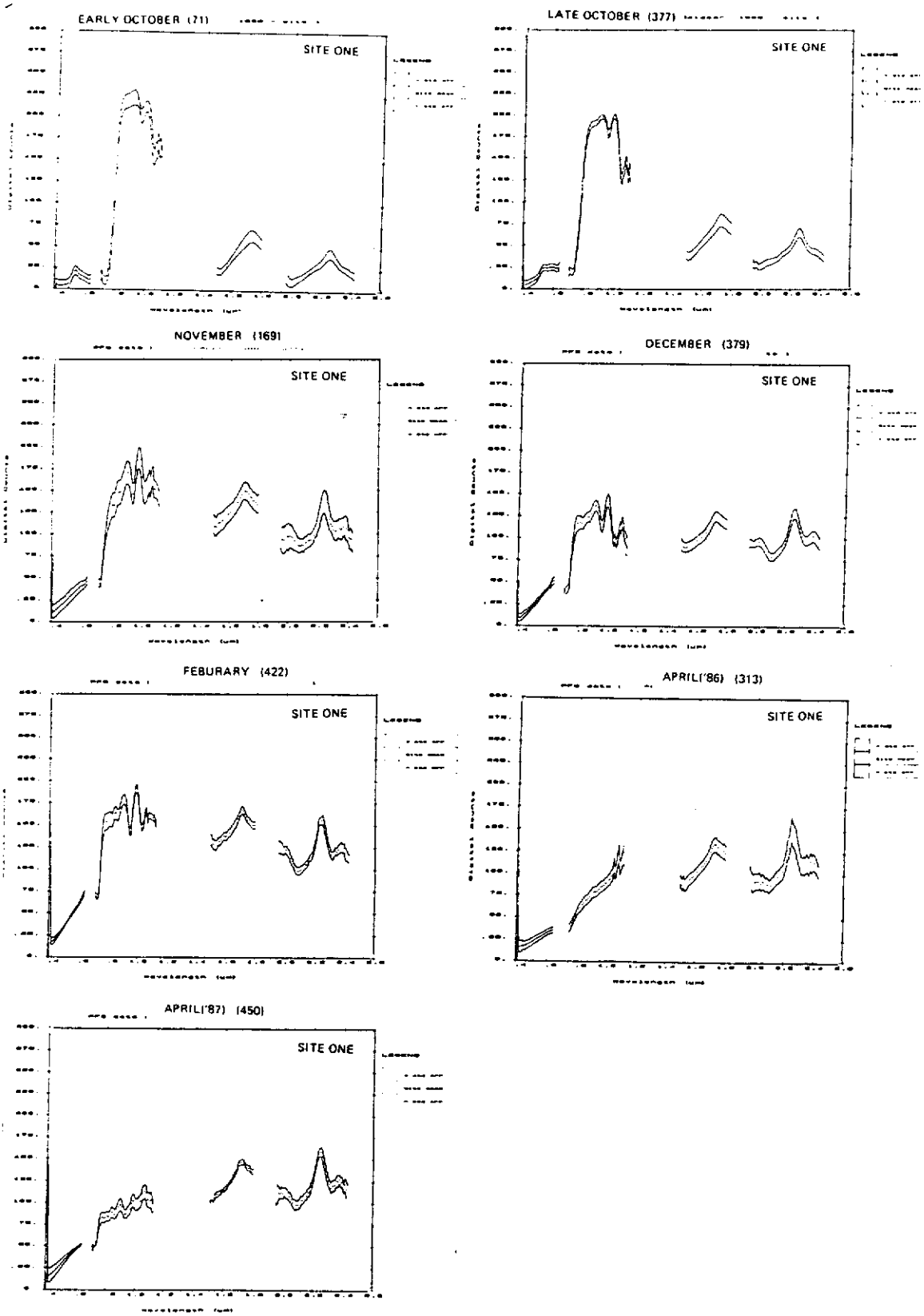

Appendix Seven (a). Masked mean PFS spectra for Site One throughout the period of the study.

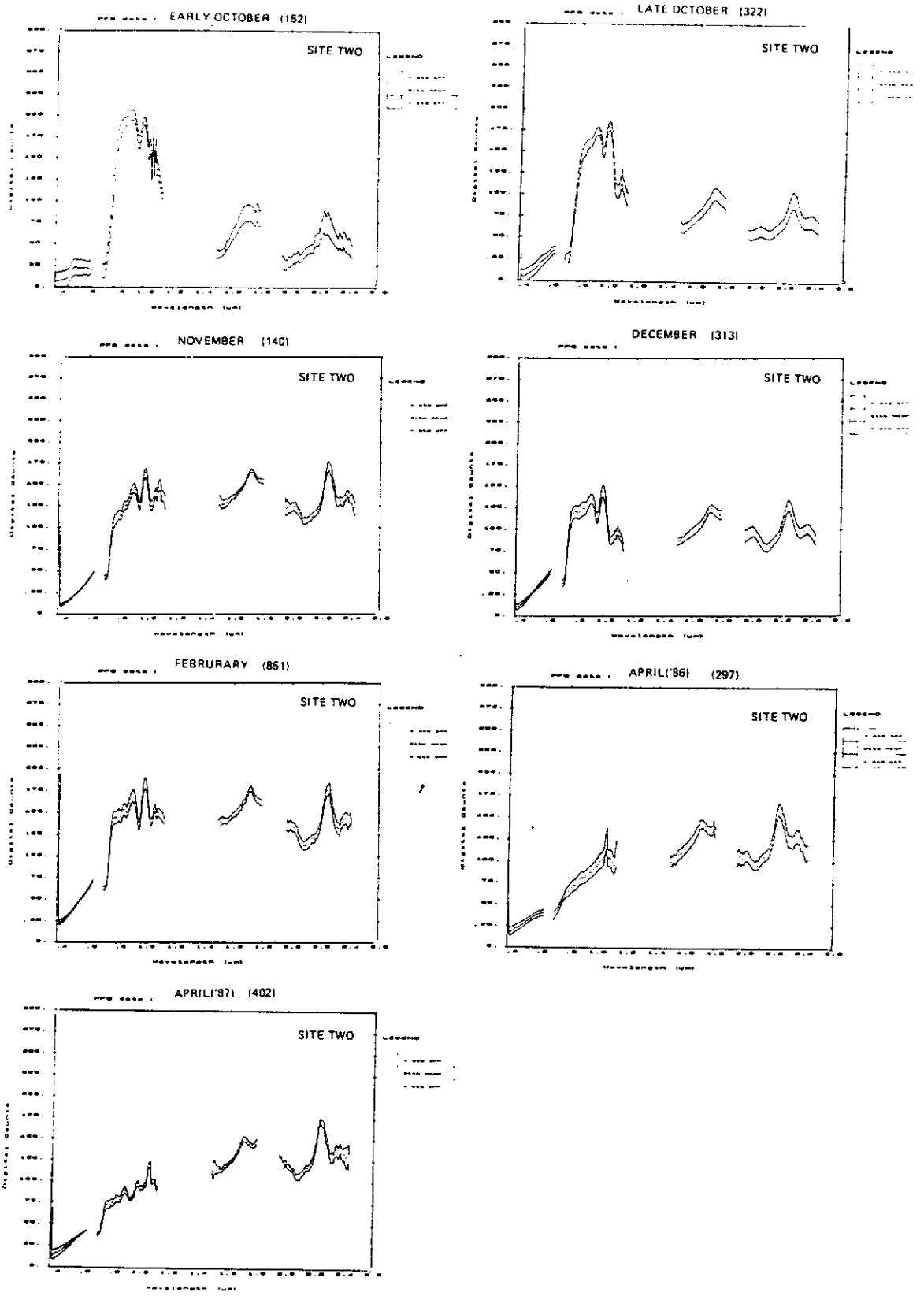

Appendix Seven (b). Masked mean PFS spectra for Site Two throughout the period of the study.

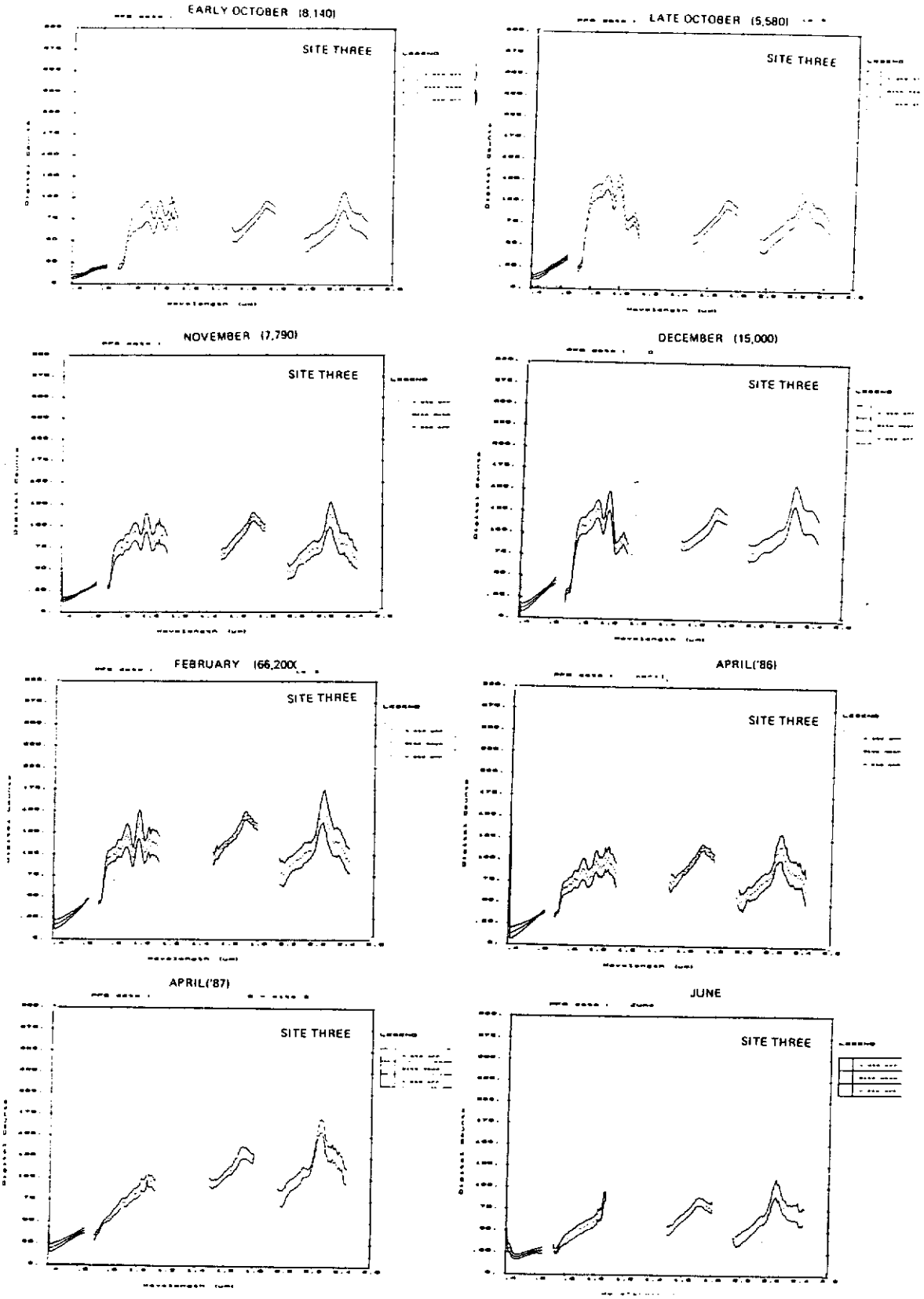

Appendix Seven (c). Masked mean PFS spectra for Site Three throughout the period of the study.

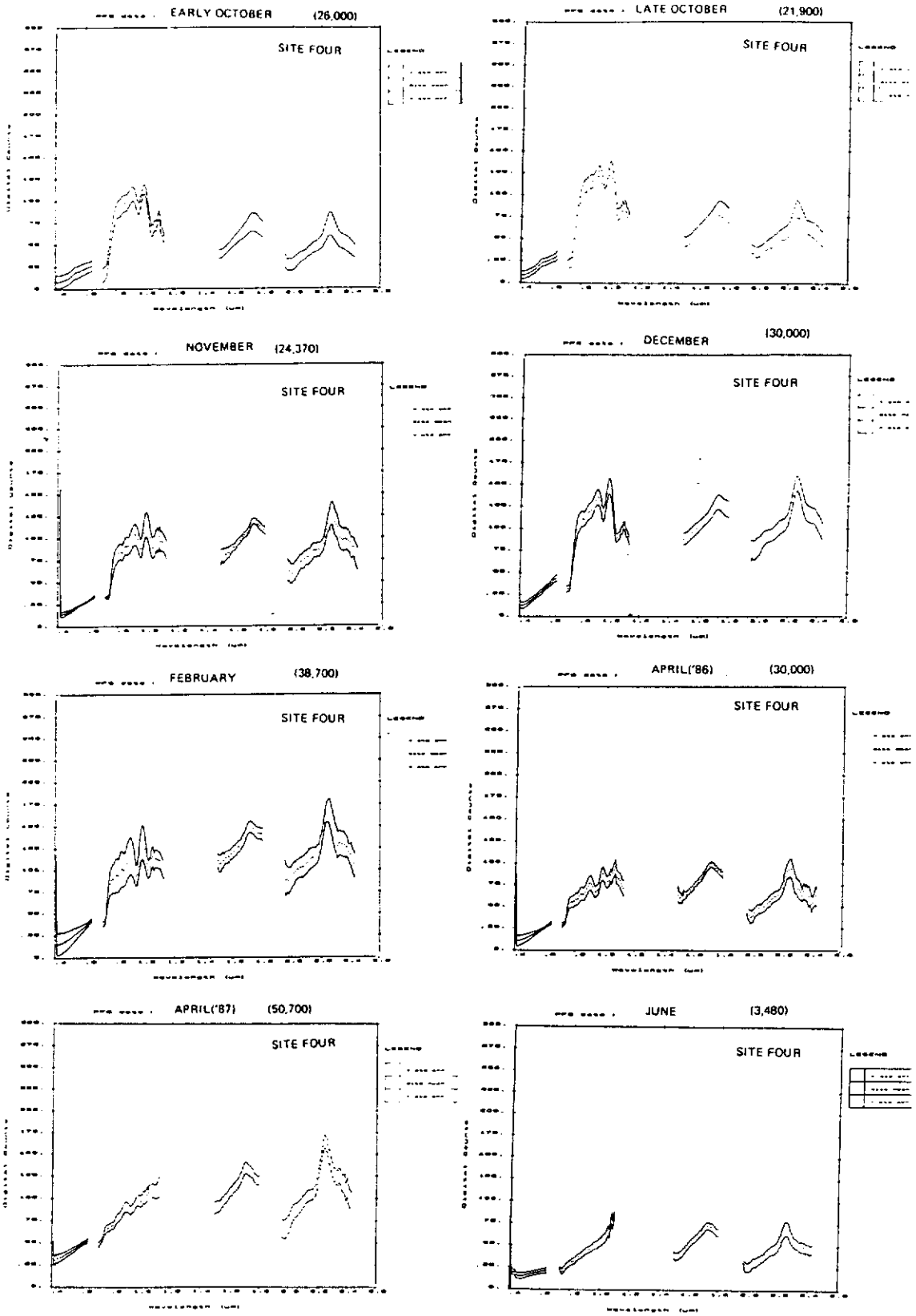

Appendix Seven (d). Masked mean PFS spectra for Site Four throughout the period of the study.

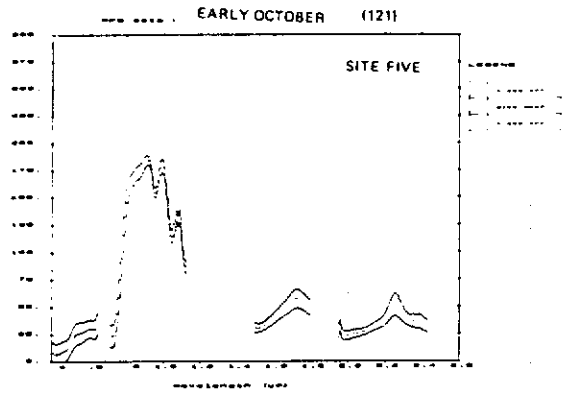

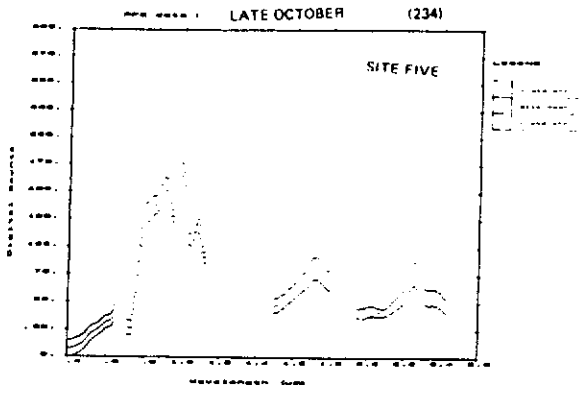

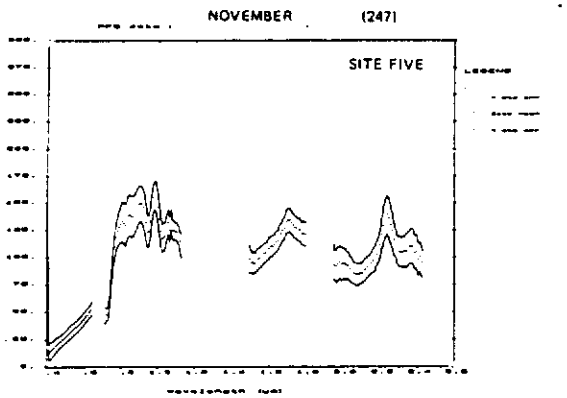

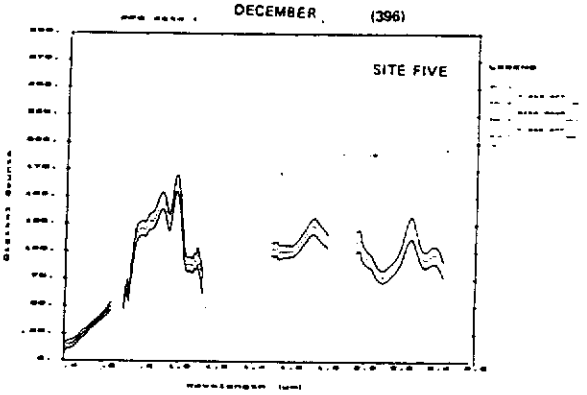

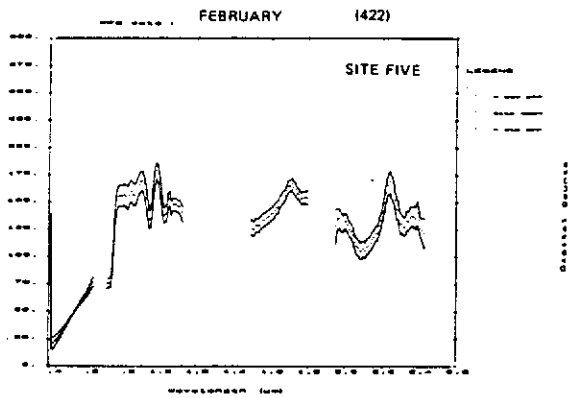

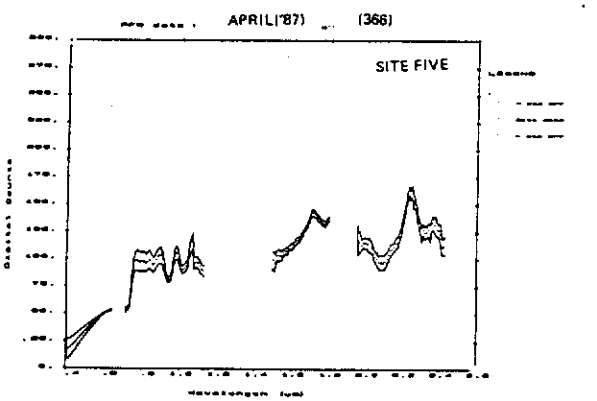

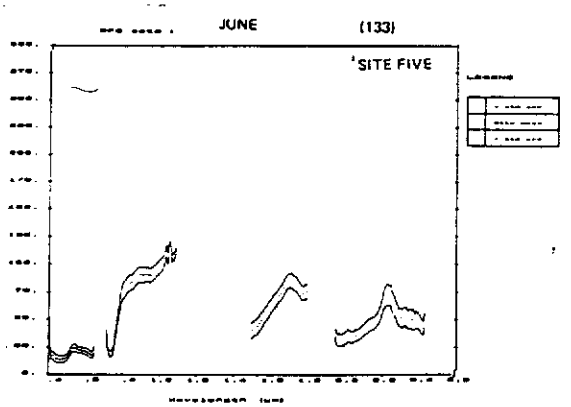

Appendix Seven (e). Masked mean PFS spectra for Site Five throughout the period of the study.

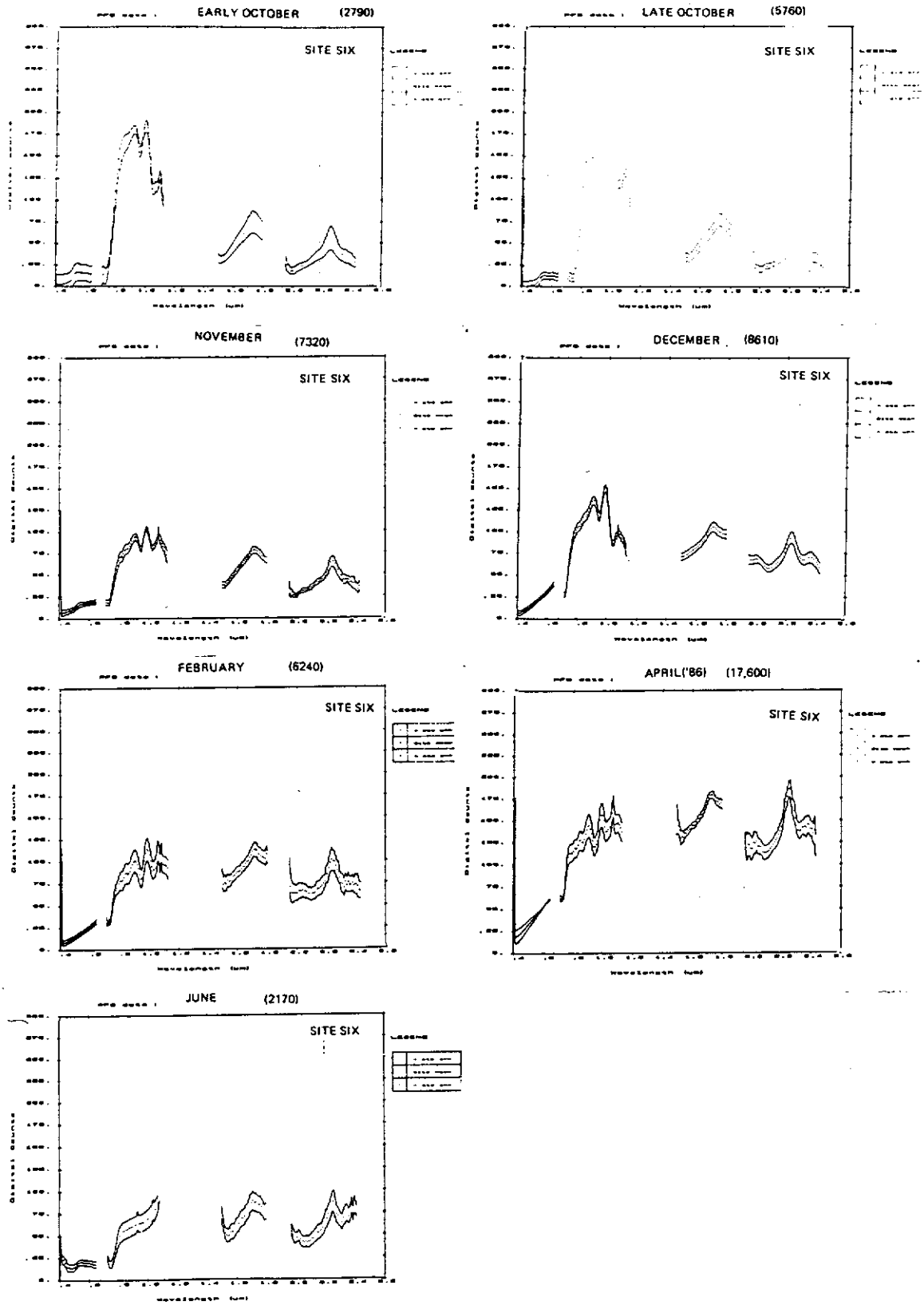

Appendix Seven (f). Masked mean PFS spectra for Site Six throughout the period of the study.

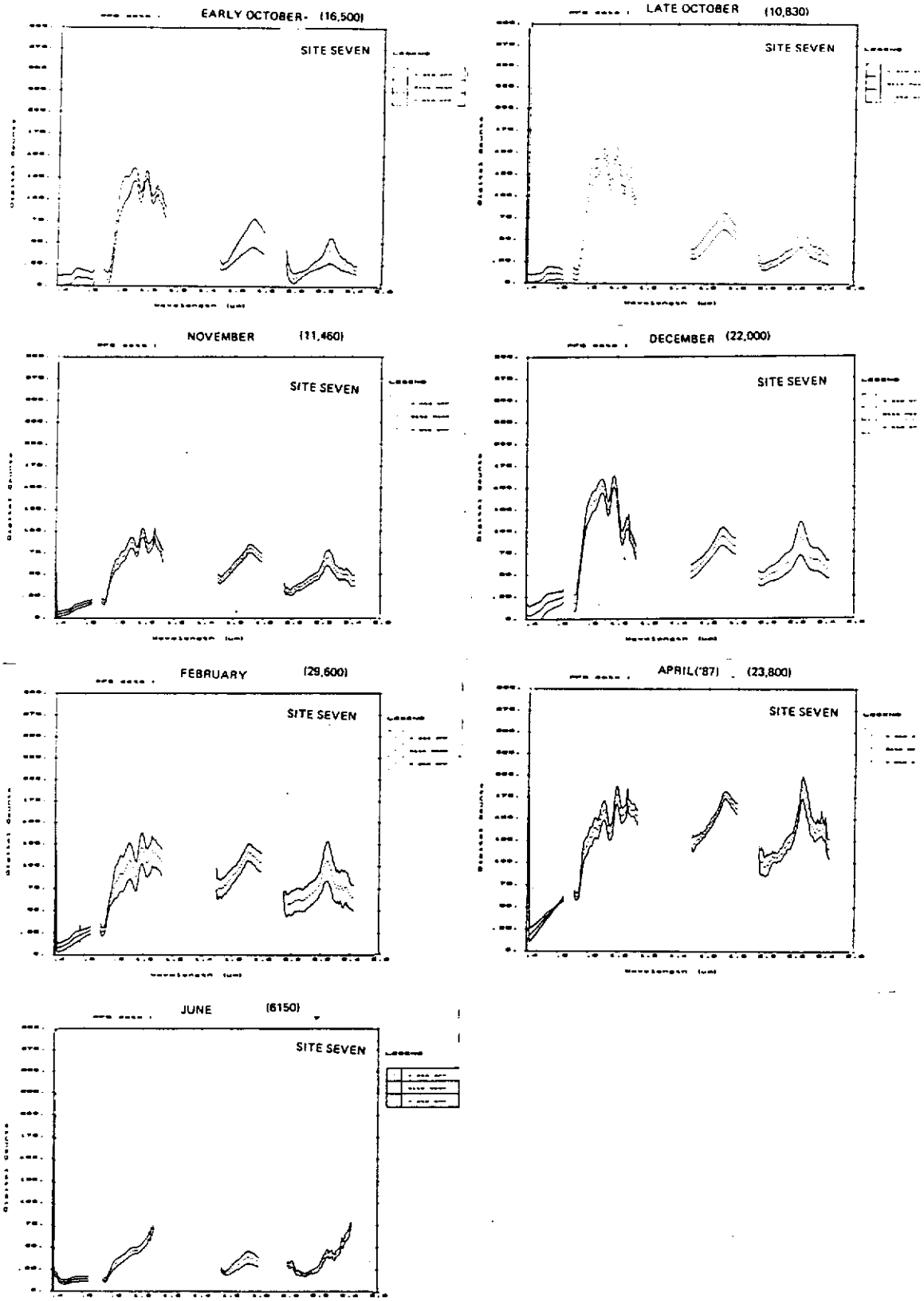

Appendix Seven (g). Masked mean PFS spectra for Site Seven throughout the period of the study.

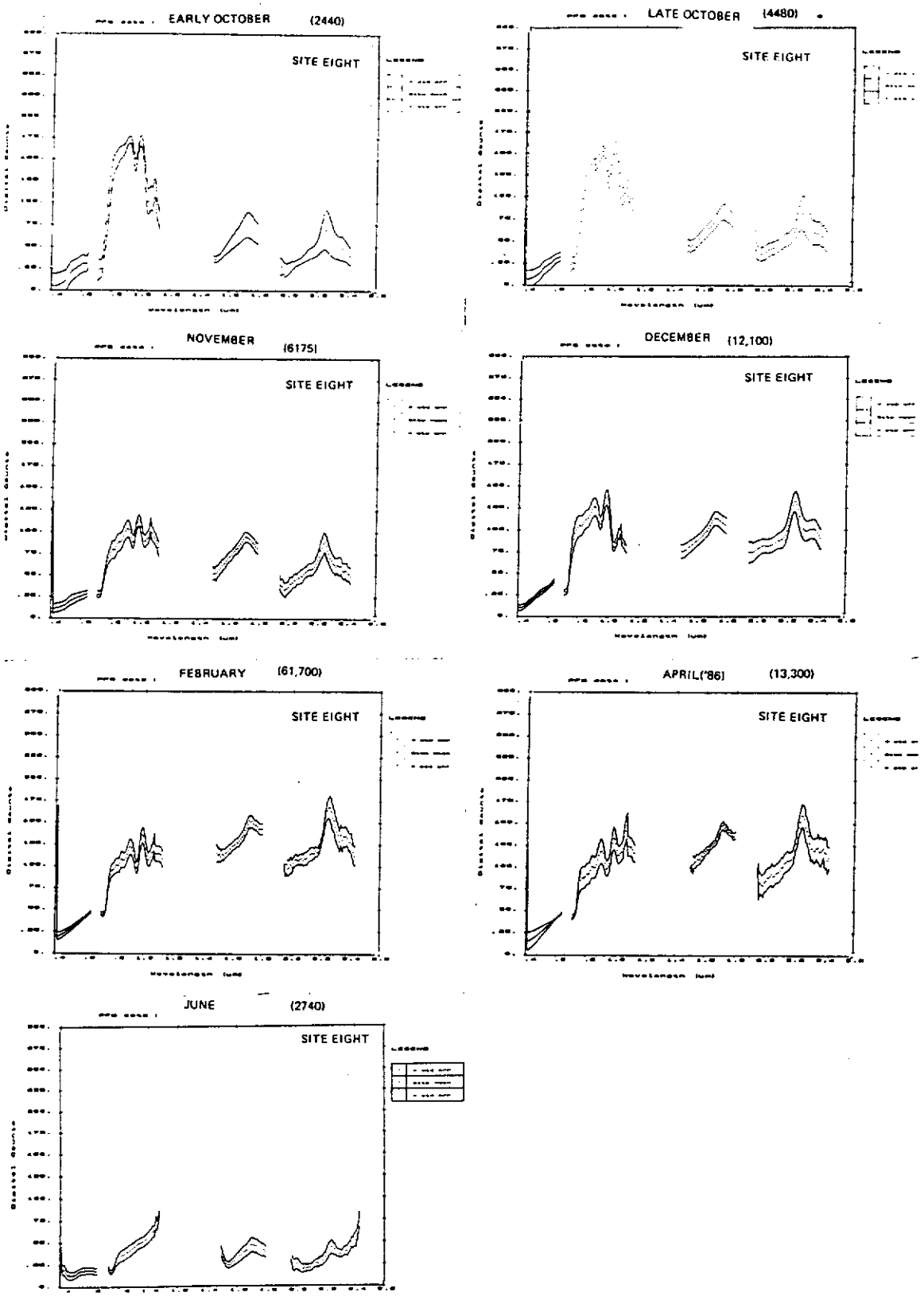

Appendix Seven (h). Masked mean PFS spectra for Site Eight throughout the period of the study.